Characterisation of autophagosomes as a source of novel citrullinated antigens for use as a cancer vaccine

Bryony Heath

Thesis submitted to the University of Nottingham
for the degree of
Doctor of Philosophy

March 2023

Funded by the Medical Research Council

Abstract

Post translational modifications of proteins are often found to be altered in tumour cells compared to normal physiological cells. These differences have been exploited in immunotherapy based treatments, where the immune system is targeted to tumour specific PTMs, as reviewed in this thesis. One particular modification, citrullination, has been shown to be an epitope that is important in the specific activation of CD4 T cells against tumour cells, leading to their cytotoxic destruction. It is thought that the citrullination of proteins and their presentation on MHCII is involved in the process of autophagy. We hypothesise that autophagy is a stress response in tumour cells, which leads to the production of citrullinated epitopes, that can be found within the tumour autophagosome. To test this hypothesis, autophagic activity in primary immune and fibroblast cells, and cancer cell lines, were tested and constitutive autophagy in tumour cells was observed. An autophagosome enrichment protocol was established and the presence of autophagosomes was confirmed by Western blot, flow cytometry, and imaging. The autophagy associated marker, LC3-II was found to be restricted to a number of density fractions. When analysed, the contents of the autophagosome positive fraction were shown to contain citrullinated proteins. Autophagosomes can

therefore act as an enriched sourced of citrullinated epitopes for identification of novel proteins by mass spectrometry or for use as immunogens to raise an anti-tumour T cell response against citrullinated epitopes. This is an exciting prospect for identifying novel citrullinated epitopes for cancer immunotherapy.

Acknowledgements

Firstly, I would like to thank my supervisors, Dr Ian Spendlove and Dr Andrew Jackson for their guidance, support and sense of humour throughout my PhD. Their advice has been invaluable in my continued progression and I appreciate them taking the time to look out for me even through turmoil, such as a pandemic!

I would also like to thank the Host-Tumour Interactions group as a whole who have all graciously parted their knowledge to help shape my research. Further thanks goes to Lindy Durrant and Scancell Ltd. for generously giving their advice and resources.

Thank you to Peter Symonds and Dr Sabaria Shah who carried out the ELISPOT assays, to MSc student, Shashwat Goyal, for preparing labelled autophagosome preps for EM, and to Jade Manning and Katie Choi who carried out the EM imaging.

Thank you to the Medical Research Council for funding my PhD and making this work possible.

Special thanks to my peers Dr Ilona Sica and Megan Greener for always being available to lend an ear during an incubation period coffee break. Your friendship is something I hold dearly and has kept me sane throughout these years!

Finally, I would like to thank my Mum, Cherry Heath, for without her unwavering support I would not have gotten anywhere near this far! Thank you to my friends and teammates for their support, with a special mention to Elizabeth Richmond who's "therapy" sessions kept me on the right path, and to Lara Doolan for supporting me through the final months, to the very end.

Table of Contents

1. Introduction

1.1 What Makes a Good Immunotherapy Cancer Vaccine?

Cancer vaccines for immunotherapy need to fulfil a number of requirements in order to successfully induce an immune response against tumour cells and unfortunately in most cases, vaccines are not able to achieve this.

Firstly, for T cell immunity, a suitable epitope target needs to be chosen. Optimal targets are antigens that the immune system will not be tolerant against, due to central or peripheral T cell tolerance[1]. A neoepitope, created due to mutation within the tumour, is a strong candidate as T cells would not be educated in the thymus to see it as a "self" peptide and become anergic due to tolerance. Other potential epitopes could include differentially post translationally modified proteins, or a protein that has been upregulated past the point of normal expression.

The next requirement is for the immune system to be fully activated against this antigen. This can occur through the full activation of specialised antigen presenting cells (APC), such as dendritic cells (DC), causing them to upregulate co-receptor molecules. This provides signal 2, in duality with signal 1 (peptide in the context of MHC) allowing for full activation of T cells. This is often achieved through the use of

an adjuvant that activates DC through their toll-like receptors (TLR)[2].

For the immune system to be in its activated state, it needs the correct cytokine environment to promote immunity rather than tolerance. Unfortunately, tumour environments can have a cytokine profile that skews the immune system in the direction of tolerance[3]. This can be overcome by using epitopes that are recognised by CD4 T helper 1 (Th1) cells that can produce cytokines that promote cell mediated immunity[4].

Not only is it useful to have a CD4 epitope to skew the cytokine environment, but a CD8 epitope can be important in the destruction and clearance of tumour cells. CD8 T cells are cytotoxic, and can release cytotoxic granules to compromise the target cell and cause cell death[5]. This is the primary goal in tumour immunotherapy.

Each epitope target needs to have good avidity between the activated dendritic cell or the tumour cell and the T cell to overcome the threshold of activation for the T cell[6]. The upregulation of second messengers on DC contributes to this, but antigen expression on the target cell also has a role. This concept is evidenced when using self-epitopes as targets,

where overexpression allows for breaking of tolerance and T cell activation[7].

Tumour masses are usually heterogeneous[8]. This means that one cell may not express the same neoantigens and therefore present the same antigens on MHC as the next cell. An optimum cancer vaccine will target an epitope that is expressed and presented on all cells within the tumour mass, instead of only targeting a small sub-population. Some vaccines use multiple epitopes to try and circumvent this issue[9,10].

Further concepts of successful cancer vaccines are reviewed by Liu et al.[11]

1.2 The Major Histocompatibility Complex and Adaptive Immunity

The major histocompatibility complex (MHC) is a complex of proteins involved in the presentation of antigen peptide fragments to T cells for activation. There are two types of MHC complex, MHC-I and MHC-II, each with different constraints on the type of antigen they bind, route of antigen processing, and subset of T cell that they interact with. In humans, MHC is called the human leukocyte antigen (HLA) and each of the MHC subtypes are coded by a number of genes, found on chromosome 6[12]. MHC-I molecules are made up of α chains,

coded by three class I genes: HLA-A, HLA-B, and HLA-C[13]. Class II molecules are made up of an α and β chain, of which there are also three pairs of immunologically important genes: HLA-DR, HLA-DP, and HLA-DQ (Figure 1.1)[13]. Unlike HLA-DQ and –DP, HLA-DR gene cluster has an additional β chain, giving two different potential -DR molecules for immune activation[13]. For this reason, each person has three different HLA-I molecules, and at least three HLA-II molecules expressed on cells. HLA are highly polymorphic[14], meaning there is great genetic variation within these genes within the population, and most individuals will be heterozygous at each loci[15], allowing for even further variation between individuals. Polymorphisms are mainly concentrated to the β1 subunit of MHC-II genes and α1 and α2 subunits of MHC-I, all of which are involved in antigen binding and T cell recognition[16]. With polymorphism and polygeny contributing to diversification, a large range of antigens can bind to MHC and be recognised by T cells, and this is largely individualised in each person.

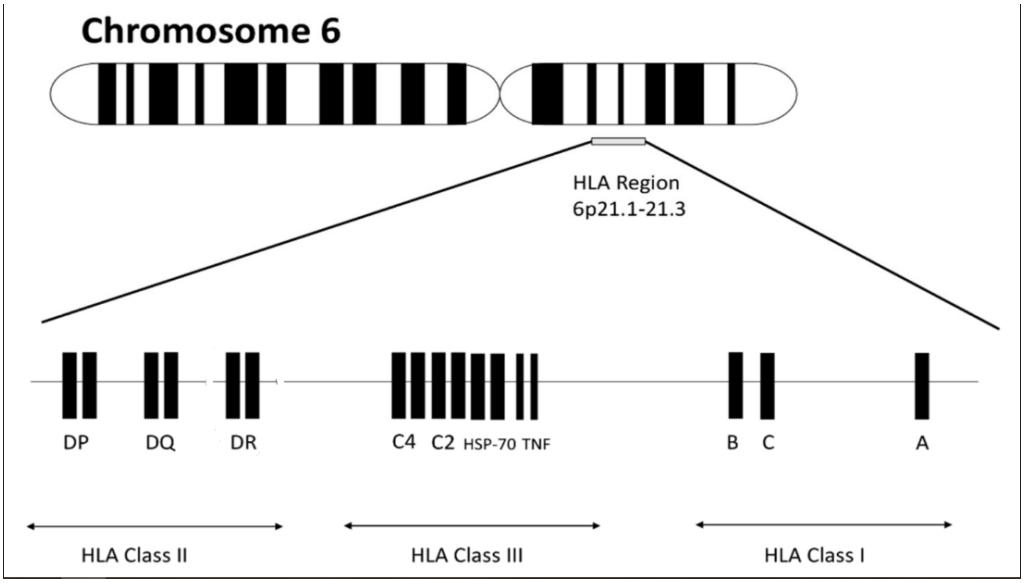

Figure 1.1 Class I, II and III HLA genes on chromosome 6[17].

Each subtype of MHC is able to bind a different repertoire of antigen. MHC-I is mostly involved in the presentation of antigens from an intracellular source, primarily as a way to combat viral infections within cells[18]. Viral peptides bind to MHC-I and are presented to CD8+ T cells, which are activated to release lytic enzymes to destroy the infected cell[19]. For this reason, MHC-I is expressed on all cells as a "window" to inside for immune cells. MHC-II typically presents antigens from extracellular origin to CD4+ T cells, inducing cytokine production that supports particular immune responses[20]. MHC-II is primarily expressed by cells of the immune system but expression can be induced in other cells in the presence of inflammatory cytokines[21]. Antigen binding clefts of both MHC subtypes are formed by two α-helices, either side of the

antigenic peptide. The subtypes differ in their tertiary structure, allowing for different types of peptide to bind. MHC-I has a closed structure at each end of the binding cleft. Shorter peptides of 8-11 amino acids can fit within these constraints[22]. MHC-II however has a more open structure allowing for longer peptides, typically of 12-25 amino acids, as the peptide can extend outside of the binding cleft[23]. Each binding domain has a number of anchor residues which bind specific amino acids. MHC-I has anchor residues in binding pockets P2 or P5/6, and stabilises binding at the amino and carboxy terminus of the peptide (due to its closed structure at both ends)[24]. MHC-II anchor residues are found at pockets P1, P4, P6, and P9[23,25]. Each MHC variants will anchor different residues giving opportunity for different peptides to bind and further amino acid variation is possible outside of these anchor residues where the precise residue is less important.

MHC molecules are unstable in their unbound state[26]. Therefore MHC found on the surface of cells are always found in a bound MHC:Peptide configuration. This means that when MHC is purified from cells, stably bound peptides co-purify with them. The peptides eluted from HLA are considered the human immunopeptidome, of which a database has been formed based on mass spectrometry investigation of peptides isolated from MHC through acid elution[27]. MHC:peptide

complexes isolated from tumour cells have an immunopeptidome which may contain tumour specific neoepitopes. For example, this method was used in 1997 by Dubey et al. to sequence the first MHC-I bound mutated neoepitope[28]. Furthermore, the same group later discovered post-translationally modified (PTM) phosphopeptides associated with tumour cells[29]. The presentation of neopepitopes and differentially modified epitopes on tumour MHC, gives an avenue for activating the immune system for specifically targeting tumour cells, leaving non-tumour cells unaffected.

1.3 Dendritic Cells

Dendritic cells (DC) are the primary antigen presenting cells (APCs) that are responsible for controlling the adaptive immune response[30]. They bridge the gap between innate and adaptive immunity by recognising pathogen associated molecular patterns (PAMPs) and danger signals, then inducing a primary immune response by presenting antigens to T cells for activation[31].

Immature dendritic cells (iDC) derive from precursors in bone marrow, and are found in tissues, blood and lymphatics. In their immature state, DC express low levels of costimulatory molecules (such as CD80, and CD86)[32], MHC, produce less

inflammatory cytokines, but have a high level of endocytic activity[33]. Immature DC also express inflammatory chemokine receptors, such as CXCR1, CCR1, CCR2 and CCR5, complement, and chemoattractant receptors, to allow them to home to infected tissue[34]. iDC are therefore specialised for finding pathogens within the tissue. Upon encountering pathogens, DCs are activated and go through maturation to become mature DC (mDC). This process involves downregulation CCR1 and CCR5 and upregulation CCR7, to home to secondary lymphoid organs[34,35]. Further functional changes that occur include the upregulation of MHC-II and co-stimulatory receptors, and the production of inflammatory cytokines, including IL-12, IL-1, and TNF[36]. These markers, amongst others, define the mDC phenotype and makes them specialised for T cell activation. mDC activate T cells through presentation of antigens in the context of MHC (signal 1), co-stimulatory molecules (signal 2), and inflammatory cytokines (signal 3) for full T cell activation. Recently activated T cells then migrate from the lymph nodes then home to inflamed tissue to carry out their effector functions.

Dendritic cells are a heterogenous population with different subsets specialised for particular functions. The three major subsets of plasmocytoid DC (pDC), and two types of conventional DC, cDC1 and cDC2. The main function of pDC is

production of type 1 interferon in response to viral infection[37,38]. Activation occurs through Toll-like receptor 7 (TLR7) and TLR9 which sense single-stranded RNA and double-stranded DNA, respectively, and pDC selectively express these receptors for carrying out this function[39]. pDC can be identified by surface markers CD123 (IL-3R) and CD45RA, as well as markers involved in their function CD303 (CLEC4C; BDCA-2), CD304 (neuropilin; BDCA-4) CD85k (ILT3) and CD85g (ILT7)[40].

cDC1 cells show particularly good ability to cross-present antigens on MHC-I and induce T helpter type 1 (Th1) and natural killer (NK) cell responses through IL-12 release, however this is more pronounced in mice than in humans[41–43]. cDC1 and 2 both express CD141, CD13, CD33, and CD11c but cDC1 has a much lower expression of CD11c in comparison. These markers plus CLEC9A (extracellular actin receptor), CADM1 (cell adhesion molecule) and BTLA antigen can lead to accurate identification of cDC1 only[43–45].

cDC2 cells are more prevalent than cDC1 but are also more heterogeneous[46,47]. They are thought to be specialised in CD4 T cell activation through MHC-II presentation. cDC2 cells are characterised by surface markers CD1c, CD2, FcεR1, SIRPA and myeloid markers CD11b, CD11c, CD13 and CD33.

Furthermore, more recent work has shown that markers CLEC10A (CD301a), VEGFA and FCGR2A (CD32A) are reliably associated with cDC2[48].

DC subsets are largely conserved within mice[49], apart from some subtle differences, as outlined above. Murine bone marrow is often used as a source of progenitor cells to differentiate into a large amount of dendritic cells for experimentation[50].

Dendritic cells present both MHC-I and MHC-II peptides for activation of CD8 and CD4 T cells, respectively. Different processes are used to load each MHC for peptide presentation. Classical MHC-I loading occurs from an intracellular source, such as viral infection. Proteins from within the cytoplasm are degraded by the proteasome[51] and the resulting peptides are translocated to the endoplasmic reticulum (ER) via Transporter Associate with Antigen Processing (TAP)-dependent translocation[52]. The Peptide Loading Complex (PLC) is located within the ER which constitutes of TAP, ERp57, tapasin and the calnexin-calreticulin system[53–56]. Newly synthesised MHC-I is stabilised by this complex. The PLC mediates the loading of MHC-I where the peptide is trimmed to the optimal size of 8-11 amino acids by the ER aminopeptidase ERAP-1[57]. High affinity peptide:MHC-I

complexes are then translocated to the plasma membrane, via the golgi apparatus.

Classical MHC-II loading occurs through endosomal routes. MHC-II is synthesised in the ER where it is associated with an invariant chain (Ii) which binds to the peptide binding groove as a pseudopeptide and stabilises the complex[58]. The complex then moves to an endocytic compartment called the MHC-II compartment (MIIC), either directly[59,60] or via the golgi apparatus[61]. Ii is digested in the MIIC by cathepsins as the compartment acidified, leaving a fragment called the Class II-associate Invarient Chain Peptide (CLIP) which continues to stabilise the complex within the MIIC[62,63]. Extracellular antigens, that have entered the MIIC through the endosomal system, are degraded by endo-lysosomal proteases[64,65]. HLA-DM then catalyses the dissociation of CLIP and association of antigenic peptides within the MHC-II peptide binding grove, provided the peptides have optimal affinity[66]. Once loaded peptide:MHC-II complexes are translocated to the membrane, either by contact of the MIIC with the plasma membrane[67], or through vesicular trafficking[68].

Extracellular sources enter the MIIC for MHC-II loading through a number of ways. Receptor-mediated or clathrin-mediated endocytosis is a targeted process for internalisation

of soluble extracellular material. Ligands such as lipoproteins, transferritin, plasminogen complexes, carbohydrates, hormones and lysosomal enzymes bind receptors to activate them, recruiting proteins to aid in the invagination of the membrane[69–74]. A key protein involved in this is clathrin, which is why the process is called clathrin-mediated however many more proteins are also involved in this process (reviewed here[75]). This process allows for the uptake of particles with an optimal size of <25nm[76]. Following uptake, the particles go through the endocytic pathway, from early endosome through to late endosome/MIIC, moving to increasingly acidified compartment where peptide processing can take place[77].

Macropinocytosis is the non-specific process by which soluble antigens in the extracellular fluid are internalised. This is an actin-dependent process by which actin causes the extension of the membrane, causing membrane ruffles, which can extend into a cup shape that ultimately seals at the distal tips, forming an intracellular macropinosome[78]. The macropinosome then joins the endocytic pathway and has access to MIIC, similarly to endosomes.

Phagocytosis is the process where large antigens (>0.5 μm, such as microbial organisms) are recognised, internalised, and

degraded. The degradation process can liberate antigenic peptides for MHC-II loading. Recognition of antigens for phagocytosis are through receptors such as Fc, complement, scavenger or mannose/fucose family receptors[79]. After recognition, the actin cytoskeleton is remodelled to extend pseudopodia around the particle and engulf it to form an intracellular phagosome. The phagosome then goes through a maturation process where it acidifies and acquires proteases. The process of loading MHC-II with phagosomal proteins may have a number of routes. There is evidence for phagosomes acquiring MHC-II for loading during maturation[80], and evidence that MHC-II does not interact with the phagosome and is loaded with phagosomal proteins outside the phagosome[81]. Nevertheless, once MHC-II is loaded with antigenic peptide, it is translocated to the plasma membrane to be seen by CD4 T cells.

There are also non-conventional ways for antigen presentation. Cross presentation allow for the presentation of extracellular antigens on MHC-I and the activation of cytotoxic CD8 T cells. Two main mechanisms of cross-presentation have been suggested: cytosolic and vacuolar. Cytosolic is sensitive to proteasome inhibitors and therefore it is suggested that proteins escape endosomes or phagosomes to access the proteasome[82]. It is currently unknown whether peptides that

are proteasomally processed are transported to the ER for MHC-I loading or if they are transported back into the phagosome for further processing[83,84]. Vacuolar cross-presentation is inhibited by lysosomal inhibitors, suggesting that MHC-I loading of extracellular antigens must first come through the lysosome before being loaded onto MHC-I[85,86].

Finally, another source of non-conventional MHC-II loading occurs through autophagy. Macroautophagy (hereafter referred to as autophagy) involves the formation of intracellular vesicles to target cytoplasmic proteins and aggregates to the lysosome. Although the exact mechanisms have not been found, proteins targeted to autophagosomes by conjugation with LC3 get presented on MHC-II, and not MHC-I, giving evidence for MHC-II loading through autophagy[87]. Autophagy activation also increases the presentation of tumour and viral antigens on MHC-II[88,89]. Further evidence comes from LC3 being found in MIICs, suggesting interactions between the two compartments[90].

1.4 Post-translational modifications

Post-translational modifications (PTMs) are used to alter the function or activity of proteins through covalent addition of groups or cleavage of amino acids in the existing protein. To date, at least 710 types of protein modification have been

MODIFICATION TYPE	TARGET	MODIFICATION
PHOSPHORYLATION	Serine/Threonine, Tyrosine	PO_4 (phosphate)
GLYCOSYLATION	Hydroxyl group	Various carbohydrates
NITRATION	Tyrosine, tryptophan, cysteine, methionine	NO_2 (Nitro group)
ACETYLATION	Lysine	CH_3CO (acetyl group)
AMIDATION	Lysine, cysteine, serine, threonine, tyrosine, arginine	NH_2 (amine group)
HYDROXYLATION	Proline, lysine, asparagine, aspartate, histidine	OH (hydroxyl group)
METHYLATION	Arginine, lysine, amino/carboxy terminus of proteins	CH_3 (methyl group)
UBIQUITINATION	Lysine, cysteine, serine, threonine, N-terminus of proteins	Ubiquitin

Table 1. The 8 most common PTMs, their targets, and the modifying group.

identified, as shown in the Delta Mass database from the Association of Biomolecular Resource Facilities[91], the 8 most common of which are summarised in table 1. PTMs allow for fast and/or transient adaptation of proteins, something that

cannot be achieved through genetics alone, and are involved in controlling protein localisation, turnover, signalling capabilities and protein-protein interactions. This in turn allows for fine tuning of the processes within an organism on a shorter time scale than transcriptional activation.

There are a number of ways that protein modifications can occur, the majority being enzymatically mediated. These are activated through several mechanisms such as cellular stress, autophagy, apoptosis and through general cell homeostasis. Some modifications can occur non-enzymatically, such as spontaneous lysine carboxylation[92], glycation[93], carbamoylation[94], and carbonylation[95], often due to stress, such as oxidative stress.

Within the thymus, the developing T cells are either positively or negatively selected depending on their strength of binding to antigen presenting cells that are presenting self-peptides on MHC. If the affinity for self-peptides is too strong, it is likely that the T cells will be self-reactive if allowed to enter circulation, which would lead to the destruction of normal, healthy cells. Self-reactive T cells are therefore deleted in the thymus if this is the case. However in a study by Raposo et al., T cells specific for post translationally modified protein were able to escape central tolerance in the thymus and enter

circulation[96]. This is either because PTMs aren't present in the thymus or aren't present in a high enough concentration for the T cell to be negatively selected. This could potentially allow generation of a subset of novel epitopes that are only generated under stress. This may have important ramifications for the immune repertoire as some PTMs are only formed under stressful conditions e.g. in infectious disease or the tumour microenvironment.

1.4.1 Post-translational modifications as T-cell epitopes

An incidence of post translational modification alters protein structure, through changes in covalent and non-covalent interactions. This can cause proteins to assume a different tertiary structure which permits increased or decreased binding to MHC[97]/TCR, or alters proteolytic cleavage of polypeptides and the generation of new epitopes[98], such as the cleavage of cytokeratin fragments creating neoepitopes in Adenocarcinomas. More effective binding to the TCR can lead to a breakdown of tolerance against this protein, leading to autoimmunity, as can be the case in rheumatoid arthritis[99] and type I diabetes[100].

1.4.2 Post-translational modifications in cancer

As in autoimmune diseases, changes in metabolism in cancer can cause differences in PTMs. A number of PTMs are

documented to be differentially produced in cancer cells and these include phosphorylation, glycosylation, citrullination, and nitration (discussed below). Modified peptides have the potential to be processed and presented on MHC, giving the immune system opportunity to be activated against them, specifically targeting cancer cells. This idea has been harnessed in some immunotherapies, using proteins with aberrant or upregulated PTMs as 'neoepitopes' with the goal of activating the immune system against them[101]. The difficulty with targeting PTMs as a neoepitope, rather than genetic mutations, is that PTMs are much harder to identify as a robust template such as the genetic code isn't available to compare them against. Genetic mutations are easily discoverable by comparing the genetic sequence of cancer cells to normal cells, and it is easy to amplify tumour genetic sequences in order to accurately do this. With protein modification, we are not able to amplify this in order to accurately investigate differences in tumour and normal cells. PTMs are often transient, adding further complication to their identification. However, some PTMs have been identified as contributing to an immune response, and have been identified as neoepitopes in cancer, as detailed below.

1.4.3 Glycosylation

Glycosylation of proteins is often dysregulated in cancer and changes in N-linked and O-linked glycans, fucosylation, as well as increases sialyl Lewis antigen have been witnessed[102,103]. This can be due to changes in the expression or specificity of sugar transferases. As a single glycosyltransferase has the ability to alter multiple sugar residues at multiple locations on different proteins, genetic changes in a glycosyltransferase can have large consequences in changing the properties of glycoproteins in cancer cells. This can then amplify changes in glycans on the cell leading to a very different glycome to normal cells, aiding targeting of cancerous cells[104]. Glycosylation impacts on cancer specific neoepitope formation in three ways, namely blocking certain cleavage sites, allowing for a protein sequence that isn't normally found for extended amounts of time, altering the affinity for MHC, or altering the affinity for TCR. This can all occur through the changes of tertiary structure due to the interference in protein sequence and non-covalent forces.

T cells were shown to specifically recognise glycopeptides in a number of early studies, presented by both MHCI and MHCII[105–107]. It was shown that large glycans would block binding of the glycopeptide to MHCII however monosaccharide or disaccharides could permit it, provided the sugar moiety

was not bound to anchor residues important for MHCII binding[108]. T cells were later shown to respond to glycopeptides, which were outside the TCR contact region, and not their deglycosylated counterpart, which lead to the hypothesis that carbohydrates change the conformation of the peptide which directs TCR reactivity[109]. Carbohydrates within the TCR interacting region could induce responses against both the sugar itself[108] and the sugar plus protein[110].

Glycopeptides may induce T cell responses when presented on MHCI. Haurum et al demonstrated they were able to induce a glycan specific CTL response. It has been shown that the glycan moiety affects both TCR and MHC binding, with the carbohydrate being able to strengthen bonds in both. With regards to processing of MHCI restricted peptides, O-linked GlcNAc peptides can be processed in the ER and transported by TAP. It is thought that N-linked GlcNAc peptides are not able to be presented on MHCI, possibly because the glycan moiety interferes with aminopeptidases that process the peptide to the right length for MHCI, or because the glycan blocks the translocation to the ER via TAP[111].

There are a number of cancer related carbohydrate antigens. Some of the most commonly found are the TF and Tn antigens which are truncated O-linked carbohydrates (Gal-GalNAc-O-

Ser and GalNAc-O-Ser respectively). These are formed due to the decrease or absence in the activity of β1-6GlcNAc transferase which catalyses the initial elongation of O-linked glycans, and an increase in activity of the α2-3-sialyltransferase which adds a terminating sialyl acid residue to galactase, preventing elongation. Due to the size of normal glycans, and their structural flexibility, it seems more likely that glycans would mask MHC biding, rather than potentiate it. However, with the partial reduction of glycans, creating TF and Tn antigens, the glycoprotein becomes immunogenic. These antigens are highly expressed on tumour cells, and infrequently on normal cells, therefore it is possible to activate T cells against it. This is what occurs with the MUC1 antigen, found to be upregulated in various adenocarcinomas[112]. The mucin-like glycoprotein is normally highly glycosylated, but these glycosylations become truncated in cancer cells. The cancer associated MUC1 with truncated glycans has been shown to induce both CD4 and CD8 responses *in-vivo* against the neoepitope.

Another glycoprotein common in prostate cancer is prostate specific antigen (PSA), where it is often found increased in cancer patients. It is unknown whether the glycan moiety contributes to MHC/TCR binding, however there are studies showing the activation of an immune response to a peptide

without glycan moiety so it is possible that it is not required[113]. In a study by Tabares et al, a difference in glycosylation between PSA of malignant or benign prostate tumours was shown[114]. If these glycans are also incorporated on MHC, it could be possible to more selectively target malignant prostate tumour cells, rather than normal prostate cells expressing PSA.

The Tn and Sialyl-Tn antigens occur due to the loss of Cosmc function, a molecular chaperone for T synthetase[115]. Without this, large amounts of Tn antigen are generated on a wide amount of glycopeptides as T-synthetase is not available to catalyse the formation of the T antigen. Tn is also a substrate for α1-6 sialyltransferase[116]. Loss of Cosmc function or overexpressed α1-6 sialyltransferase can lead to the generation of sialyl-Tn. As these two antigens are not normally present on physiological cells in the quantities found on tumour cells, they are a good marker for cancer and potential target for immunotherapy. Dendritic cells have receptors for glycosylated proteins and can bind to and internalise both Tn and sTn antigens through C-type lectin receptor (CLR) and sialic acid-binding immunoglobulin-type lectin (Siglec) receptors respectively[117,118]. This increases the chance of the immune system becoming activated against these antigens, after the DC has taken up, processed and presented it.

1.4.4 Phosphorylation

Phosphorylation is one of the most common post-translational modifications and is involved in the control of signalling cascades for cell growth and metabolism. It is often found to

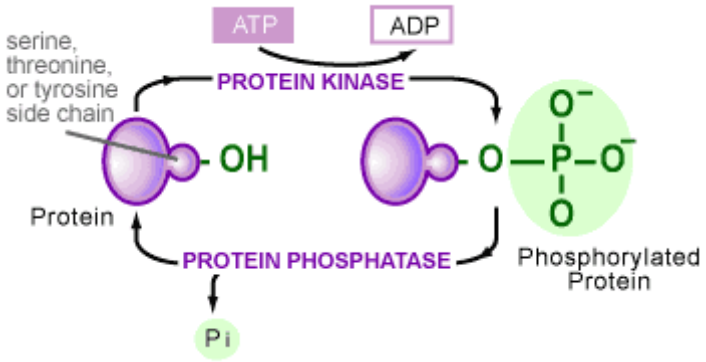

Figure 1.2 Schematic of the phosphorylation reaction on a serine/threonine/tyrosine side chain. [102]

be dysregulated in cancer and can contribute to a more malignant phenotype through dysregulated cell signalling.

Cancer cells have been shown to display phosphopeptides on the major histocompatibility complex (MHC) *in vivo*. In the case of MHCI, the phosphate moiety has been shown to increase the affinity for MHC due to the phosphate group forming stabilising interactions with the binding cleft[119]. The phosphate group remains solvent exposed when the peptide is bound to MHC, leaving it available for direct interaction with the T cell receptor (TCR). CD8 T cells selectively bind to phosphopeptide-MHC and do not cross react with the

unphosphorylated protein. Zarling et al analysed phosphopeptides presented on MHCI in melanoma, ovarian, and EBV transformed B lymhoblastoid cells.[120] 36 phosphopeptides were found bound to HLA-A*0201 from 35 independent proteins. Seven of these proteins are involved in cell cycle control (e.g. CDC25b), and 10 are involved in cell signalling (e.g. Tensin-3, IRS2, β-catenin, and BCAR3). The group then went on to show that cells expressing these proteins, phosphorylated them and presented on MHC (most likely through a proteasomal degradation pathway[121]), and this allowed for specific activation of T cells against the phosphopeptide bound to MHCI. As these proteins are integral to the malignant phenotype, they are ideal targets for immunotherapy, as they are more likely to be upregulated in cancer cells than normal cells.

Phosphorylated MART-1, a common phosphoprotein found in melanoma cells, has been studied by Li et al[122] bound to MHCII. In contrast to MHCI, the group showed that the phosphate group has no direct contacts to MHC and creates all of its contact through water-mediated hydrogen bonds. The phosphopeptide actually shows a lower affinity compared to its unphosphorylated counterpart, however this may not be the case for all phosphopeptides bound to MHCII. As with MHCI bound phosphopeptides, the phosphate moiety is solvent

exposed, suggesting direct interaction with CD4 TCR. Li et al showed that the phosphate group is essential for TCR recognition as the unphosphorylated protein does not induce a T cell response.

There have been a number of examples of phosphopeptide presentation on MHCII in cancer cells. As well as the above example for MART-1, MHCII has been shown to present 150 unique phosphopeptides on melanoma patient cell lines and EBV transformed B cell lines[123]. The peptides were sourced from 53 proteins, the majority of which are transmembrane proteins and involved in important cellular functions, increasing the chances of these proteins being expressed in a wide amount of cells within a tumour mass and between patients. Some phosphopeptides were presented by both melanoma cell lines (e.g. MART-1 and Tensin-3 peptides) and EBV transformed B cell lines (e.g. CD20 peptides), suggesting global therapeutic potential for these types of cancer and HLA type, with upregulated proteins.

1.4.5 Nitration

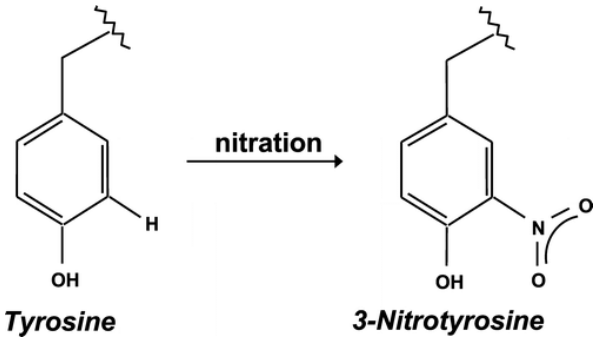

Figure 1.3 Schematic of the nitration reaction on tyrosine [124].

Tyrosine can become nitrated which is mediated by reactive nitrogen species which are often increased due to inflammation, one of the hallmarks of cancer. This type of modification has mostly been explored in lung cancer patients, where an increase in $3NO_2Tyr$ of has been seen on a number of proteins [125,126]. Under basal physiological condition, nitration is a widespread process, occurring on many proteins, tissues and organs, however its actual number of occurrences on total tyrosine residues remains relatively low[127]. Protein nitration is found to be significantly increased or found exclusively on certain proteins in lung cancer[126].

The induction of T cell responses to nitrated proteins has not been extensively looked at in tumour tissue specifically, however there have been multiple studies of T cell induction in other tissues. CD4 T cell activation has been seen in response to various nitrated proteins in mice and can lead to the

formation of autoreactive antibodies against the non-nitrated proteins due to the T cell help[128, 129, 130, 131, 132]. CD4 T cells remain tolerant to the non-nitrated protein. CD8 T cells have also been shown to become activated due to nitrated gp33 (a Lymphocytic Choriomeningitis virus glycoprotein), by both direct and indirect recognition[133]. The nitrate moiety is therefore able to either directly interact with the CD8 TCR or changes what part of the protein is exposed to TCR through changes in MHC binding.

Conversely, Galbrilovitch et al. showed that nitration of proteins was able to disrupt the TCR binding, and therefore is able to mask an immune response against cancer and cause tolerance[134]. This is another mechanism of immune evasion that could occur in tumours, leading to immune escape.

As nitration of proteins is increased in lung cancer, it is probable that nitrated proteins are presented on tumour cell MHC, and could potentially allow T cell responses against the tumour.

1.4.6 Deamidation

Deamidation involves the removal of an amide group from amino acids. This can convert asparagine to aspartic acid or glutamine to glutamic acid within a polypeptide chain. This process is closely linked to deglycosylation of N-linked glycans

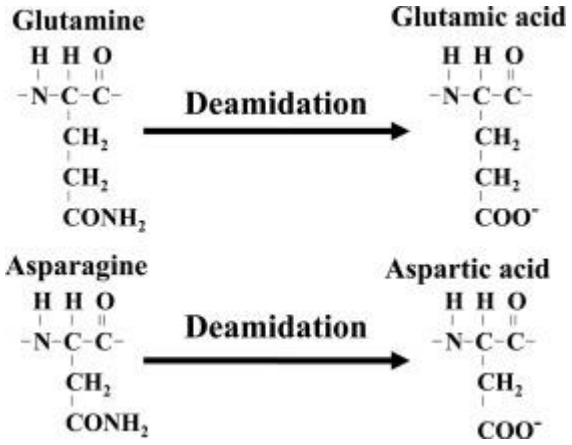

Figure 1.4 Schematic of the deamidation reaction on glutamine or asparagine[135].

as asparagine is often deamidated in conjunction with this. Protein deamidation has been shown to increase T cell reactivity to antigens and is the basis for celiac disease where gluten epitopes are deamidated, turning them into epitopes that can be recognised by the TCR in the context of MHC[136].

In cancer, deamidation has been shown to occur on tyrosinase in Melanoma patients, causing activation of CD8 T cells when the deamidated peptide is presented on MHCI[137, 138]. The change of asparagine to aspartic acid does not alter the affinity of the peptide for MHC, however the peptide with

aspartic acid is able to induce a CD8 response at 100 fold lower concentrations. This increased sensitization is accounted for by increased affinity of the TCR for the deamidated protein.

Dalet et al has shown that a tyrosinase CD8 antigen is made up of two deamidation and a reverse splicing event to give a melanoma specific epitope[138]. This, however, was also shown to occur in normal melanocytes as well, as PNGase and the proteasome, which are key in creating the epitope, are also found in normal melanocytes.

Deamidation can also alter the proteolysis of a protein by removing the target for asparagine endopeptidases[139]. This in turn can cause changes in available MHC epitopes due to the availability of differently processed tyrosinase peptides.

1.4.7 Cysteinylation

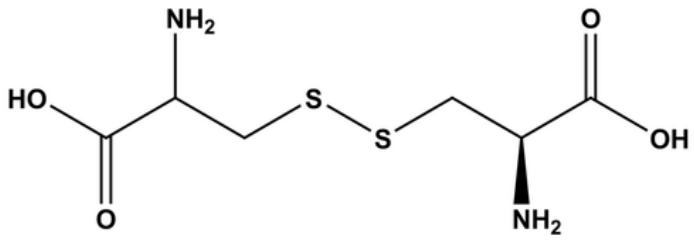

Figure 1.5 Diagram of a cystine dimer, joined by a disulphide bond[140].

Cysteine residues are susceptible to spontaneous cysteinylation where two residues interact to form a dimer.

The addition of cysteine causes conformational changes in the protein and therefore alter the potential binding domains for MHC or TCR. Cysteinylated proteins have been described to mask TCR contact sites in MHCI[141,142] and MHCII[143] presented peptides. Without the removal of PTM cysteine residues, T cells fail to be activated against the ligand. It is possible that peptides presented on cancer cells could become cysteinylated and therefore an effective response against tumour cell epitopes cannot be launched.

Cysteinylation potentially has roles in cancer. For example, heparinase, which is involved in the metastic capacity of cancer cells through its degradation of heparin sulphate, has been shown to be activated by cyteinylation[144]. However, due to the reasons stated above, cysteinylation in cancer is unlikely to be a source of neopepitopes.

1.4.8 Acetylation

Acetylation of histones is normally associated with the activation of genes, and there are cases of histone hyperacetylation being found in cancer, as is the case with H3K14 acetylation in oral cancers[145] and H3 and H4 hyperacetylation in hepatocellular carcinoma[146]. Acetylation of

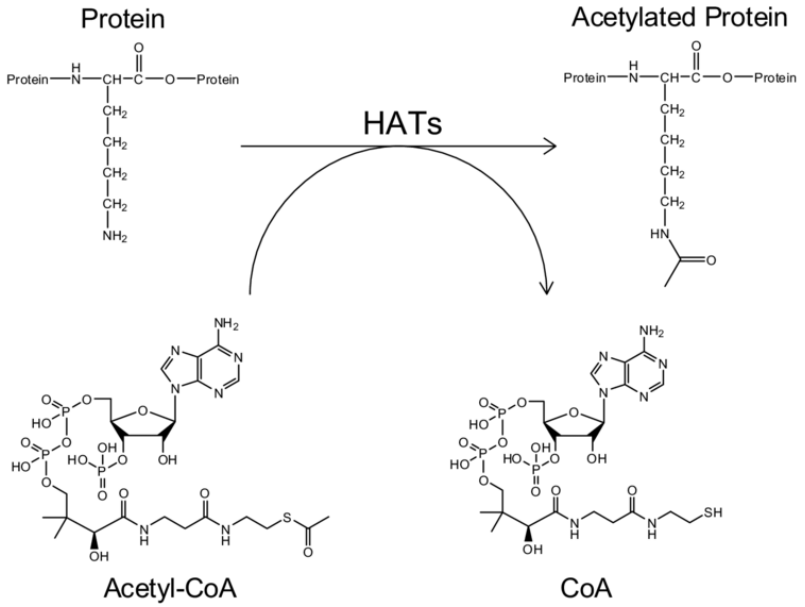

Figure 1.6 Schematic of the acetylation of proteins, catalysed by histone acetyl transferase[147].

proteins other than histones is also found to be increased in cancer cells, for example acetylated androgen receptor is found increased in prostate cancer cells[148]. Increased acetylation in cancerous cells tends to lead to an increased production or increased activity of proteins involved in cellular growth and metabolism.

Sun et al. showed that acetylated NAc-SL9, bound to MHCI, had its acetylserine residue solvent exposed which allowed it to interact with the TCR[149]. This is due to the unfavourable energetics of the N-terminal residue binding in pocket A, which is the MHC pocket in which its non-acetylated protein would be found to give the lowest Gibb's free energetic state. The acetylated protein is still stabilised in pocket A by new hydrogen bonds. The addition of the acetyl group also forces the Arg residue at position 62 of MHC into a position that is available for TCR recognition. In multiple studies, the N terminal acetylation of the protein lowers the thermodynamic stability of the protein-MHC complex[149,150]. TCR engagement is likely to occur at the now solvent exposed N-terminal, at the conformational change points of MHC (e.g. Arg62), and new points on the target protein that come about due to conformational changes after acetylation has occurred[149]. Although the modification weakens the binding to MHCI, acetylated peptides are still found bound to MHCI, demonstrating that the terminal NH_2 group is not essential for MHCI binding[151].

He at al. showed that the acetylated MBP bound to mouse I-A (MHCII) and that the acetylated N-terminal residue was required for MHC binding and induction of autoimmune T cells

causing encephalomyelitis. The acetyl residue stabilises the structure through hydrogen bonds with the MHC pocket[152].

In cancer, p53 can become acetylated at position 120. Proteins with this modification have been found to be presented on MHCII and induce a T cell response against tumour cells presenting this modified protein[153]. Although p53 and acetylated p53 are present in normal cells, both the upregulation of p53 and dysregulation of acetylation are both commonly found in cancer, therefore an immunotherapy against acetylated-p53 could be more effective against cancerous cells than normal cells.

1.4.9 Methylation

Overexpression of protein arginine methyl transferases (PRMTs) has been found in a variety of cancers. This leads to hypermethylation of histone and other proteins which can contribute towards tumorigenesis. Examples of increased methylation in cancer include methylation of H4R3 in prostate cancer, causing transcriptional activation[154,155], and methylation of the oestrogen receptor in breast cancer, contributing positively to the SRC-Pi3K-FAK signalling pathway

for cell proliferation and survival[156]. There is also evidence of protein being solely methylated in cancerous cells, giving a possible specific target for immunotherapies without the complication of self-tolerance[157].

The methylation of arginine masks the hydrogen bonding groups, changing the molecules shape. This can cause a

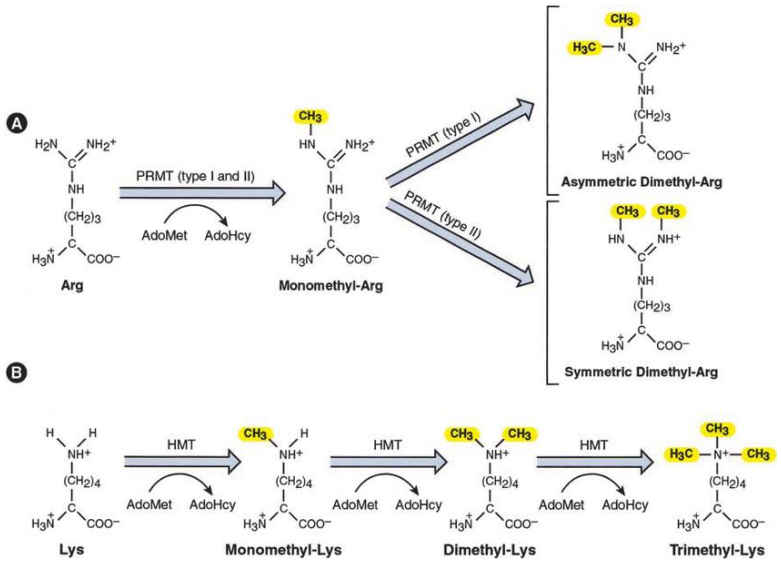

Figure 1.7 Schematic of the methylation of arginine and lysine[158].

change in whether the protein is able to bind to MHC and induce a T cell response, by allowing changes in protein-protein interactions.

HLA-B*07 has been shown to favourably bind di-methylated proteins. This is because it binds the same consensus sequences as arginine methyl transferase, and also is able to harbour the di-methyl groups at the P3 position[159]. On looking

at HLA-B*07 associated peptides in B lymphoblasts, Marino et al observed that a subset of proteins are known to be associated with cancer, for example NCoA-3 and CARM1[159]. These are therefore a possible immunotherapeutic avenue for cancers overexpressing these proteins. It remains to be seen whether T cells that are reactive to this self-peptide are present.

Jarmalavicius et al. showed that melanoma cells present a monomethylated GPS-2 which is capable of activating CD8 T cells to a much higher degree in cells taken from melanoma patients, than in healthy donors, suggesting the epitope is tumour specific and an appropriate target for anti-cancer immunotherapies[160].

1.4.10 Lipidation

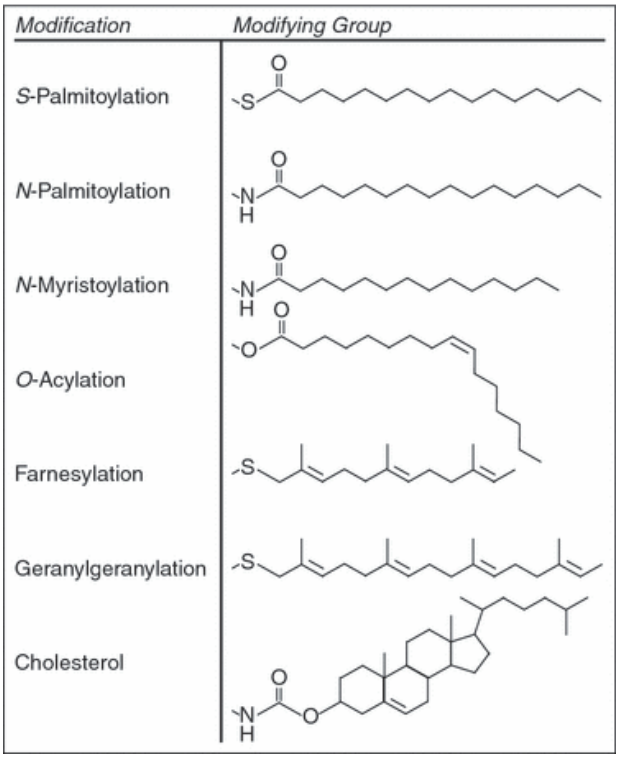

Figure 1.8 Structures of covalent lipid modifications[161].

Protein lipidation is increased in cancer cells due to upregulation of lipid metabolising enzymes and as a by-product of the upregulation of other metabolic pathways, such as increased glycolysis. Proteins that have been post-translationally lipidated, such as Ras, Wnt, and urokinase-type plasminogen activator-receptor (uPAR), contribute to the pathogenesis of cancer and the lipidation of them controls their cellular localisation and activation states[162].

N-myristoylated proteins have been shown to bind to the rhesus monkey Mamu-B*098 (MHCI) and presented to CD8 T cells to activate them against the lipidated protein[163, 164]. The

receptor has the usual A-F pockets however these are adapted to accommodate an uncharacteristically short (4/5mer), N-myristolated peptide. Pocket B is lined with hydrophobic residues and smaller amino acids, such as serine and threonine, to allow for the bulky hydrophobic lipid molecule. This is supported by Van der Waals forced from residues in the D pocket. The F pocket is small, with the side chains of tyrosine and glutamine pointing into the pocket, so that the peptide is limited to short lengths of amino acids (4/5mer).

Viral lipopeptides are known to be presented as an effective immune response against foreign pathogens. Multiple studies have also shown that lipidation of synthetic peptides for immunotherapy can improve an immune response, possible due to better antigen uptake and/or the lipid moiety acting as an adjuvant[165,166]. Stittelaar et al were able to show that palmitoylated peptides were able to induce a CTL response without uptake and processing, suggesting the palmitoy group was still present on the epitope, however the response was much less efficient and required high concentrations of peptide[167].

1.4.11 Splicing

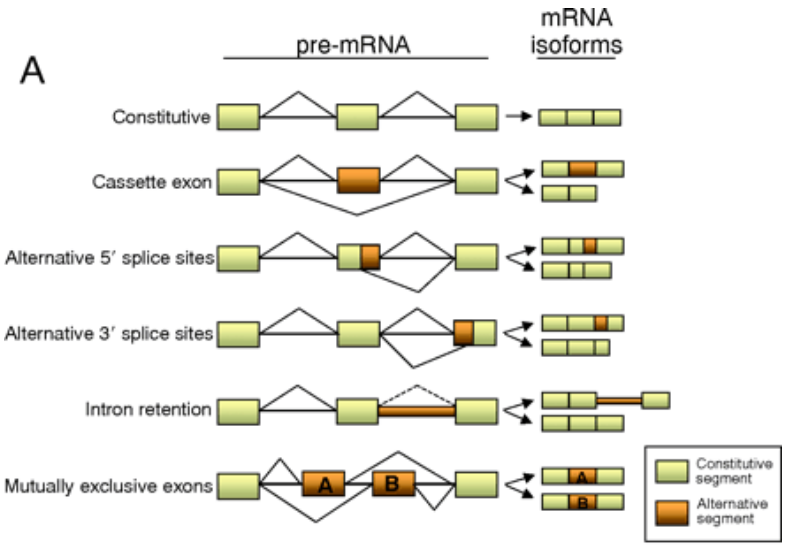

Figure 1.9 Possible splicing events found in cancer[168].

Changes in mRNA splicing occurs in cancer and can further the cancerous phenotype of cells. Upregulation/downregulation or mutation of splicing regulator proteins (including the spliceosome itself), mutation of splicing regulatory sequences, and changes in chromatin and transcriptional regulators can all effect the splicing of proteins and lead to the production of proteins that cause cancer progression[169].

In a study by Kahles et al, 8705 patients were analysed for alternative splicing events. 30% of tumours had an increased amount of alternative splicing events, giving on average 930 new splice junctions[170]. This gives a large amount of potential neoeptiopes where the new structure of the protein, due to

the changes in amino acid sequence, allows for better binding to MHC or TCR.

Evidence in alternative splicing potentially leading to T cell responses comes from a study showing epitopes presented on MHCI[171]. Splicing errors can lead to the retention of introns in the mRNA transcript, which then go on to be included in the translated protein. These neoepitopes can then bind to MHC and be presented on the cell surface. It remains to be demonstrated whether these peptides are capable of inducing a T cell response.

Mutations in cancerous cells can also create novel splice sites which can then allow for neoepitopes to be created[172]. T cell markers are shown to be increased in tumours with increased splice-site inducing mutations, however T cell reactivity against these neoantigens has not been tested.

1.4.12 Citrullination

Citrullination is a PTM where arginine is converted to citrulline by the removal of an imino group. This is catalysed by the peptidylarginine deiminase (PAD) enzyme, of which there are 5 isotypes: PAD 1-4 and 6. These enzymes have specific tissue localisation, which influences their targets. However there is evidence for extracellular PAD enzymes, suggesting

that their specificity is not only controlled by their locality. PAD1 is localised to epidermis and hair follicles[173]. PAD2 is more widely expressed and found in the central nervous system, pituitary gland, muscle, and uterus[174]. PAD3 is located in skin and hair follicles[175]. PAD4 is found in immune cells such neutrophils and monocytes[176]. Finally, PAD6 is found in embryonic stem cells and oocytes[177].

Arginine is strongly basic and is positively charged. The deiminisation of it removes this positive charge and reduces its potential to be protonated. This has strong consequences for protein folding and interactions due to ionic bonding. Arginine's charge and large size means that it is difficult to accommodate in MHC, whereas citrulline is much more easily accommodated due to its flexibility and polar characteristics, allowing for more favourable electrostatic interactions with the P4 binding pocket of MHCII[178].

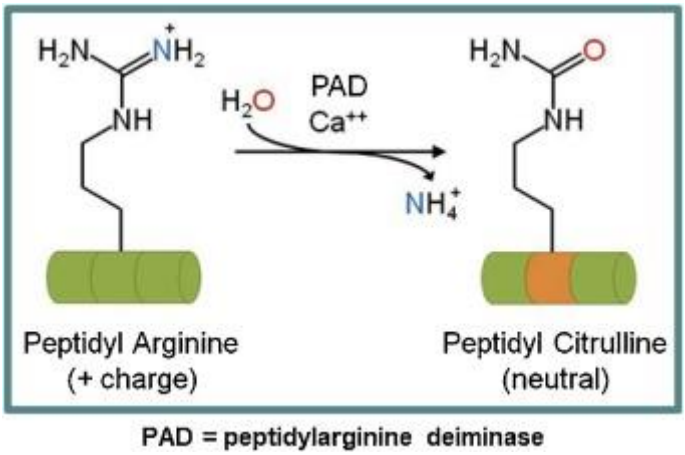

Figure 1.10 Schematic showing the citrullination of arginine, as catalysed by PAD[179].

Citrullinated epitopes are most heavily studied in the context of rheumatoid arthritis (RA), where autoreactive CD4 T-cells are activated against citrullinated epitopes in the synovium. Environmental stresses, such as smoking, are thought to cause an increase intracellular calcium to micromolar levels which allows for activation of PAD enzymes and hypercitrullination of proteins such as vimentin and collagen, amongst others[178,180]. CD4 T cells are activated against citrullinated proteins, which leads to activation of B cells, class switching, and the production of anti-citrullinated-peptide antibodies. This all leads to the further inflammation of the joint and a more severe disease phenotype.

PAD expression levels, most notably PAD2 and PAD4, are increased in multiple types of tumour[181]. It is thought that PAD is activated due to the high metabolic demands and low nutrient availability in the tumour mass. Increased PAD activity has led to the citrullination of proteins and their presentation on MHC. The loading of citrullinated peptides onto MHCII has also been implicated in the autophagy process[182], which is increased in cancer cells to aid in their survival and skew the cell away from the route of apoptosis.

Citrullinated proteins have already been shown to be good potential for immunotherapy targets in the work of Brentville et al. The group has shown that both citrullinated vimentin and α-enolase are produced by tumour cells and then presented on MHCII, most likely through the process of autophagy[183,184]. They were able to produce a robust CD4 T cell response against the citrullinated proteins, which was effective at clearing tumour cells. With Lee et al. identifying 209 proteins with possible citrullination sites, it is likely that there are other citrullinated proteins presented on cancer cells which can be utilised for immunotherapy[185]. We know that in the case of RA, citrullinated fibrinogen, filaggrin, and type II collagen are also presented on MHCII.

Molecularly, the citrullination of vimentin has been shown to increase the affinity for binding of vimentin to HLA-DRB1*0401 compared to its non-citrullinated counterpart[186], which is due to the preferential binding of citrulline to a conserved amino acid sequence in the P4 pocket of HLA, known as the shared epitope sequence[187]. It has also been shown that certain polymorphisms outside of the shared epitope sequence, such as the P1 and P9 pocket residues, are also important in the preferential binding of the citrullinated proteins[188]. HLA-DRB1 allele is genetically associated with rheumatoid arthritis because of this. Brentville et al went on to

show that citrullinated epitopes are not just limited to binding HLA-DRB1 in cancer[184], therefore the available pool of epitopes to target is increased for cancer therapies and we are less limited by the HLA alleles that patients express.

1.5 Physiological Role for Citrullination

The citrullination modification changes the ionic charge of amino acids and therefore has the potential to alter a proteins tertiary structure[189]. This can have consequences on a proteins function or interaction mechanics with other proteins. It has been shown in various substrates that, if more than 10% of arginines are citrullinated, the protein becomes denatured[189]. Arginine placement within a peptide effects the ability for PAD to catalyse citrullination with varying efficiencies. N-Arg-Asp-C sequences give the best efficiency and is therefore the most susceptible areas for this modificationc, as well as at beta turns[190]. PAD enzymes are activated by high calcium levels that may only be achieved in situations of high cellular stress or in terminal differentiation events. It is possible that citrullination could be used as a way to denature proteins and therefore turn off particular processes within the cell.

Physiologically, many cytoskeletal proteins are citrullinated, such as vimentin, glial fibrillary acidic protein, trichohyalin,

filllagrin, and cytokeratin. This has various functional consequences, such as the dissolution of vimentin networks during apoptosis[190], or allowing cytokeratin molecules to bind together by reducing their isoelectric point. Citrullination is also used in altering the charge of myelin basic protein, which allows for fine tuning of the myelin sheath[191]. Citrullination of MBP reduces the available basic residues for binding to the neuron, and so a less compact sheath is formed and neural plasticity is maintained. Citrullinated-MBP is reduced in adulthood as neural plasticity is reduced. MBP citrullination also alters tertiary structure so that sites that can be cleaved by metalloproteinases are exposed, increasing MBP degredation[191]. As citrullination effects the tertiary structure of proteins, it is possible citrullination is used to increase degredation of other proteins too.

PAD4 is found in the nucleus and is therefore available for gene regulation. In granulocytes[192], it antogonises oestrogen signalling by demethyliminating histones (removal of methyl-arginine resulting in citrullination)[193]. This acts as a negative feedback for the activation of genes through oestrogen signalling. It is possible that PAD4 also aids in the dissolution of the nucleus and its contents during apoptosis. The citrullination of nuclear lamina and histones leads to the

disintegration of the nuclear lamina and nucleosomes respectively[194,192].

PAD4 is also activated following innate immune activation due to infection[195]. In activated neutrophils, histone H3 is deiminated which allows for the decondensed chromatin required for NET formation, which is used in the effective clearance of pathogens. Neutrophils with PAD4 knocked down are unable to form NETs[196]. PAD4 is also involved in the pluripotency of cells which require chromosomes to be in a decondensed state. Citrullination of histone H1 allows chromatin decondensation for the transcription of pluripotency related genes during initial embryonic development and cell reprogramming in mice[197].

An additional immune process which is effected by citrullination is chemotaxis. Various chemokines have been found naturally citrullinated, with a reduction of activity with CXCL12[198], a reduction in chemoattractant abilities of CXCL10, CXCL11, and CXCR3[199], and mixed effects on CXCL8, depending on whether it occurs in the peritoneum or in circulation[200].

PAD4 has been found to have differing effects on p53 signalling in different studies. In one study, PAD4 activation was shown to be increased due to stress induced p53

activation, and that this led to multiple proteins being citrullinated, including nucleophosmin, inhibiting its signals for cell homeostasis and growth[201]. Alternatively some studies have shown that PAD4 represses p53 signalling by citrullinating the promotor of p53 target genes[202,203]. Additionally, PAD4 citrullinates inhibitor of growth 4 (ING4), inhibiting its interaction with p53, so that it can no longer enhance the action of p53[204].

PAD enzymes need millimolar concentrations of calcium to be activated, however this type of concentration is not found physiologically. It is therefore not entirely clear how PAD enzymes become activated when the cell membrane isn't compromised, leading to a high concentration of calcium[205].

1.6 Citrullination in Rheumatoid Arthritis

Citrullination has been implicated in the pathogenesis of anti-citrullinated protein antibody (ACPA)-positive rheumatoid arthritis, with approximately 60% of RA patients also having ACPAs, with the antibodies being found in circulation well before the onset of disease. The mechanism behind the development of ACPA-RA is not clear, however there have been a number of studies that show potential genetic and environmental associations that give clues to how this disease develops. As the formation of class switched antibodies is an

adaptive process, the immune system first needs to become activated against citrullinated epitopes. There is a strong dose-dependent association between smoking and ACPA-RA when paired with the genetic risk factor of the HLA-DRB1 allele[206]. HLA-DRB1 which contains the 'shared epitope' sequence within its binding cleft, which allows for good binding to citrullinated proteins. It is hypothesised that smoking causes the activation of PAD2 in the lungs, which causes the formation of citrullinated proteins. The smoke then also acts as an adjuvant to activate the immune system against the epitope[207]. It is possible that other forms of inflammation could also trigger anti-citrulline immunity, such as other pollutants or infection. Infection is especially of interest with pathogens that express PAD enzymes, such as Porphyromonas gingivalis[208].

After the development of ACPAs, it is thought that a second cause of inflammation occurs in the joint, causing the production of citrullinated epitopes. Neutrophils could be a source of PAD enzymes in the synovial fluid as they both secrete PAD2 and PAD4 on their cell membrane[209]. ACPAs then bind the new citrullinated proteins in the joint. This possibly leads to the formation of aggregates, causing a vicious cycle of increased inflammation and chronic disease. Citrullination in dense cultures of dendritic cells and the binding of ACPAs has

also shown to cause transdifferentiation of DCs into osteoclasts, possibly contributing to bone erosion in RA patients.

1.7 Citrullination in Cancer

PAD4 is overexpressed in a variety of tumours, including invasive carcinomas[210,211]. This translates to an increase in citrullination of various targets such as transcription factors, coregulators and histone proteins. Functionally, citrullination can act as an antagonist to methylation modifications, such as for the regulation of p53 target genes, leading to decreased cell cycle arrest and apoptosis[203]. PAD4 also citrullinates antithrombin, stopping its inhibition of thrombin, a protein used in tumour angiogenesis[212]. PAD4 activity and citrullination is therefore a survival mechanism for tumour cells.

PAD4 mediated citrullination is an intermediate step in mitogen signalling, such as EGF and oestrogen, in cancer[193]. This culminates in the activation of downstream target genes, such as c-fos, leading to cell survival and growth[213].

PAD2 is also overexpressed in multiple cancers, particularly in breast cancer. In a study by Katayama, both transcription and translation of PAD2 was found to be increased, and this correlated with citrullinated protein production.[214].

Furthermore, they showed that presentation on MHCII and antibody-citrullinated antigen complexes were shown to increase in patients.

Proteins such as α-enolase, HSP60, tubulin and cytokeratin proteins are also citrullinated in tumour cells[215]. These proteins are linked to the survival and metastases of cancers and therefore it is possible that citrullination alters the function of these proteins and contributes to malignancy.

1.8 Autophagy and Citrullinated Epitopes

Autophagy, is a process of "self-eating" where proteins within the cytoplasm are targeted for lysosomal degradation and the resulting amino acids recycled. Non-selective autophagy refers

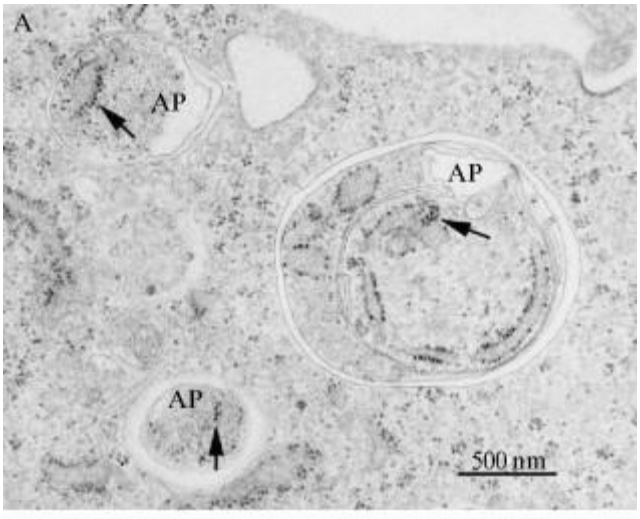

Figure 1.11 Electron micrograph of autophagosomes (AP). Arrows indicate engulfed ribosomes[216]

to engulfment of portions of the cytoplasm, allowing for non-specific degradation of the proteins/lipids/nucleotides

enclosed[217]. This is typically induced in response to stress signals such as starvation, for an intracellular source of new materials for biosynthesis. Selective autophagy is used to target species like protein aggregates, faulty or unrequired organelles, lipid droplets, or pathogens for degradation. Both are therefore involved in continued cellular homeostasis.

Autophagy initiation, in mammals, is mediated by two main complexes: unc-51-like autophagy activating kinase 1 (ULK1) complex, and class III PI 3-kinase complex I (PI3KC3–C1). Both complexes come together at a specialised area of the ER, called the omegasome. ULK1 complex is made up of ULK1, FAK family-interacting protein of 200 kDa (FIP2000), ATG13, and ATG101[218]. There are three requirements for autophagy activation via this complex which are: the activation of the kinase domain (ULK1), recruitment to the omegasome, and the ability of the complex to act as a scaffold for other proteins. ULK1 activation is through autophosphorylation at Thr180 which takes place due to autophagy induction and the co-assembly of the complex subunits[219–221]. Examples of autophagy activating signals include the inactivation of master energy signalling node, mTORC1 (due to starvation)[222], or the activation of AMPK (through energy depletion) and its subsequent phosphorylation of ULK1[223]. Recruitment of ULK1 complex to the omegasome is via the EAT domain on ULK1,

and ATG13 phosphorylation[224]. Further interactions occur with ULK1 and ATG13 LC3 Interacting Regions (LIR) which bind LC3[225]. Activated ULK1 phosphorylates BECN1, VPS34 (catalytic subunit), and AMBRA1 of the PI3KC3-C1 complex, activating it[226–228].

There has been some evidence that ULK1 complexes are delivered to the omegasome on recycling endosomes and hybrid pre-autophagosomal structures (HyPAS)[229]. Furthermore ATG9-containing vesicles from the trans-golgi network, and ATG16L1 containing vesicles from the plasma membrane converge at the recycling endosome, in addition to ULK1[230,231]. ULK1 and FIP200 then targets these vesicles to the ER by binding VAPA, VAPB, and Syntaxin 17 (STX17) on the ER membrane[232,233]. This can also deliver a potential source of membrane for the phagophore[234].

The PI3KC3-C1 complex is made up of VPS34 (the catalytic subunit), VPS15, ATG14L, and BECN1[235,236]. The main function of the complex is to phosphorylate phosphatidylinositol to give PI(3)P, which is essential for autophagy initiation. Translocation of the complex to the omegasome is mediated by ATG14L[237,238]. The NRBF2 protein facilitates dimerization of the complex for activation. This displaces Bcl-2 from VPS34, allowing for kinase activity[239]. The phosphorylation of AMBRA1

by ULK1 is proposed to release PI3KC3-C1 from microtubules[226]. A number of kinases converge pro-autophagic signalling on BECN1. As well as ULK1, BECN1 phosphorylation occurs through AMPK (in response to glucose starvation), MAPKAP2 (as a stress response) and death associated protein kinase (DAPK), to induce autophagy[240–242].

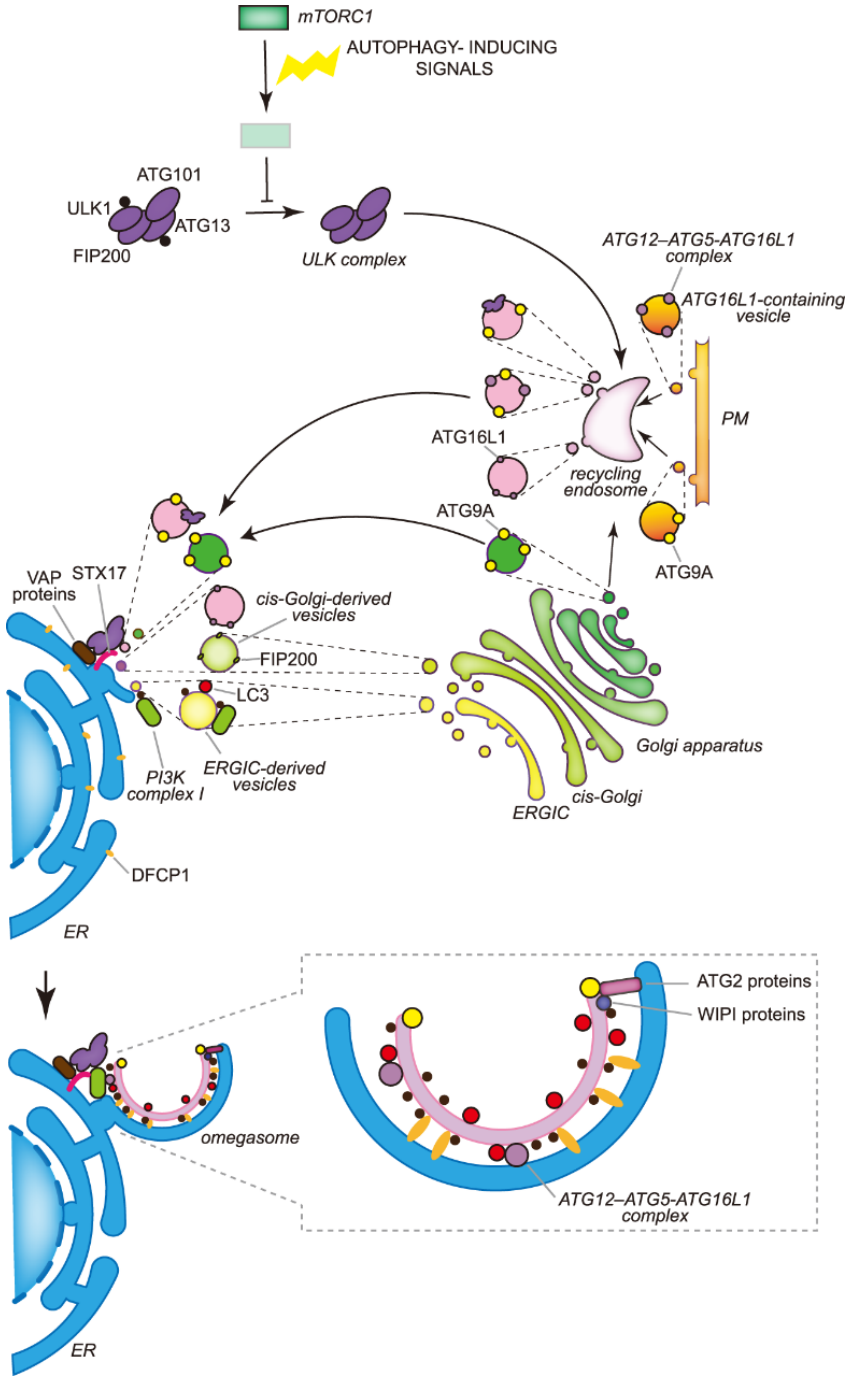

Figure 1.12 The molecular mechanism of autophagosome initiation in mammals. Autophagy inducing signals, such as starvation, leads to the inhibition of mTORC1, which allows for activation of the ULK1 complex, which includes proteins such as ULK1, FAK family-interacting protein of 200 kDa (FIP2000), ATG13, and ATG101. Activated ULK1 complex associates with the endosomal compartment and potentially aids in directing to the ER omegasome. Other autophagy associated proteins such as ATG12-ATG5-ATG16L1 complex and ATG9A can also be recruited at the endosomal compartment. Phagophore formation could be aided through the fusion of membranes from endosomal, golgi or ERGIC origins. Endosomes can be directed there through the binding of ULK1 to VAPA, VAPB or STX17. With the coming together of compartments and their accessory proteins, elongation of the phagophore can be initiated. Key in this step is the lipidation of LC3 if the formation of PtdIns3P by PI3K complex 1. PtdIns3P is also involved in WIPI and ATG2 recruitment which could help in the transfer of lipids from ER to the phagophore[243].

The production of PI3P allows for the binding of DFCP1, an ER membrane protein, to give close associate between the phagophore and the ER, creating the omegasome[244]. ATG2-WIPI complex binds PI3P and aids in the transfer of lipids from the ER to the phagosome[245]. ATG12-ATG5-ATG16L1 complex is then recruited to the omegasome via WIPI. LC3 is lipidated

by the covalent addition of phosphatidylethanolamine (PE). Upon autophagy activation, LC3-I is cleaved by ATG4B at Methionine 121, exposing Glycine 120 for lipidation. This is carried out by E1 enzyme ATG7, E2 enzyme ATG3, and E3 activity of ATG12–ATG5–ATG16L1 complex, converting LC3-I to LC3-II. Under basal conditions, LC3-I is localised to the cytoplasm. Although the exact contribution of LC3-II to membrane biogenesis is unknown, it is thought to be involved in membrane expansion[246]. ATG12–ATG5–ATG16L1, LC3-II, and actin filaments are all thought to be involved in the shaping of the nascent autophagosomal membrane[247–249].After membrane elongation, pore closure is the final step in autophagosome biogenesis. This is mediated by the endosomal sorting complexes required for transport (ESCRT) which catalyses membrane fission[250]. After closure, autophagosomes mature through the release of almost all ATG proteins and dephosphorylation of PI(3)P[251]. LC3-II (Atg8 in yeast) remains conjugated to the inner and outer membrane of the autophagosome. Throughout the autophagosome lifecycle, autophagosomes interact with different compartments. Electron microscopy studies have shown that early autophagosomes fuse with early endosomes, forming amphisomes[252]. Furthermore autophagosomes have been shown to fuse with multi-vesicular bodies (MVB)[253]. There is

evidence to show that fusion with other vesicular compartments is essential for the progression of autophagy[254]. Autophagosomes/amphisomes ultimately fuse with the lysosomes, form autolysosomes, to degrade the contents for recycling. Studies have also shown the a kiss-and-run fusion, where portions of the autophagosomal/lysosomal lumen are exchange but the vesicles never fuse[255]. Fusion of autophagosomes with endosomes/MVB/lysosomes involves the action of a number of proteins, including SNARE, tether,

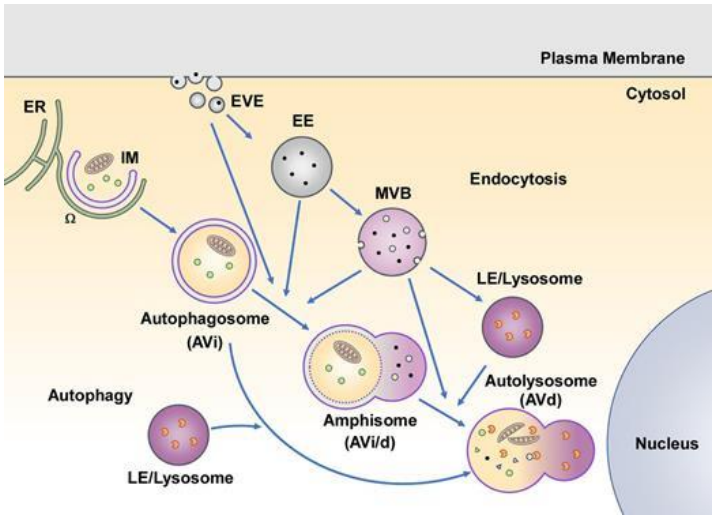

phosphoinositides, and RAB proteins[256].

Figure 1.13 Summary of the autophagosome lifecycle.

Autophagosomes are initially formed at specialist areas of the ER called the omegasome. A cup-like structure is formed (iM) and the membrane elongates until it is able to fuse together, enclosing a portion of cytoplasm and forming the mature autophagosome (AVi). Mature autophagosomes interact and fuse with the endolysosomal system, including early vesicular endocytic, endosomal (EE), multi-vesicular body (MVB), and lysosomal compartments, allowing for

the formation of amphisomes (AVid) and the transfer of contents. Autophagosomes can the ultimately fuse fully with the lysosome for form the autolysosome (Avd), allowing for the degradation of its contents. [256].

Autophagy is integral in many of the functions of DCs. It has been shown to be involved in cellular migration, activation, TLR signalling, cytokine production, antigen presentation, and maturation[257]. With regards to antigen presentation, autophagy is one of the pathways used to load, primarily MHC-II, but also MHC-I through cross-presentation of exogenous antigens[258,259]. MHC-II loading compartments were shown to fuse with autophagosomes in dendritic cells and autophagy was shown to enhance CD4 responses against cytosolic and nuclear antigens[258]. DCs capable of cross-presentation increased autophagy on activation, and autophagy increases the presentation of exogenous soluble antigen on MHC-I, possibly through LC3 associated phagocytosis (LAP). LAP involves the direct recruitment of LC3 and autophagy proteins to the phagosome, after Dectin-1 or TLR2 stimulation, and is a pathway for prolonged MHCII loading[260, 261]. It is also involved in the clearance of dead cells[262].

Not only can autophagy contribute to the availability of peptides for MHCII, but it can also contribute neoepitopes for binding MHCII. Ireland et al. showed that autophagy was responsible for the citrullination of endocytosed hen egg-white lysozyme (HEL) in murine DCs, which led to the presentation of citrullinated HEL and activation of T cells against it[182]. Furthermore, Sorice et al. showed that autophagy activation in human synoviocytes also led to the presentation of citrullinated vimentin, α-enolase and filaggrin[263]. More recently, Sugawara et al has also shown in synovial fibroblasts that autophagy induction and citrullinated vimentin production are linked, and that induction of autophagy leads to the presentation of citrullinated peptides on MHCII[264].

1.9 Citrullinated Epitopes as a Cancer Vaccine

Citrullinated epitopes fulfil a number of the requirements for an effective cancer peptide vaccine. The cit-epitope is not a neoepitope per se, however it is unlikely to be seen on normal cells in large quantities due to being a by-product of cellular stress and autophagy. Tumour cells are under stressed conditions, so is likely that their cells are going through autophagy to provide for this, and are producing cit-epitopes that will be presented on MHC.

Brentville et al. used CpG and MPLA as adjuvants *in vivo*, to provide activation of dendritic cells and upregulation of second messengers[183]. This successfully led to CD4 T cell activation against cit-epitopes of tumour cells, leading to IFNγ and granzyme secretion, and long term survival.

The avidity of citrullinated-vimentin on melanoma and lung cancer models is high enough to activate a CD4 cell response, which is promising for *in-vivo* vaccinations of melanoma or other cancers in human patients[183].

An interesting occurrence for using citrullinated-vimentin as a peptide vaccine is that it induced a cytotoxic response against tumour cells via CD4 cells, rather than the normal cytotoxic CD8 cells. The CD4 cells release IFNγ and granzyme in response to cit-vimentin, allowing for direct cytotoxicity, as well as skewing the immune environment of the tumour towards immune activation, and destroying tumour cells directly[183].

Citrullinated proteins are also an attractive cancer vaccine due to the absence of patient specificity as citrullinated proteins could be identical in multiple patients. This allows for a wider application, unlike the use of neoepitopes from mutation that are patient specific.

1.10 Hypothesis and Aims

The aim of this project was to develop a reliable method of enriching autophagosomes. Then to characterise them as a source of citrullinated epitopes, potentially giving an opportunity for the discovery of novel tumour associated citrullinated epitopes that may be used to as potential vaccine candidates.

The main hypotheses are as follows:

1. We hypothesised that autophagy is dysregulated in tumour cells. This can be used to enrich autophagosomes, a vescicular population that is transient in normal cells.

   The presence of autophagosomes in tumour cell lines and primary immune and fibroblast cells were examined in vitro by SDS PAGE and Western blot to observe any differences present in tumour cells. Autophagy modifying drugs were tested on tumour cells to identify dysregulated signalling.

2. We hypothesised that tumour autophagosomes are a source of citrullinated proteins

This was investigated examining protein content of autophagosomes and probing for citrulline residues using a phenyl glyoxal probe

3. We hypothesised that citrullinated proteins from autophagosomes can stimulate T cell response to citrullinated epitopes

   Autophagosomes were used in an ELISPOT assay with splenocytes from citrullinated peptide immunised mice to observe T cell activation. The assay was further developed for the uptake of autophagosomes by dendritic cells prior to stimulation of T cells using autophagosome primed DC.

2. Materials and Methods

2.1. Cell Culture and Reagents

B16F1 (ATCC-CRL-6323) were cultured in complete medium of RPMI 1640 (Gibco) supplemented with 10% Foetal Bovine Serum (FBS) (Sigma), at 37°C with 5% CO_2. MCF-7 (ATCC), T-47D (ATCC) and MBA MD 231 (ATCC) cells cultured in Dulbecco's Modified Eagle Medium (DMEM) (High glucose) (Sigma) + 10% FBS (Sigma) at 37°C with 5% CO_2. All cell lines were grown to 70-90% confluency before passaging 1:10.

Primary immune cells were isolated from heparinised whole blood which was layered onto a Histopaque-1077 (Sigma) gradient and centrifuged at 800g for 25 minutes. The PBMC layer was harvested and anti-CD14 magnetic beads (Miltenyi) were used for positive selection in a magnetic separation column (Miltenyi). If CD4 T cells were to be isolated, the negative flow through would be taken and anti-CD4 magnetic beads (Miltenyi) would be used for positive selection.

Monocyte and monocyte derived dendritic cells were cultured at a density of $1x10^6$ cells/ml in supplemental RPMI-1640 (Sigma) + 10% foetal calf serum (FCS, Sigma) + 1% sodium pyruvate (Sigma). Granulocyte-macrophage colony stimulating factor (GM-CSF, Peprotech UK) and interleukin-4

(Immunotools), at a concentration of 1000 IU/ml, were used to differentiate monocytes to dendritic cells. Cells were fed at day 3 or 4 with 50% of the previous amount of medium and cytokines, and harvested at day 5-7.

CD4 T cells were cultured in RPMI 1640 (Gibco) +1% L-glutamine (Sigma), 1% Penecillin/Streptomycin (P/S), 1% Non-essential amino acids (Sigma), 1% Sodium pyruvate (Sigma), 2% HEPES (Sigma) and 10% FBS (Gibco). T cells were supplemented with IL-2 (30U/ml) (made in house) after 24 hours rest. CD4 cells were activated with PMA (25ng/ml) (Sigma) and Ionomycin (0.5ug/ml) (Sigma).

Patient fibroblasts were cultured in Dulbecco's Modified Eagles Medium (DMEM) (High glucose) (Sigma) supplemented with 5% FBS, 1% P/S, hydrocortisone (1:2000), insulin (1:2000), transferrin (1:5000), and fibroblast growth factor (FGF) (1:10000).

HEK-293 cells were cultured in Dulbeccos Modified Eagle's Medium – High Glucose (Sigma) + 10% foetal bovine serum + 1% L-Glutamine and incubated at 37°C. Cells were grown to 70-90% confluence before passaging.

Autophagy was induced using rapamycin (Calbiochem), carboplatin (Sigma), and Thapsigargin (Sigma) at 800nM, 125µg/ml, and 150nM respectively. Autophagy induction by

starvation was carried out by culturing B16F1 cells in Earle's balanced salt solution[265]

Autophagy flux was inhibited using chloroquine (Sigma) at 50μM and autophagy initiation was inhibited using LY294002 at 10μM.

2.2 Antibodies

Primary antibodies used for western blot include anti-LC3B antibody (CST, 2775S, used at 1:1000), -PHB1 antibody (CST, 2426T, polyclonal, used at 1:1000), -EEA1 (C45B10) Rabbit mAb (CST, 3288T, monoclonal, used at 1:1000, -Rab7 (D95F2) XP Rabbit mAb (CST, 9367T, monoclonal, used at 1:1000, -Rab5A antibody (CST, 2143T, polyclonal, used at 1:1000), -Rab11 (D4F5) XP Rabbit mAb (CST, 5589T, monoclonal, used at 1:2000), -Calnexin (C5C9) Rabbit mAb (CST, 2679T, monoclonal, used at 1:1000), SQSTM!/p62 antibody (CST, 5114T, polyclonal, used at 1:1000)human LAMP2/CD107b antibody (R&D Systems, MAB6228-SP, monoclonal, used at 2μg/ml), -GM130 (R&D Systems, MAB81991-SP, monoclonal, clone 2059C, used at 1μg/ml), anti-citrullinated HSP70 (Eurogentec, monoclonal, stock concentration 1.5 mg/ml, used at 1:1000), anti-peptidyl-citrulline (Millipore, MABN328, monoclonal, clone F95, used at

1:500), and anti-β-actin (Sigma, A5441-100UL, monoclonal, clone AC-15, used at 1:5000).

Secondary antibodies used were IRDye® 680RD Donkey anti-Mouse IgG (H + L) (LI-COR, 926-68072, polyclonal, used at 1:20,000) and IRDye® 800CW Donkey anti-Rabbit IgG Secondary Antibody (LI-COR, 926-32213, polyclonal, used at 1:20,000

Primary antibodies for flow cytometry and confocal microscopy include Human LC3B Alexa Fluor® 647-conjugated Antibody (R&D, IC9390R, monoclonal, clone 1251A, used at 5µl/10^6 cells), anti-CD11c-FITC (Miltenyi, 130-110-700, clone REA754, used at 1:50), anti-CD80-PerCP/Cy5.5 (Miltenyi, 104722, monoclonal, clone 16-10A1, used at 1:50).

2.3 Generation of Bone Marrow Derived Dendritic Cells

Bone marrow cells were harvested from femurs and/or tibia of either naïve BALB/c (Charles River) (for BMDC optimisation experiments) or naïve HHDII/DP4 (EM:02221, European Mouse Mutant Archive) (for ELISPOT assays) mice. Bone marrow cells were cultured in complete medium (RPMI 1640, 10% FBS, 5% PenStrep, mGM-CSF (10ng/ml), mIL-4 (10ng/ml)) at 1x10^6 cells/ml for 7 days, replacing 75% and 50% of media on day 3 and day 6 respectively. Dendritic cells were selected for by harvesting lightly adherent cells on day 7

and used for subsequent experiments. The percentage of CD11c positive cells (dendritic cells) was determined by flow cytometry.

2.4 FITC-Dextran Assay

$1x10^5$ BMDC were cultured in complete media supplemented with Fluorescein isothiocyanate–dextran (MW 40,000) (Sigma) at 25µg/ml, for the indicated time points, at 37°C with 5% CO_2. Cells were cultured on ice as a negative control. After incubation, cells were washed with PBS, centrifuged down at 300g for 5 minutes, and fixed in 200µl 4% Formaldehyde. Fluorescence was detected using flow cytometry.

2.5 Peptides

Mixed cit-peptide vaccination included: alpha-enolase 241-260cit (VIGMDVAASEFF-cit-SGKYDLD), vimentin 28-49 cit (cit-SYVTTST-cit-TYSLGSAL-cit-PSTS) and vimentin 415-433cit peptides (LPNFSSLNL-cit-ETNLDSLPL), which were provided by Genescript as a lyophilised powder. Peptides were made up at 1mg/ml in PBS/20% DMSO and 25ug (25ul) of each peptide were mixed together with 5ug of CpG and 5ug MPLA (each at 1mg/ml in dH20), then made up to a final volume of 100ul with PBS for injection. The SNAPvax formulation uses 4nmol of each peptide/TLR7/8 adjuvant conjugate stock in DMSO,

mixed, and made up to 100ul with PBS, instead of CpG and MPLA.

2.6 In-vivo Immunisation of Peptides

All mouse studies were done under Home Office approved project licence (PP2706800) with ethical reviews by University of Nottingham and Nottingham Trent University Animal Welfare and Ethical Review boards (AWERB). HHDII/DP4 were dosed with a single injection of peptides with adjuvants or with peptides conjugated to TLR7/8 adjuvant (SNAPvax) via subcutaneous or intramuscular route on days 1, 8 and 15. Mice were culled on day 21 and splenocytes were harvested and used in further ELISPOT assays.

2.7 ELISpot Detection of IFNγ

Mabtech ELISpot kits were used to manufacturer's protocol. Briefly, IFNγ capture antibodies were coated onto 96-well Immobilin-P plate at a concentration of 10µg/ml and incubated overnight at 4°C. Plates were blocked for 1hr at room temperature using 100µl of complete medium (RPMI-1640 (Gibco) + 10% FBS (Gibco), HEPES (Sigma), L-Glutamine (Sigma), PenStrep (Sigma)) per well. Splenocytes from immunised HHDII/DP4 mice were harvested and seeded at $5x10^5$ cells/well in complete medium, plus 2-mercaptoethanol (1:250000, Sigma). Peptide, autophagosome or dendritic cell

preps were added to splenocytes and incubated together for 40 hours at 37°C, 5% CO_2. Following incubation and washing of wells with PBS 0.05% Tween-20 (Sigma), biotinylated anti-IFNγ was diluted in PBS (1:1000) and 50ul was added to each well. The detection antibody was incubated at room temperature for 2.5 hours. Following incubation the well plate was washed with PBS-T. Streptavidin Alkaline Phosphatase was added to each well in a 1:1000 dilution in PBS and incubated for 1.5 hours at room temperature. Wells were then washed with PBS-T and 50µl of development solution was added and left for approx. 35 minutes at room temp until colour developed. The reaction was stopped by washing plates, which were then left to dry at room temperature. Once dry, plates were read using an ELISpot plate reader (CTL Europe GmbH, Aalen, Germany).

2.8 Western Blot

Cells were lysed in RIPA buffer (Sigma) with protease inhibitor cocktail 2 (Sigma), protease inhibitor cocktail 3 (Sigma), benzonase (Sigma), and phosphatase inhibitor cocktail (Sigma) added in a 1/100 dilution. The lysis buffer was added at 100µl per 500,000 cells and incubated for 1 hour on ice with occasional agitation. Cells were then centrifuged at 14,000g for 15 minutes at 4°C. Soluble lysate was then decanted, leaving the insoluble pellet behind, and stored

frozen at -20°C. Protein concentration of each lysate was determined using the BCA assay kit (Sigma).

For 4-15% gradient polyacrylamide gels, the Bolt Bis-Tris gel system with MES running buffer (Thermofisher) was used to manufacturer's protocol. Proteins were transferred to 0.45µm nictrocullulose membrane (Amersham) and detected using LI-COR Odyssey Fc imaging system

Primary and secondary antibodies were diluted in 5% (w/v) Milk to manufacturer's dilutions. Bands were quantified using the LI-COR Odyssey Fc imaging system and Image Studio 4.0 software. Bands were normalised to β-actin loading control when possible.

2.9 Autophagosome Enrichment

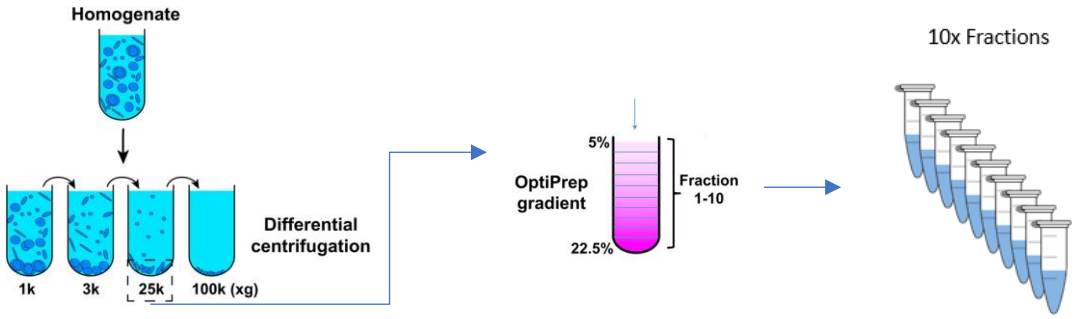

Figure 2.1 Summary of autophagosome enrichment/organelle fractionation. Tumour cell homogenate is differentially centrifuged. The 25k pellet is layered on top of an Optiprep gradient. Following

centrifugation ten 1ml fractions are harvested and taken forward for further investigation. Images are adapted from[266].

Tumour cell lines grown to 70-90% confluency in 4 or 8 T225 flasks, with chloroquine (50μM) conditioned media for final 3 hours. Cells were harvested and resuspended in 5ml or 10ml homogenisation media (250mM sucrose, 1mM EDTA, 20mM HEPES, pH7.4) respectively. Cells were homogenised on ice by 50 draws through 21G needle. Homogenate was differentially centrifuged at 1000, 3000, and 25000g. The 25000g pellet was resuspended in 2ml homogenisation media and layered onto an OptiPrep gradient consisting of 1.6ml 5, 10, 16, 24, and 30% OptiPrep. Homogenate was centrifuged at 100,000g for 17 hours. 10 times 1ml fractions were harvested. Fractions were centrifuged down and resuspended in PBS, or lysed in lysis buffer, for further experimentation.

For autophagosome enrichment from ex-vivo tumours, HHDII/DP4 mice were implanted on the right flank with $1x10^5$ B16/HHDII/iDP4 (B16FI MHC K/O, transfected with HHDII and IFNγ inducible DP4, as previously described[267]) cells in 100μl of DPBS on day 1. Group A mice received tumour only, whereas group B mice received peptides, as described above, intramuscularly at day 4, 11, and 18. Mice were terminated when tumour measured 15mm in any direction. Tumours were

harvested from mice and flash frozen in liquid nitrogen. After freezing, tumours were cryo-fractured using the BioPulverizer (Biospec Products) which was pre-chilled using liquid nitrogen. Cryo-fractured tumour from group A and B were combined and suspended in 20ml homogenisation media and processed as above.

2.10 Rhodamine-Phenylglyoxal (Rh-PG) Labelling of Citrulline for SDS-PAGE

Cell/organelle lysate was mixed with trichloroacetic acid (20% final concentration) and Rh-PG probe (Caymen biologicals) (80μM final concentration), and incubated at 37°C for 1hr. Reaction was quenched with free L-citrulline (Sigma) (100mM final) and incubated at 37°C for a further 30 minutes. Labelled samples were then cooled at -20°C for 30 minutes. Precipitated protein was pelleted at 18,000g for 30 minutes, at 4°C. The pellet was washed with cold acetone. Acetone was removed and the protein pellet was dried. Protein was resuspended in Tris-HCl (20mM, pH7.4) and used in SDS-PAGE/Western blot. Rhodamine was visualised using the 600nm channel of the LI-COR Odyssey XF.

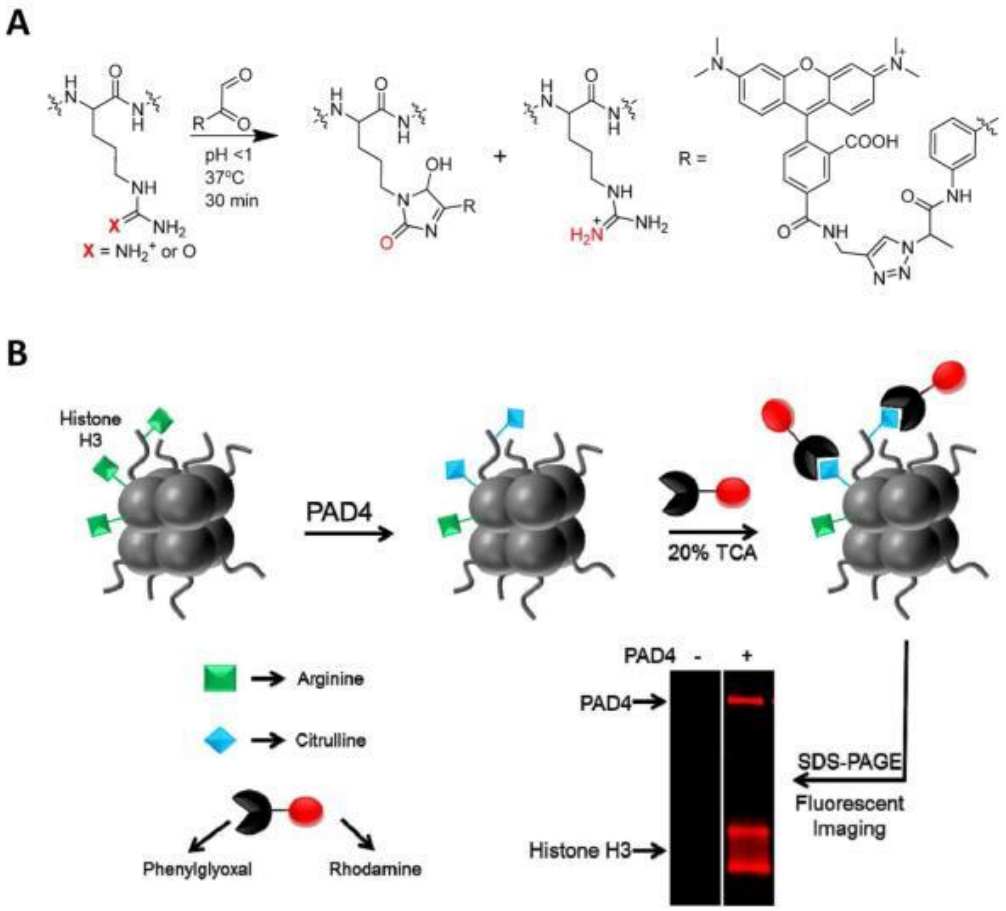

Figure 2.1 Mechanism of action of rhodamine-phenylglyoxal probe. A) Structural formula of the reaction between a citrulline residue and glyoxal of the rhodamine-phenylglyoxal probe. B) PAD4 converts arginine on Histone H3 to citrulline. The Rh-PG probe then reacts with citrulline under acidic conditions. Citrullinated residues are then visible through rhodamine fluorescence at 600nm, after protein separation by SDS-PAGE. Figure taken from Bicker et al[268]

2.11 Flow cytometry

For extracellular staining cells were incubated with fluorophore labelled antibodies at 4°C, at the manufacturers recommended dilution and incubation period, or for 30 minutes if not

specified. Following incubation cells were pelleted at 300g for 5 minutes and resuspended in 200µl 4% formaldehyde.

For intracellular staining, cells were fixed and permeabilised using Miltenyi staining buffer set, to manufacturer's instructions. Cells were incubated with primary antibody and/or hoescht staining for 1hr prior to washing steps.

Detection was carried out using Miltenyi MACSQuant10, or ImageStream for whole cells. Autophagosome enrichment preps were investigated using the Beckman Coulter MoFlo Astrios EQ flow cytometer.

Cells were firstly gated out of debris events using forward scatter vs side scatter plots. Doublet events were excluded using forward scatter (area) vs forward scatter (height). Imaging flow cytometers required gating for cells in focus by taking the gradient RMS high population. Positive fluorescence was determined using isotype control antibodies for the relevant fluorophore. The peak in fluorescence from isotype antibody was taken as the negative population.

Flow cytometry data was processed using FlowJo V10, IDEAS 6.2, or Kaluza Analysis 2.1.

2.12 Confocal Microscopy

Cells were seeded on glass cover slips in a 24-well plate. Following experimental conditions, cells were fixed in 4%

paraformaldehyde and permeabilised with 0.3% Triton X-100 (Sigma). Cells were then blocked with 3% bovine serum albumin (BSA) (Sigma) for 1hr at room temperature. Cells were then incubated with primary antibodies, diluted in blocking solution, for 1hr at room temperature. Cells were then washed three times in 1:1000 Triton X-100 and a further two times in PBS. Coverslips were then mounted onto a glass slide using Prolong Glass Antifade Mountant with NucBlue Stain (Thermofisher) and left to cure for at least 24 hours.

2.13 Electron Microscopy

Organelle samples were labelled with anti-LC3 antibody (Cell Signalling Technologies), and F(ab')2-Goat anti-Rabbit IgG (H+L) Secondary Antibody, Qdot 655 (Thermofisher) as per manufacturers protocol. Samples were incubated in succession in cacodylate buffer (Agar Scientific R1102), 2.5% glutaraldehyde, 2% OsO4 (Agar Scientific R1017) and 3% aqueous uranyl acetate (VWS EMS 100504-336). Post dehydration with 60%, 80%, 90%, 96% and 100% EtOH, samples were baked in Epon resin (Agar Scientific R1043) for ~48 hours. Sectioned samples were positioned on to 300 copper mesh grids supported with carbon film. The grids were imaged on the Tecnai TEM.

2.14 Statistical Analysis

All statistical analyses were performed on Graphpad Prism 7.04. Significant values were taken as $p \leq 0.05$.

3. Autophagy is Constitutively Active and Functional in a Variety of Tumour Cells

3.1 Introduction

Cancer cell lines are a useful model system for studying cancer, allowing for a potentially unlimited source of genetically identical cells to the origin cancer source. The advancement of omics technology has allowed for detailed comparisons between cancer cell lines and the tumours of which they are derived from. Studies in breast cancer[269] and ovarian cancer[270] show mutational concordance between cell lines and tumours, although slight differences in copy number alterations (CNAs) are seen. However, studies into head and neck[271] and colorectal cancer[272] cell lines showed large differences in mutations, where mutations were shown to be more abundant in cell lines. However, Barretina et al.[273] and Garnett et al.[274] achieved an impressive feat of genetically characterising 947 human cancer cell lines, establishing the Cancer Cell Line Encyclopaedia (CCLE), and showed that a strong genetic concordance between cell lines and primary tumours was found.

Despite genetic similarity between cell lines and tumours, a genetically identical model does not represent the diversification of cells found in a tumour mass *in-vivo*, as cells within the mass may be genetically dissimilar depending on

the mutations obtained through the cancers life cycle. Furthermore a 2D culture of identical cells does not consider the spatial effects of cells in 3D, where the conditions of cells within the centre of the mass may be very different from the outer edge, and does not include the effects of the extracellular matrix and other cell types (such as immune cells). For this reason, only specific questions may be asked of cancer cell lines, and further work may be needed in order to give a wider understanding in a more physiologically relevant environment.

Autophagy in tumour cells can have a paradoxical role. It can act as a tumour suppressor, particularly for the onset of cancer/early in tumour progression, through its role in degrading dysfunctional and/or aggregated proteins and organelles[275–280]. However once tumour cells are established, autophagy acts to protect against microenvironmental stresses such as nutrient starvation and hypoxia, clears damaged organelles, such as mitochondria, protects against genome instability, and reduces inflammation[281–284]. Many proteins involved in autophagy are shown to be upregulated, such as autophagy essential protein Beclin1 and Ras, and key signalling nodes, such as mTOR, are dysregulated[285–287].

As cancer cell lines are genetically similar to their primary tumour counterparts, similarly dysregulated autophagy could be expected. For example, Ras is shown to be upregulated in many cancer cell lines, as well as tumours, and has been shown to contribute to elevated autophagy in PDAC cell lines and PDAC tumours[285]. Furthermore resting cancer cell lines consistently show evidence of autophagy taking place. Compared to primary cells, cancer cell lines appear to show an increased level of autophagy at basal level, within the literature. Where primary cells are shown to have negligible LC3-II on western blot, the corresponding band is visible in cancer cell lines.

Rapamycin is most commonly used as an autophagy inducer. It was first isolated from *Streptomyces hygroscopicus* in 1975 and was investigated as an antibiotic and shown to inhibit *Candida albicans*, Microsporum gypseum and *Trichophyton granulosum*[288]. Since then, more has been elucidated of its mechanism of action. Rapamycin acts by forming a complex with 12-kDa FK506-binding protein (FKBP12)[289] which then acts as an allosteric inhibitor of serine-threonine protein kinase, mammalian TOR (mTOR). mTOR itself operates as part of a complex of proteins of which there are two distinct types: mTOR complex 1 (mTORC1) and mTORC2[290]. These complexes differ in their mTOR binding partners and signalling

cascades and is depicted in figure 3.1. Shared proteins between both complexes include mTOR, Dep domain-containing mTOR-interacting protein (Deptor)[291], mammalian lethal with sec-13 (mLST8)[292], and the Tti1/Tel2 complex[293]. mTORC1 specific proteins include regulatory associated protein of mTOR (Raptor)[294], and proline-rich Akt substrate of 40 kDa (PRAS40)[295] whereas mTORC2 specific proteins include rapamycin insensitive companion of mTOR (rictor)[290], protein observed with rictor 1/2 (protor 1/2)[296], stress-activated protein kinase-interacting protein 1 (mSIN1)[297]. mTORC1 is a signalling node, taking input from energy, oxygen, nutrient and growth factor status of the cell, to manage anabolic cell growth and proliferation through effector functions in protein, nucleotide and lipid synthesis, glutamine metabolism, glycolysis, and autophagy[298]. mTORC2 also functions as a signalling node but is involved in different processes such as cytoskeleton organisation and cell survival as a response to growth factor input[298]. Both complexes act differently in response to rapamycin treatment, with mTORC1 inhibited by acute and chronic exposure, whereas mTORC2 is only inhibited after chronic exposure[299]. Autophagy activation is caused through the inhibition of mTORC1 only. After rapamycin dimerises with FKBP12, the complex binds FKBP−rapamycin binding domain (FRB) on mTOR, blocking the

active site from binding substrate[289,300]. Under nutrient rich conditions, mTORC1 inhibits autophagy by phosphorylating Unc-51-like kinase 1 (ULK1) at Ser757, which inhibits it from forming a complex with focal adhesion kinase family interacting protein of 200KDa (FIP200) and ATG13, inhibiting the initiation of autophagy[301,302]. Blocking mTORC1 with rapamycin removes this inhibition and allows for the activation of autophagy. Rapamycin-FKBP12 cannot bind to mTORC2 however it is able to bind to free mTOR[303]. Upon mTORC2 complex turnover, rapamycin-FKBP12 bound mTOR will be unavailable for new complex formation and therefore the downstream effector functions of mTORC2 will be inhibited.

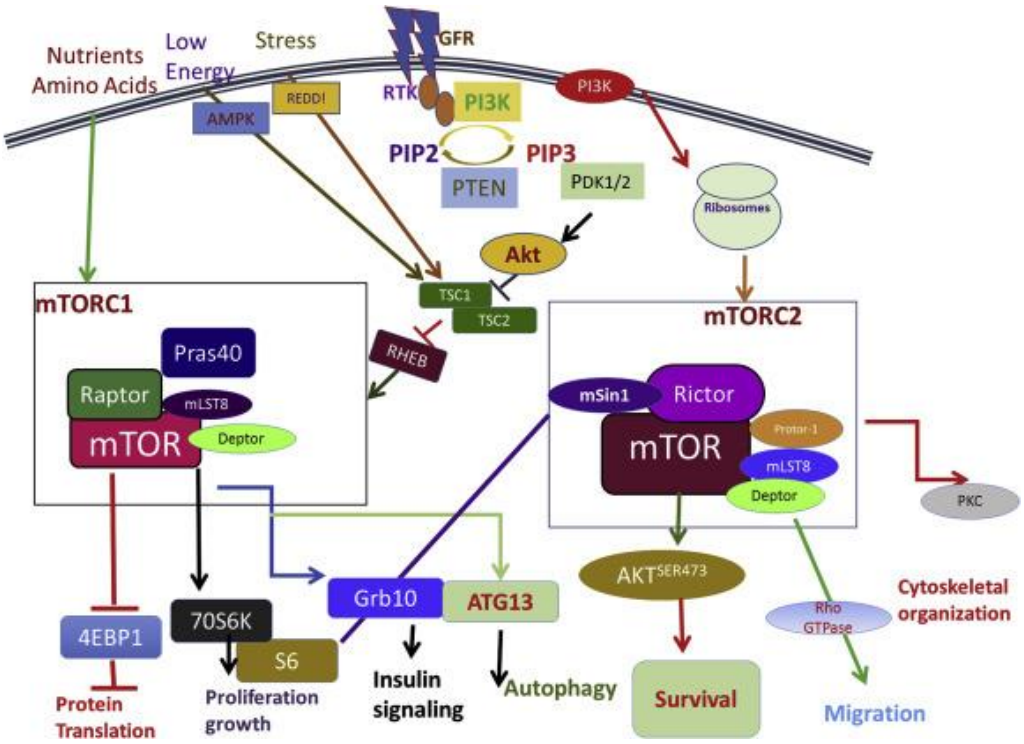

Figure 3.1 mTOR complexes mTORC1 and mTORC2 and an overview of their signalling pathways[304]

Chloroquine was discovered by Hans Andersag in 1934, as part of Bayer IG Farbenindustrie, to be used as an antimalarial drug[305,306]. It was however thought to be too toxic for consumption by humans and research using this drug was halted[307]. It wasn't until Chloroquine was re-discovered through a new drug pipeline, initially called SN-7619 and re-named to chloroquine, that work was continued on developing it as an anti-malrial drug[307]. The effects of chloroquine on autophagy were first identified by Trout et al. whom observed an increase in autophagic vacuoles in muscle cells on the addition of chloroquine[308]. This occurred due to the inhibition of fusion between the autophagosome and lysosome. Initially the mechanism of action was thought to be due to an increase in pH within the lysosome, as chloroquine is a basic compound[309,310]. However research by Mauthe et al. has shown that it is the fusion process between lysosome and autophagosome that is inhibited and lysosomal pH is, conversely, unchanged[309]. It was shown that chloroquine induced changes to the recruitment of SNAP29, a protein important to autophagyosome-lysosome fusion, to autophagosomes and that this may cause a decrease in fusion events. The blocking a lysosomal fusion causes accumulation of autophagosomes within the cell as autophagic flux is halted.

Pan-phosphoinositide-3-kinase (PI3K) inhibitors are often used to inhibit autophagy in the earlier stages of activation signalling. Class III PtdIns3K catalytic subunit PIK3C3/Vps34 is part of the PI3KC3-C1 complex, involved in the production PI(3)P for autophagy induction[311]. Class I PI3K is involved in mTORC1 activation through the PI3K-AKT-mTOR signalling pathway and inhibits autophagy. PI3K inhibitors also inhibit class II PI3K but this class is currently not proven to have a role in autophagy, although there is some evidence that it contributes PI(3)P for autophagy activation in yeast[312]. LY294002's was first shown to specifically inhibit PI3K while leaving other lipid kinases unaffected in 1994[313]. Its effect on autophagy was discovered by Blommaart et al. in 1997[314] whom showed that LY294002 inhibited PI3K activity and the formation of new autophagosomes. The assumption was made that this was due to PI3K involvement in membrane trafficking. Further research has shown that it is through the inhibition of Class III PtdIns3K and the subsequent disruption of complex formation involved in both autophagosome formation and maturation that causes autophagy inhibition[315]. However, as a pan-PI3K inhibitor, LY294002 inhibits both Class I PI3K, which is anti-autophagy, and class III PtdIns3K, which is pro-autophagy. Class I PI3K is activated in growth factor-rich conditions whereas class III PtdIns3K is activated

in growth factor low conditions, therefore the presence of growth factors has to be taken into account when using this inhibitor[316,317]. LY294002 used with high growth factor conditions may actually cause activation of autophagy through its inhibition of class I PI3K.

3.2 Aims

Although autophagy has been shown to be increased in cancer *in vivo*, it is important to determine whether this still applies to cell lines *in vitro*, to determine their applicability to be used as a model system. If we aim to capitalise on differences between autophagy in cancer and physiological cells, we are required to determine autophagy in native cells as well. This chapter explores the differences in autophagy between physiological cells and cancer cell lines, whether the autophagy is functional in these cells, and characterise changes in autophagy when cells are exposed to stress that could occur in the tumour microenvironment.

3.3 Results

3.3.1 Autophagy in Primary Cells

In order for the epitope products of tumour autophagy to be targeted by the immune system, there should ideally be a substantial difference between autophagy in normal and malignant cells. Therefore, we tested the hypothesis that such differences are present between primary, non-transformed, immune and fibroblast cells and tumour cell lines. The content of autophagosomes within primary cells was measured at basal levels and following activation of autophagy by rapamycin. Chloroquine was used to block autophagic flux.

Expression of LC3-II was undetectable in resting monocytes (fig 3.2.A). However, when degradation of autophagosomes was blocked by exposure to chloroquine LC3-II expression was detected. When normalised to the β-actin loading control, autophagy is negligible in these cells and therefore only occurs in very small amounts. Similarly low levels of autophagy were characteristic of other resting primary cells including CD4+ T-cells (fig 3.2.B), monocyte derived dendritic cells (moDC) (fig 3.2.C), and fibroblasts isolated from within and outside the tumour (fig 3.2.D). Nevertheless, despite their basal low level of autophagy, these cells were responsive as LC3-II expression increased upon addition of chloroquine. This

suggested autophagy flux was occurring within these cells, however not at the levels witnessed in tumour cell lines.

Minimal levels of LC3-I or LC3-II species were identified in resting CD4 T cells. A modest increase in LC3-II expression was observed upon the addition of chloroquine. Upon activation of T cells by TLR agonist, LC3-I levels were elevated. Furthermore, the expression of LC3-II was further enhanced by rapamycin/chloroquine as noted with other primary cells.

Minimal LC3-II was detected in resting moDC, suggesting low levels of basal autophagy. Similar to observations in monocytes, LC3-II expression increased following the addition of chloroquine, and this was accompanied by a corresponding decrease in LC3-I.

Figure 3.2

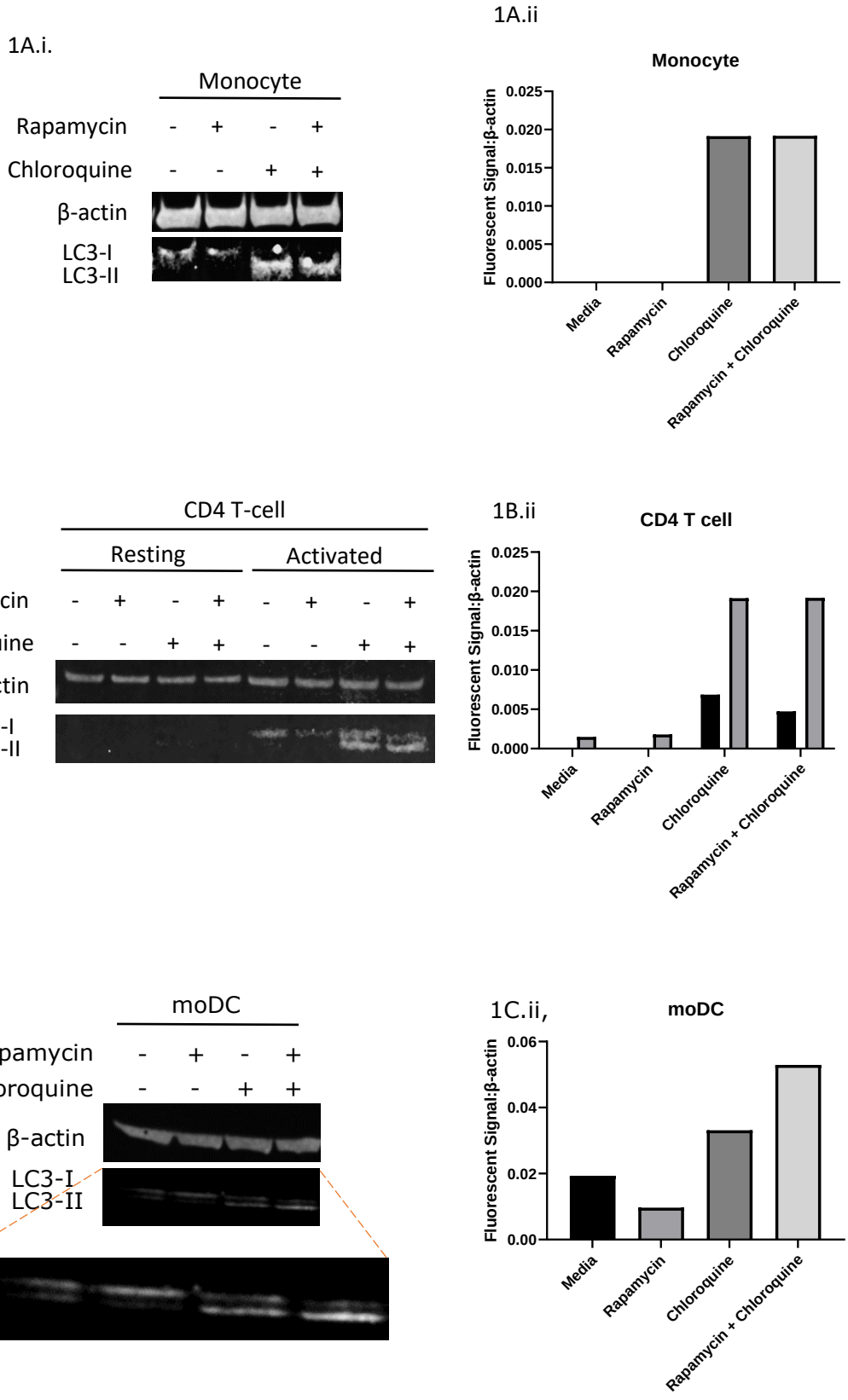
1A.i.
Monocyte
Rapamycin - + - +
Chloroquine - - + +
β-actin
LC3-I
LC3-II
1A.ii
Monocyte
Fluorescent Signal:β-actin
0.025
0.020
0.015
0.010
0.005
0.000
Media
Rapamycin
Chloroquine
Rapamycin + Chloroquine
1B.i.
CD4 T-cell
Resting
Activated
Rapamycin - + - + - + - +
Chloroquine - - + + - - + +
β-actin
LC3-I
LC3-II
1B.ii
CD4 T cell
Fluorescent Signal:β-actin
0.025
0.020
0.015
0.010
0.005
0.000
Media
Rapamycin
Chloroquine
Rapamycin + Chloroquine
Resting
Activated
1C.i
moDC
Rapamycin - + - +
Chloroquine - - + +
β-actin
LC3-I
LC3-II
1C.ii,
moDC
Fluorescent Signal:β-actin
0.06
0.04
0.02
0.00
Media
Rapamycin
Chloroquine
Rapamycin + Chloroquine

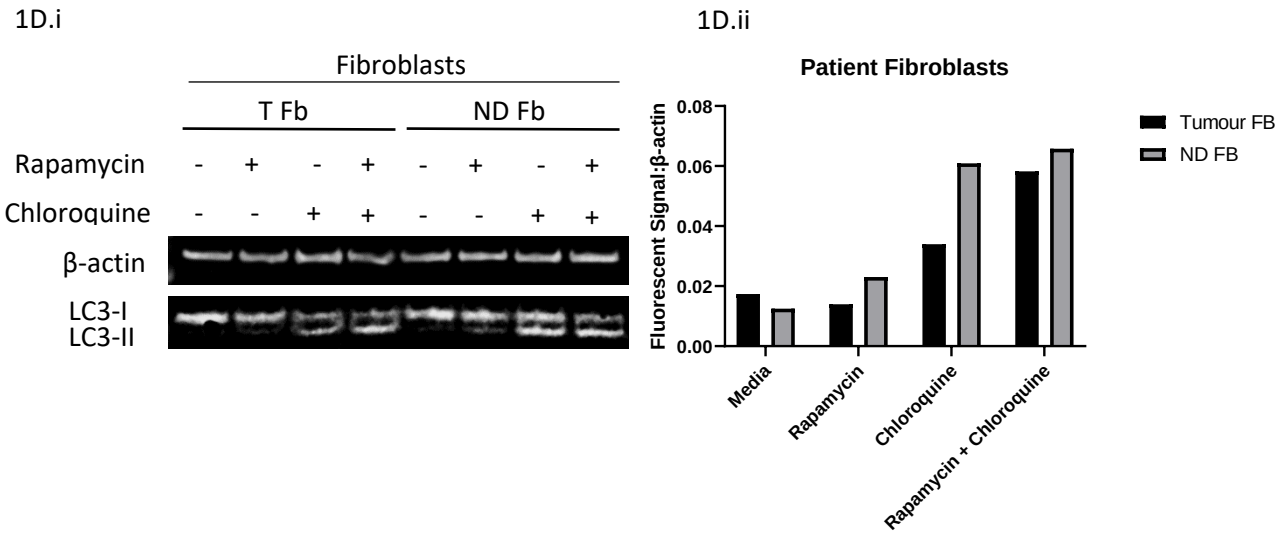

Figure 3.2. Autophagy in resting and activated primary cells. Cells were rested or activated with a combination of chloroquine and rapamycin prior to extraction of protein content. Representative western blots show autophagosome levels as inferred by the level of LC3-II expression in monocytes (Ai-ii), CD4 T-cells (Bi-ii), and monocyte-derived dendritic cells (Ci-ii) isolated from the blood of healthy donors, and patient fibroblast cells (Di-ii) from within the tumour (T FB) and outside the tumour mass (ND Fb). β-actin was used as loading control and normalised signal is shown in the corresponding bar charts. n=1

3.3.2 Autophagy in Tumour Cell Lines

Higher LC3-II signals were observed across all tumour cell lines and conditions, compared to primary immune and fibroblast cells. B16F1 (fig 3.3.Ai), MCF-7 (fig 3.3.Aii), T47D (fig 3.3.Aiii) and MDA MB 231 (fig 3.3.Aiv) cells showed high LC3-II levels in basal conditions, which was further exacerbated on the addition of chloroquine. This was shown to be significant in MCF-7 cells ($p=0.0151$). Treatment with rapamycin did not cause any detectable increase in LC3-II, and in the case of B16F1 and MCF-7 cells, a decrease in LC3-II was observed (figure 3.3.Ai, Aii, Bi, Bii). For MCF-7, this decrease was shown to be significant ($p=0.0109$). The expression of p62 (a substrate of autophagy) was determined in B16F1 and MCF-7 cells and found to be consistent across all conditions, although expression was higher in B16F1 cells compared to MCF-7.

When comparing LC3-II levels between cancer cell lines and primary immune cells grown in complete media (figure 3.3.D), a marked difference can be seen, with an elevated level of LC3-II (and therefore autophagosomes) within cancer cells. These difference were shown to be statistically significant ($p=0.0244$).

Figure 3.3

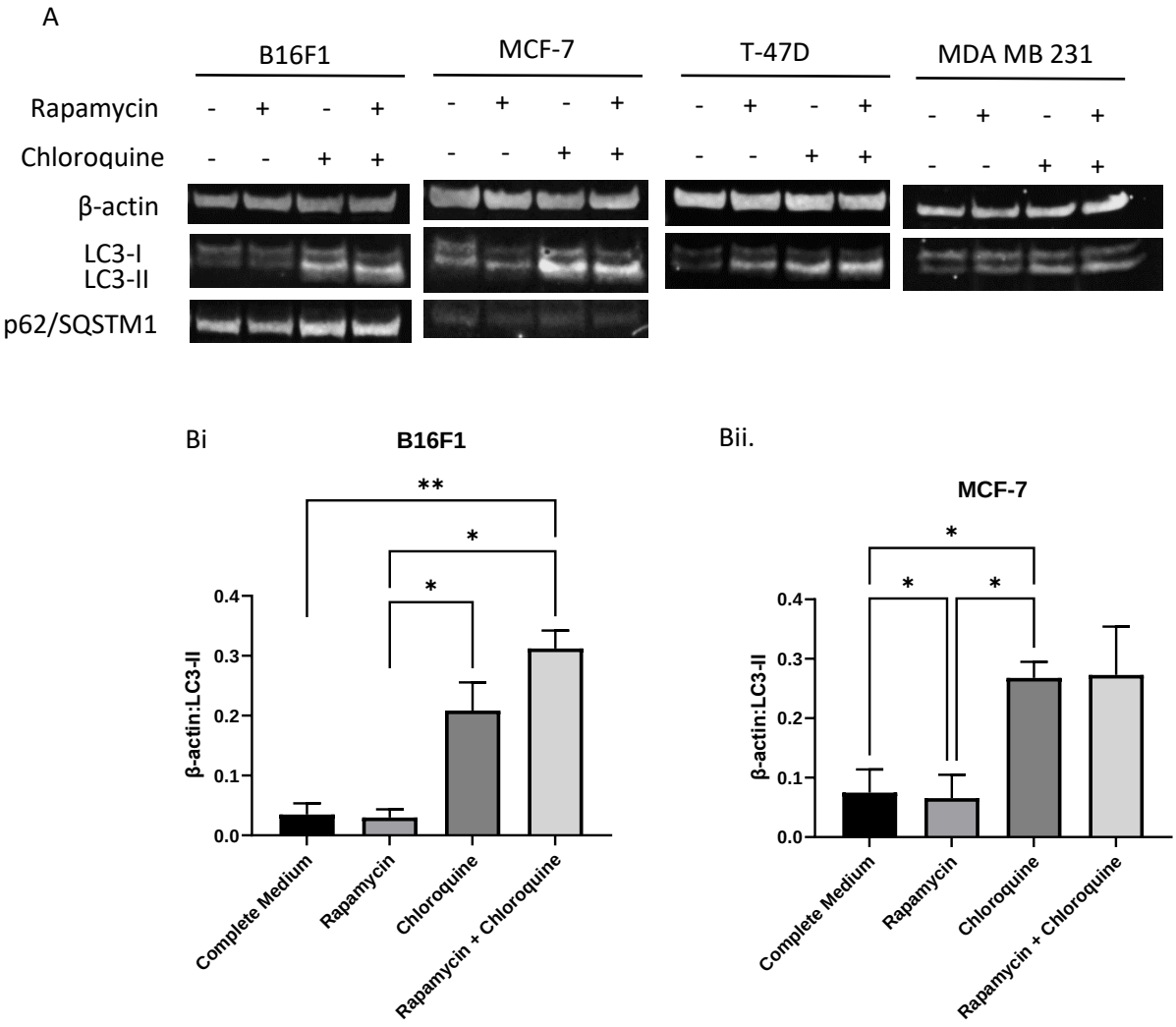
A
B16F1
MCF-7
T-47D
MDA MB 231
Rapamycin
Chloroquine
β-actin
LC3-I
LC3-II
p62/SQSTM1
Bi
B16F1
β-actin:LC3-II
Complete Medium
Rapamycin
Chloroquine
Rapamycin + Chloroquine
Bii.
MCF-7
D.
Basal LC3-II Signal
Basal LC3-II Signal [Normalised to actin]
Primary cells
Cancer cell line
P value
0.0244

Figure 3.3. The effect of rapamycin and chloroquine on autophagy in cancer cell lines. A) Western blot showing the level of LC3-II in B16F1, MCF-7, T-47D and MDA MB 231 cell lines. Fig B shows LC3-II signals normalised to β-actin control in B16F1 cells (Bi) and MCF-7 (Bii) (n=3, independent experiments of differing cell passage numbers). Statistics were performed using RM one way ANOVA, with Geisser-Greenhouse correction, and Tukey's multiple comparisons. D) Graphical representation of normalised LC3-II expression, as determined by western blot, in resting cells of both primary cells (monocyte derived dendritic cell (n=1) and macrophages (n=2), patient fibroblasts(n=2), monocytes (n=2), and CD4 T cells (n=1)) (total n=8) and cancer cell lines (B16 (n=5), MCF-7 (n=4), T47D (n=1) and MDA MB 231 (n=1)) (total n=11) Statistics were performed using an unpaired T-test. p=0.0244. Bars indicate mean expression and standard-deviation is shown by error bars. * $p<0.05$ **$p<0.01$.

3.3.3 Intracellular staining for LC3-II in cancer cell lines

Having established that long term cultured cells display higher levels of LC3-II than primary cells, the distribution of LC3+ vesicles in a selection of long-term cell lines (B16, MCF7) was investigated. Using confocal microscopy LC3-II vesicles were observed in the cytoplasm of resting cells (Fig 3.4.Ai). LC3-II+ vesicles were evident in most resting cells. Upon treatment with rapamycin/chloroquine there was no marked evidence of altered number of LC3-II+ vesicles, nor of their intracellular distribution (Fig 3.4.Aii).

Intracellular autophagy in B16F1 cells was further characterised using imaging flow cytometry, allowing analysis of LC3 presence both globally, and on an individual cellular level. Figure 3.4.B shows representative images of stained cells from each culture condition. Background levels of fluorescence are high, most likely due to binding of cytoplasmic LC3-I. However, when cells are exposed to chloroquine, an accumulation of fluorescent extranuclear puncta is seen.

Fluorescent intensities of anti-LC3-AF647 antibodies in each population (figure 3.4.C, table 1) showed a modest LC3 expression for cells grown in complete media and rapamycin

conditioned media. This was drastically increased in cells exposed to chloroquine conditioned media.

Autophagosomes can be identified as extranuclear concentrated spots of fluorescence within the cell. Spot counts for autophagosome puncta (figure 3.4.D, table 1) showed low numbers in complete and rapamycin conditioned media, with a median of 0 in both. Cells grown in complete or rapamycin conditioned medium have a spot count range of 0-6, showing that autophagosome puncta was occasionally present but in low numbers.

The spot count was increased with exposure to chloroquine to a median count of 2. Combined treatment with rapamycin and chloroquine increased the median spot count to 4. A larger effect on spot count range was seen following chloroquine treatment, increasing the range to 0-14 spots, which was slightly increased to 0-20 upon the addition of rapamycin.

Figure 3.4

Ai. Complete medium

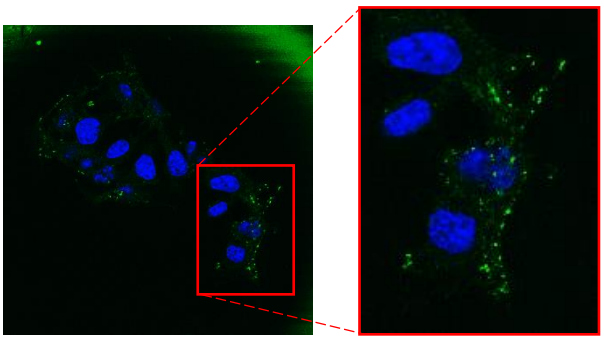

Aii. Rapamycin and chloroquine conditioned medium

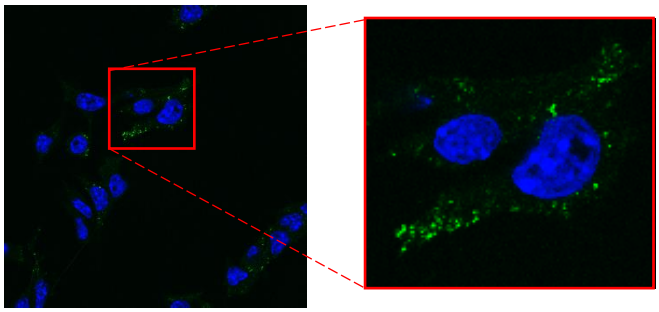

B.

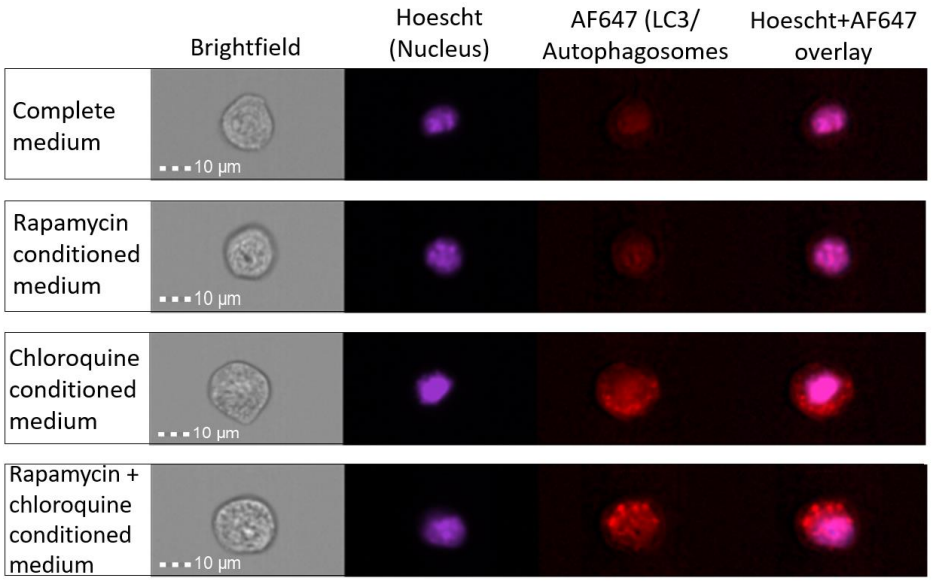

C.

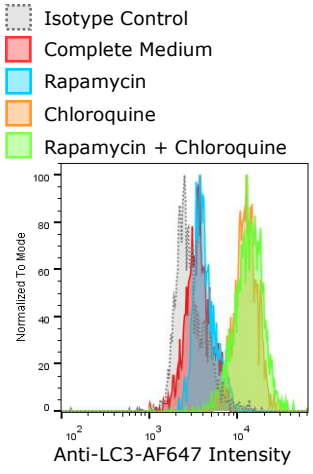

D.

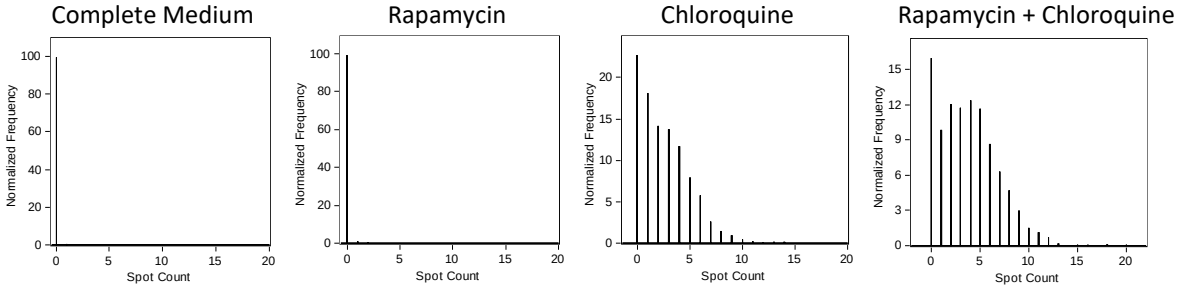

	Isotype control	Complete medium	Rapamycin	Chloroquine	Rapamycin + Chloroquine
Median Spot count		0	0	2	4
Spot count range		0-4	0-6	0-14	0-20
MFI	2674	3499	3970	12131	13273

Table 1. Spot count and median fluorescence intensity values for each experimental condition for B16F1 cells.

Figure 3.4 Intracellular labelling of autophagosomes in B16F1 cells. A) Confocal images of B16F1 cells under 630X magnification. Cells were either grown in complete medium (Ai) or medium conditioned with rapamycin and chloroquine (Aii). Anti-LC3 AlexaFluor647 labelling for autophagosomes and a Hoescht stain mountant labelling the nucleus (blue). B-D) ImageStream analysis of B16F1 cells labelled with hoescht (nucleus) and anti-LC3-AF647 (autophagosome) after 6hr treatment with rapamycin and/or chloroquine conditioned media vs complete medium control. (B) Representative images of cells grown in each condition. (C) Histogram overlay of AF647 fluorescent intensities in each condition. (D) Spot count histogram for AF647 puncta

3.3.4 Changes in B16F1 Autophagy over time in response to autophagy inducers

To further analyse a tumour cells ability to carry out autophagy and whether tumour cells autophagy is functional, LC3-II levels were investigated in tumour cells in response to various autophagy inducers that are commonly experienced by tumour cells in patients.

B16F1 cells were cultured in Earle's Balanced Salt Solution to starve them from amino acids and serum. Resting cells expressed detectable levels of both LC3I and LC3II although LC3I was the dominant species (Figure 3.5). When cells were starved of nutrients for 2 hours the basal level of both LC3I and LC3II decreased. After 4 hours of starvation LC3 was barely detectable. Prevention of autophagosome-lysosome fusion by the addition of chloroquine to starved cells resulted in a marked accumulation of LC3II that was evident after 2 hours. Cells grown in the presence of rapamycin conditioned media alone showed consistent levels of both LC3-I and LC3-II species across all time points.

B16F1 cells were grown in the presence of carboplatin, a commonly used chemotherapy in the treatment of cancer, to confirm whether autophagy is still functional when cells are treated with this drug. The presence of autophagosomes were

detected using western blot (figure 3.5.B). Again, LC3-I was the dominant species at basal levels. LC3-I levels remained consistent across all conditions until the 24hr time point, where it was found to be increased almost two-fold in cells grown in complete medium and in chloroquine and carboplatin conditioned medium. LC3-II levels stayed consistent throughout all conditions except cells grown in carboplatin and chloroquine conditioned media, which saw an 8-fold increase over 2 hours, rising to a 71-fold increase over 24 hours.

Figure 3.5

A.i.

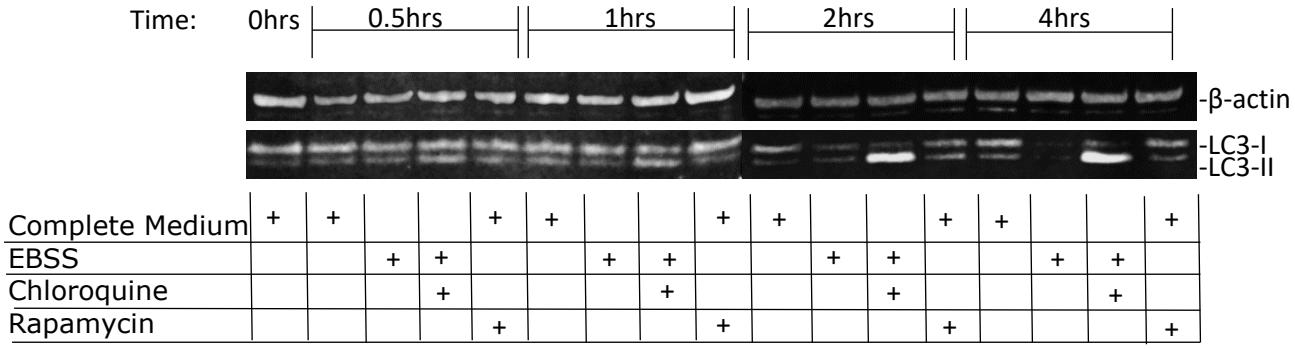

A.ii.

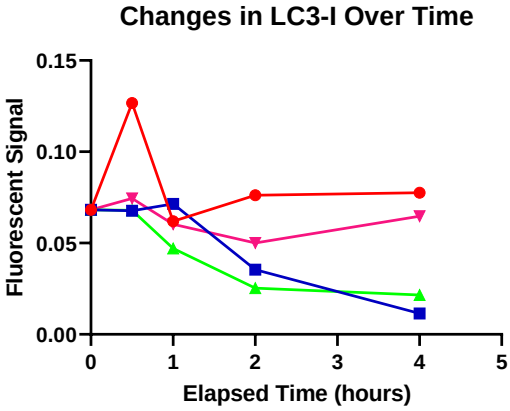

A.iii.

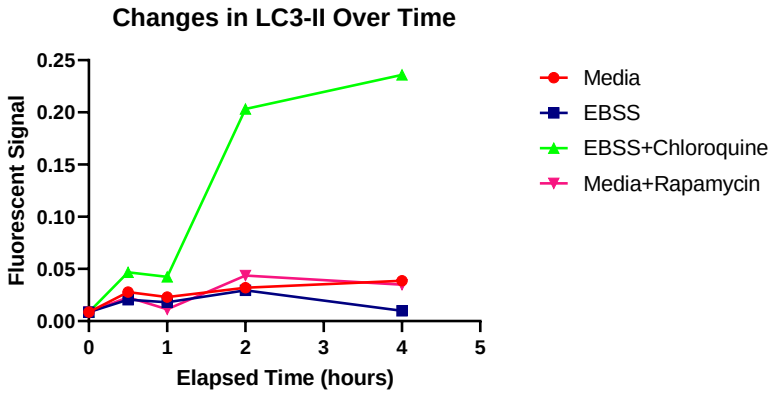

Bi.

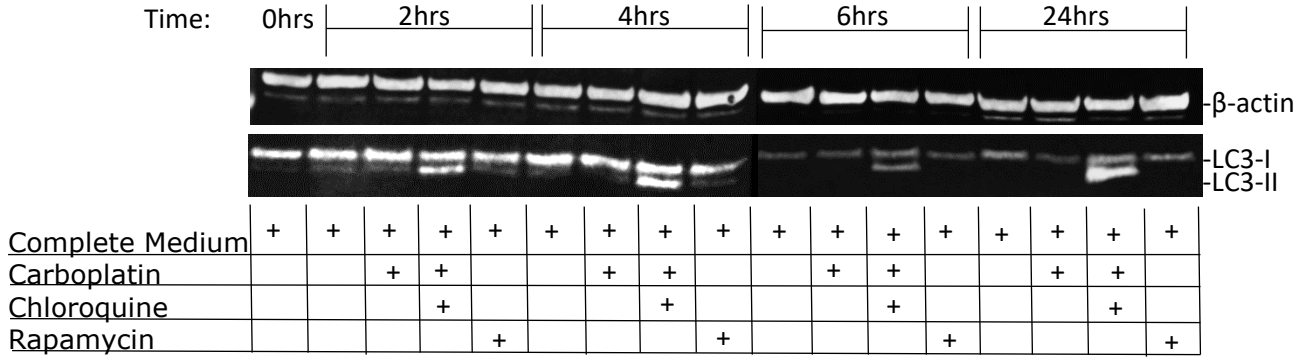

B.ii.

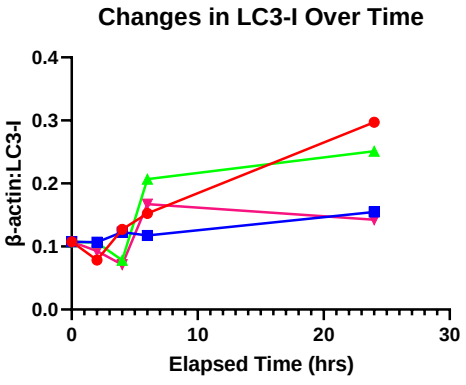

B.iii.

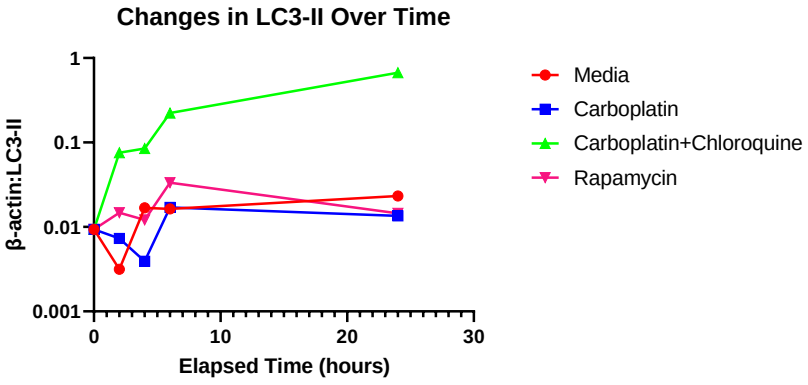

Figure 3.5. Changes in LC3-I and –II over time in response to nutrient starvation and chemotherapy drugs. Ai. Western blot of B16F1 lysate showing changes in LC3-I and –II over time, against a β-actin loading control. Cells were cultured in four different conditions: RPMI+FBS (complete medium), EBSS, EBSS+Chloroquine, and RPMI+FBS+Rapamycin and lysed at five different time points (0, 0.5 hours, 1 hour, 2 hours, and 4 hours). Aii and Aiii.) Graph of changes in fluorescence detection of western blot bands over time. Signal was normalised to actin loading control. B.i.) Western blot of B16F1 lysates after being grown in complete medium, carboplatin conditioned medium, carboplatin and chloroquine conditioned medium and rapamycin conditioned medium over five time points (0, 2, 4, 6, and 24 hours). Bii and Biii.) Graph of fluorescence signal of western bands, normalised to β-actin loading control.

3.3.5 p62 as an indicator for autophagy-mediated protein degradation in B16F1 cells 8/2/22

p62 is degraded through autophagy and therefore its reduction is a good indicator that autophagy is catabolising proteins effectively. As observed in western blot images (figure 3.6.A), p62 protein expression appeared to be stable through all conditions, except for cells treated with chloroquine for 24 hours. Under this condition there was a reduction in overall protein and p62 expression, most likely due to cell death, as cells were observed to be detached and suspended within the medium.

When p62 signal was normalised to β-actin, subtle changes were observed (figure 3.6.B). Cells grown in complete medium had consistent p62 levels within the first 4 hours, with normalised signal between 0.06 and 0.14. Beyond 4 hours, p62 began to accumulate, reaching a maximum signal of 1.5 at 24 hours. Increasing p62 signal over time was also observed in rapamycin treated cells, with a minimum signal at 1 hour of 0.07 and a maximum at 24 hours of 1.1. Both groups treated with chloroquine showed an overall increase in p62 over time, up until 24 hours where levels began to decline again. The increase in p62 in both groups was not linear as both groups showed decline at 6 hours but then increased to a

maximum at 10 hours of 1.2 and 0.9 for chloroquine treated and rapamycin plus chloroquine treated cells respectively.

The overall increase in p62 expression over time was not correlated with LC3-II expression. In complete medium, autophagosomes were present at low levels from 0 hours to 6 hours. The LC3-II band was not visible at 10 and 24 hours. This was also observed in rapamycin treated cells. In both groups of chloroquine treated cells, LC3-II signal increased at each time point, suggesting an autophagosome accumulation over time, consistent with the literature and previous experiments for chloroquine treated cells. At 24 hours however, there was a decrease in LC3-II signal in rapamycin and chloroquine treated cells.

Figure 3.6

A.

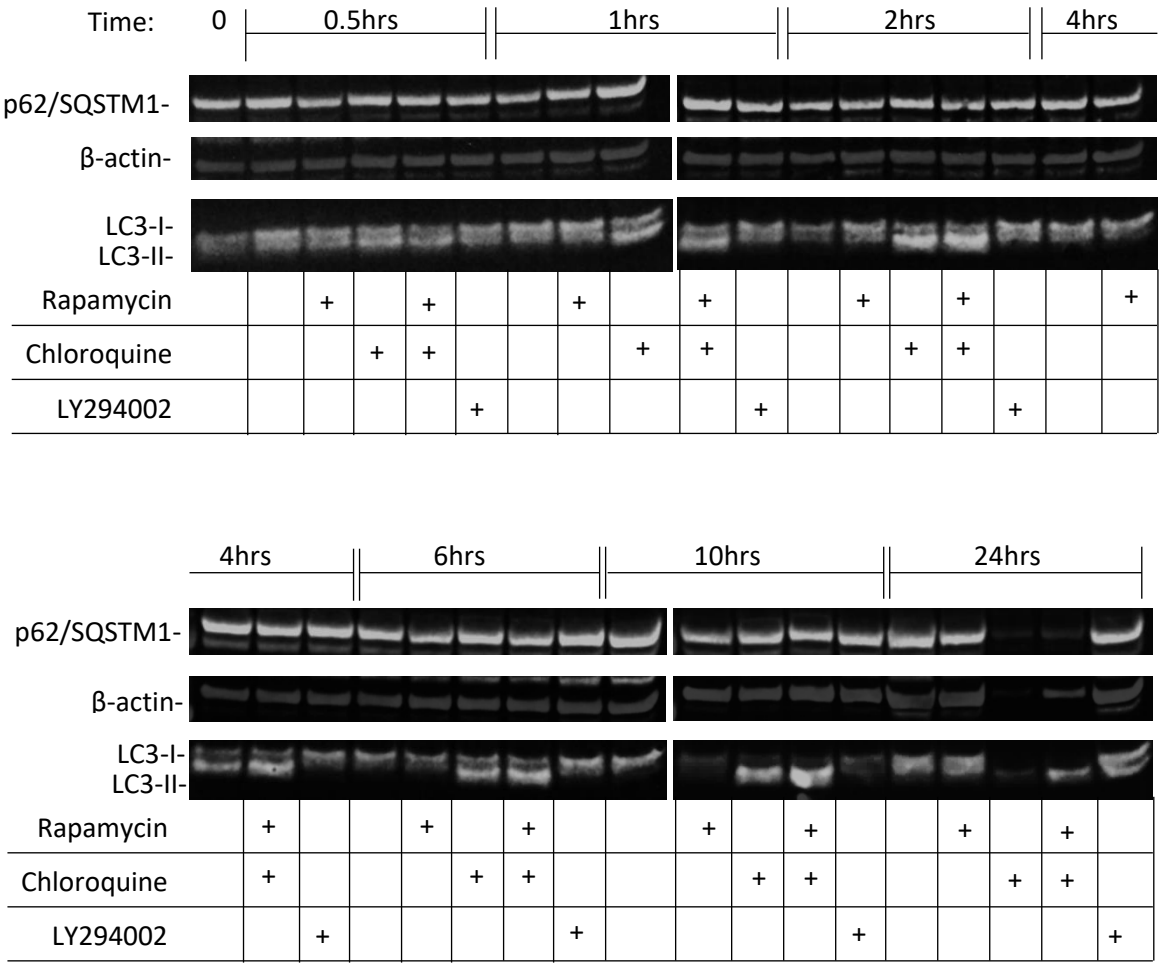

B.

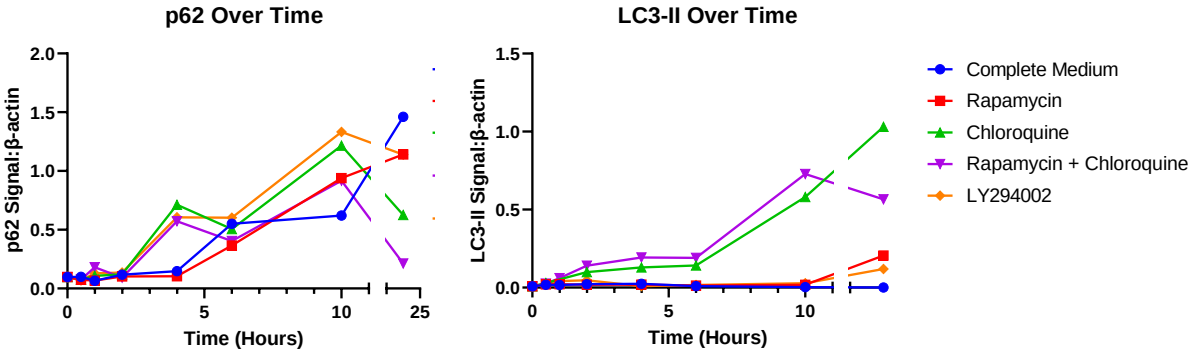

Figure 3.6 Changes in p62 and LC3-II over time in response to autophagy inducers and inhibitors. Cells were cultured in complete media or media conditioned with autophagy inducer rapamycin, or inhibitors chloroquine or LY294002 for various time points, as indicated in the figure. Expression of p62, β-actin, and LC3 were determined by western blot as shown in A. Fluorescent signal was quantified and plotted as shown in figure 3.5.B.

3.4 Discussion

For the purpose of these experiments, the level of LC3-II was taken as a measure of the amount of autophagosomes within cells, as the lipidated species of LC3 is found inserted within the membrane of autophagosomes. This does not however comment on the cells progress through autophagy flux (i.e. the progress through autophagosome formation through to fusion with the lysosome and degradation). Primary cells showed minimal basal LC3-II, indicating a low level of autophagy, which reflects the physiological nature of the cells. Autophagy is often increased as a stress response and primary cells in a nutrient-rich media are unlikely to be stressed. In primary cells autophagosomes could only be increased by blocking the fusion with lysosomes. Rapamycin, often used as a means to increase autophagy, was not able to increase the amount of autophagosomes above baseline in primary cells. This could be due to autophagosome turnover being increased with the addition of rapamycin, with autophagosomes being degraded at the lysosome as quickly as they are formed. This is supported by rapamycin plus chloroquine treatment often showing a higher signal for LC3-II than chloroquine alone. This suggests that rapamycin does induce increased autophagosomes but the fusion with lysosomes needs to be blocked in order to see this effect in primary cells. However

this was not the case with Jing Zhou, Shi Hao Tan et al.[318] whom showed that rapamycin does not cause lysosomal activation, possibly due to the allosteric inhibition of mTORC1. Rapamycin may induce the fusion of autophagosomes with lysosomes however, as inhibition of mTORC1 stops the phosphorylation of UV-irradiation-resistance-associated gene (UVRAG)[319]. UVRAG association with Beclin1 influences autophagosome formation and UVRAGs further interaction with class C vacuolar protein sorting (Vps) complex (a complex essential in endosome/vacuole tethering[320,321]) allows for tethering of the autophagosome at the lysosome and fusion events. mTORC1 inhibition allows UVRAG and class C Vps' effects on autophagosome-lysosome fusion to take place. This action of UVRAG is contested in other studies however[322,323]. Regardless of the absence/low level of LC3-II bands at basal conditions for primary cells, the addition of choloroquine alone caused an increase in LC3-II bands suggest that autophagy is taking place in these cells. This corroborates with the function of autophagy as a housekeeping degradation system, to maintain amino acid supply and degrade protein aggregates that are not associated with cellular stress. This is especially pertinent in APCs which use autophagy as a source for MHCII[324]. Therefore the low

autophagy detected in primary cells in this study aligns with current knowledge of autophagy.

In comparison to primary cells, cancer cell lines gave a level of autophagosomes that was in excess at basal conditions. This could be reflective of cancer cells being in a constantly stressed state, due to the high energy demands of immortal growth, amongst other cellular changes. A study by Pan and Kumar et al. found that in hepatic cancer cell lines, 50% of the cell proteome expression was changed at least 2-fold or more[325], compared to primary hepatocytes, showing that a physiological phenotype is not upheld in cancer cell lines. However, as autophagy is a self-regulating process, and is usually activated in conditions of starvation, media containing glucose and amino acids should provide an environment where autophagy activation should not take place. Nevertheless autophagosomes were present in much higher levels in cancer cell lines, with complete medium, and this is shown to be the case in other studies as well[326–331]. The dysregulated signalling in cancer cell metabolism is therefore likely to be inducing autophagy in a starvation independent manner. One exemplary oncogenic signalling process is through the protein, Ras, which is often upregulated in cancer, which leads to increased autophagy[332]. Ras upregulation is also found in

B16F1 cancer cell lines[333] which suggests this holds true in this case.

Like primary cells, the majority of cancer cell lines also did not show an increase in autophagosomes upon treatment with rapamycin alone. A possible reason for this is that rapamycin acts as an allosteric inhibitor of mTORC1, and competes with phosphatidic acid (PA) for its binding site. PA is synthesised by phospholipase D (PLD) which is known to have elevated activity in cancer cells[334]. This is especially true of cancer cell line MDA MB 231[335]. The same concentration of rapamycin was used throughout all experiments which may have been incorrect due to the different concentrations of PA competing for the binding site on mTORC1. Instead, a dose response curve should have been generated for each individual cell line, and the effectiveness of mTORC1 inhibition could have been determined by observing the phosphorylation status of its targets: Ribosomal protein S6 kinase (S6K) and eukaryotic initiation factor 4E (eIF4E) binding protein 1 (4E-BP1)[336]. However, cell line MCF-7 has shown inhibition of mTORC1 with a rapamycin concentration of 20nM. 800nM is therefore in excess of what is required for autophagy induction in this cell line however an increase in LC3-II is still not seen with rapamycin treatment. This could again be due to the fast turnover of newly formed autophagosomes. Nevertheless, the

addition of chloroquine in cancer cell lines causes an increase in LC3-II compared to basal and rapamycin treated cells, suggesting the autophagy flux is taking place in these cells. Furthermore, over time the high level of basal autophagy is shown to be decreased. This may be due to the increased confluency of cells over time. Previous work by Poonam Vaghela[337] has shown that B16F1 cells show a reduced level of LC3-II when confluency exceeds 90%, as was the case at later time points in the above experiments. This could be through the inactivation of YAP/TAZ signalling due to high confluency[338].

The effects of Earle's balanced salt solution appear to show reduced autophagy over time. This is shown by the reduction of LC3-II after 4 hours. Autophagosomes have been shown to be reduced after prolonged starvation in other cell lines too, which can be rescued on the addition of chloroquine[339]. This suggests that there is an increase in autophagosome flux which converts LC3-I to LC3-II quicker than LC3-I can be reformed. This is further evidenced by the concurrent reduction in LC3-I over time. Autophagy in B16F1 cells therefore appear to respond to autophagy inducers, such as starvation, as physiological cells would.

Carboplatin does not appear to significantly alter autophagy taking place in B16F1 cells. This is shown by the minimal differences between LC3-II in cells treated with media alone and with carboplatin. Carboplatin does not however reduce the cells ability to go through autophagy flux, as the addition of chloroquine does cause an accumulation of autophagosomes. This gives a good outlook for using autophagosomal processes as a target for cancer therapy, for patients that have either previously or are concurrently going through chemotherapy.

Reduction in p62 is often used as an indicator for autophagy flux. For this reason, p62 levels were investigated over time to give evidence on whether autophagy is functional as a degradation process in cancer cell lines. It was hypothesised that p62 would be reduced on the addition of rapamycin, as autophagy will be induced. The addition of chloroquine was expected to rescue the reduction in p62, since fusion with the lysosome is blocked and therefore proteins would not be degraded. This was not the case, as p62 continued to increase over time, regardless of treatment group. p62 has been shown to accumulate over time due to prolonged starvation of cells[340]. As B16F1 cells are shown to have autophagosomes present in all conditions, and these accumulate when the cells are treated with chloroquine, it suggests that autophagosome flux is taking place within these cells at all time points. With

prolonged, constitutive autophagy, p62 could be accumulating over time due to this positive feedback mechanism. In chloroquine treated groups, there is a reduction in p62 at the 24hr time point. This is likely to be due to the prolonged inhibition of the lysosome triggering apoptosis signalling cascades[341], as also shown by the reduction in β-actin protein signal. LY294002 failed to inhibit autophagy and an increase in autophagy was seen, however due to the addition of growth factors within the media and LY294002s effect of class I PI3K it is not surprising that this occurred. Furthermore, Eskilinen et al showed that PI3K inhibition in mitotic cells activates autophagy[342]. B16F1 cells are continuously dividing and therefore likely to be going through mitosis, suggesting PI3K inhibition would activate autophagy in these cells too. This could therefore explain the increase in LC3-II over time. Nevertheless, these data give further evidence that autophagy is constitutively taking place in cancer cell lines, although it may be dysregulated and perform unlike physiological autophagy.

A high level of basal autophagy was also confirmed by confocal microscopy. Here, fluorescent puncta that would be typical of autophagosome formation was seen in both basal and rapamycin and chloroquine induced conditions, suggesting that autophagy was constitutively activated in B16F1 cells.

However these data differ by way that induced conditions did not show an increase in puncta compared to untreated B16F1 cells.

Basal and rapamycin induced autophagy appeared to be low in data observed by the imaging flow cytometer (ImageStream). Unlike a confocal microscope, ImageStream images are not able to remove fluorescence from outside the focal plane, and therefore resolution is reduced. Combining this with anti-LC3-AF647 detection antibody also binding cytoplasmic LC3-I, as well as LC3-II, the background fluorescence caused by binding LC3-I may make it difficult to see puncta formed by the insertion of LC3-II in autophagosome membranes. Furthermore, this may reduce the software's ability to count spots which could lead to an underestimation of LC3-II puncta. Nevertheless, an increase in puncta is seen, both in images and in spot count, on treatment with chloroquine, suggesting that the puncta are numerous enough to be seen above background. The fluorescent histograms showing LC3 expression show a complementary picture to western blot and confocal data, with similar MFI for basal and rapamycin induced conditions which have shifted from the isotype control, and a larger increase for chloroquine treated conditions.

4. Autophagosomes as a Source of Citrullinated Epitopes

4.1 Introduction

Cancer cell lines were shown to have a constitutive presence of LC3-II. This suggests constitutive presence of autophagosomes and therefore a possible enriched source of citrullinated proteins. In order to characterise autophagosomes and their contents as a source of citrullinated epitopes, autophagosomes must be correctly identified after isolation. LC3-II is widely regarded as the gold standard marker for mature autophagosomes. LC3-II consistently stays inserted into the mature autophagosome membrane until degradation and therefore is the best available for labelling this organelle. Nevertheless, other LC3-II positive vesicular bodies do occur and therefore further techniques are required to reliably characterise autophagosomes.

One such characterisation is through electron microscopy (EM). Autophagosomes appear as double membrane, cytoplasm containing vesicles, allowing for distinction from other single membrane organelles[343]. An increased level of information can be gathered using EM such as autophagosome cargo, and position in the autophagosome life cycle. Autophagosomes can however be confused with other double membrane species such as swollen mitochondria, endoplasmic reticulum cross-sections, and endocytosed apoptotic bodies[344].

Identification can therefore be aided by immune-labelling against LC3.

There are alternative markers for autophagy however the majority of proteins are only present on the initial formation of the autophagosome. ATG9[345], ATG12-ATG5[346], ATG14/ATG14L/BCN1[347–349], ZFYVEI[350], and ATG16L[351] are all involved in the induction of autophagy and puncta can be seen as these proteins localise to the phagophore. However, the majority of these proteins dissociate on the formation of a mature autophagosomes. BECN1 can be found on mature autophagosomes, but is also found associated with the ER and therefore is not a reliably specific marker[352]. ATG16L is phosphorylated upon autophagy induction and the phosphorylated species is used as a marker for autophagy induction, similarly to LC3-II is, however expression levels do not always correlate[353]. STX17 is involved in the fusion of autophagosomes with endosomes and lysosomes[354] and has been found localised to the omegasome[355], so can be used to aid in determining autophagy flux and induction, however cannot be used as an autophagosome marker as not all autophagosomes are STX17 positive. WIPI is the only protein to show correlation with LC3-II. Upon autophagy induction, WIPI binds phosphatidyl 3-phosphate on the membrane of autophagosomes and phagophores and WIPI puncta has been

shown to co-localise with LC3 puncta[356,357]. Furthermore WIPI oligomerises on binding, giving opportunity to amplify signal by immunodetection[358]. However WIPI is not reliably detected in all cells[357] and may have alternative functions to autophagy. This may be why LC3-II continues to be the preferred marker across autophagy studies.

There are two other occasions LC3-II is associated with membranous vesicles. In both, the level is lower and not as consistent. LC3-associated phagocytosis (LAP) is the process where LC3-II directs phagosomes to the lysosome for degradation[359]. While this process is not affected by Rapamycin, unlike autophagosomes, it is affected by chloroquine[20]. The second vesicle associated with LC3-II is exosomes, a process sometimes called secretory autophagy. This is a proposed mechanism by which IL-1b is secreted by cells involving TRIM16 and SNARE proteins that help avoid lysosomal degradation[360].

The contents of autophagosomes firstly depends on the type of autophagy taking place, of which there are four main types: macroautophagy, selective autophagy, chaperone-mediated autophagy (CMA), and microautophagy. Macroautophagy refers to the non-specific degradation of cytoplasmic components. Therefore the contents will be similar to that of

the cytoplasm as a whole. Selective autophagy is for the degradation of a specific substrate by crosslinking it via selective autophagy receptors (SARs) and their LC3-intereacting region (LIR)[361]. Targets of selective autophagy include damaged organelles, large protein aggregates, lipid droplets, ferritin, and glycogen[362–366]. CMA and microautophagy do not involve the autophagosome so will not be discussed in this work. Additionally, autophagosomes can fuse with endosomes to form amphisomes, allowing for membrane proteins and lipids, and extracellular fluid to be found within LC3-positive species[367,368]. Amphisomes can be differentially identified from autophagosomes as single membrane LC3-positive vesicles[369,370]. Furthermore, in the context of the target of interest, citrullination, a study by Ireland et al.[182], the presentation of citrullinated peptides by immune cells was dependent on autophagy, and PAD activity was found localised to the organelle, giving further evidence that autophagosomes were the site of citrullination and therefore citrullinated proteins could be found within.

4.2 Aims

Autophagy is cited to be involved with the citrullination of proteins. A technique for isolation autophagosomes was developed in order to investigate its contents.

4.3 Results

4.3.1 Autophagosomes can be enriched from tumour cells by ultracentrifugation on density gradients.

Investigating tumour cells identified that autophagy is constitutively active, compared to normal cells. To analyse the contents of Autophagosomes for potential citrullinated proteins we aimed to enrich autophagosomes for further analysis. Differential centrifugation and ultracentrifugation on an OptiPrep gradient was employed, to resolve organelles by their isopycnic point[371].

Large particles, such as the nucleus and whole cells, were removed by differential centrifugation. The pellet after each centrifugation step was analysed for autophagosome content via the presence of LC3-II (figure 4.1.A). The 25K fraction showed the highest level of LC3-II, therefore this was taken forward for further separation via an OptiPrep density gradient.

MCF-7 cell extracts were separated into 10 fractions from the gradient and protein was extracted using lysate buffer. Organelle contents in each fraction were identified using antibodies against known organelle markers (figure 4.1.B). Organelles were seen to be dispersed across multiple fractions with autophagosomes (identified through anti-LC3-II) found

between fractions 3-8, peaking at fraction 6 or 7 depending on sample preparation. Other organelles were identified, such as early endosomes (EEA1) in fractions 3-7, endoplasmic reticulum (Calnexin) in fractions 3-9, mitochondria (PHB1) in fractions 4-9, and lysosome (LAMP2) in fractions 3-7, however peak amounts of organelles were found in different fractions to autophagosomes.

An organelle enrichment was carried out from B16F1 cells and autophagosome content was established in each fraction. A representative example is shown in figure 4.1.C, where autophagosome fractions were shown to be spread across fractions 5-9, with signal peaking in fraction 6 and 7. When signal was normalised to protein loaded, fraction 6 was shown to have the highest LC3 signal per µg of protein, suggesting this fraction was the most enriched for autophagosomes. Multiple autophagosome enrichments were carried out and fractions with high concentration of autophagosomes were consistently shown to be in fractions 5, 6, and 7 (figure 4.1.Civ. For this reason, these three fractions were used in future experiments where autophagosomes were required.

The same organelle enrichment process was carried out on ex-vivo B16 tumour samples and the LC3 enrichment profile in each fraction was determined by western blot (figure 4.1.D).

Fractions containing LC3-II showed a similar spread to previous samples of in-vitro tumour cell line organelle fractions. The most concentrated fraction for LC3-II was fraction 5, different from in-vitro tumours (fig 4.1.Diii). Furthermore, ex-vivo tumour organelles were also shown to contain LC3-I in similar fractions to that of LC3-II (fractions 4-9), albeit to a lesser extent.

Figure 4.1

A.

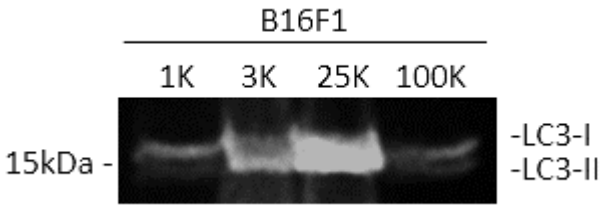

Bi.

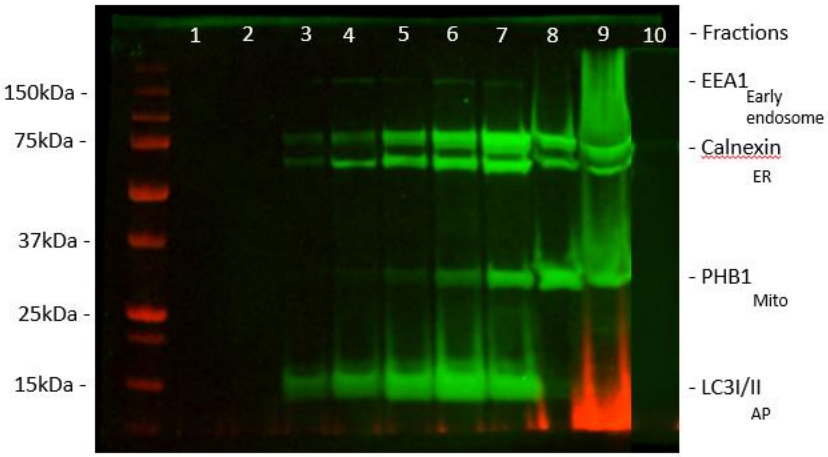

Bii.

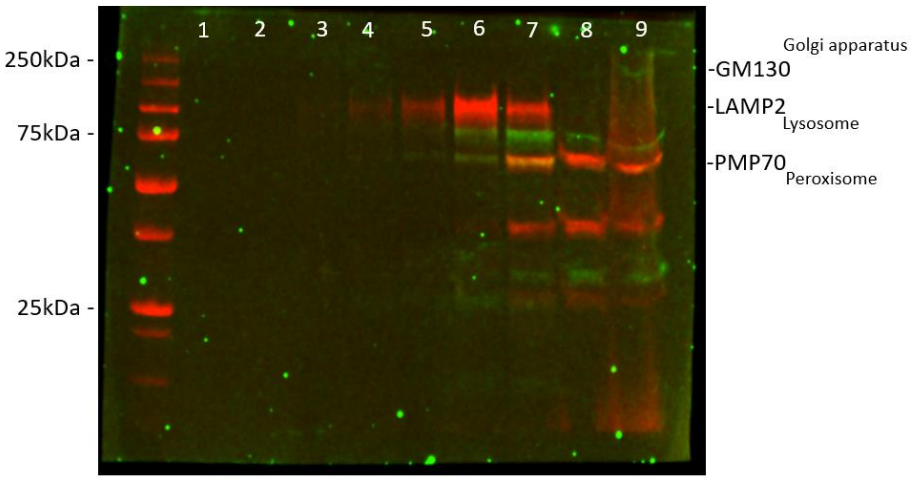

Ci.

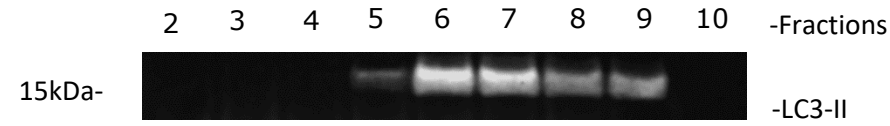

Cii.

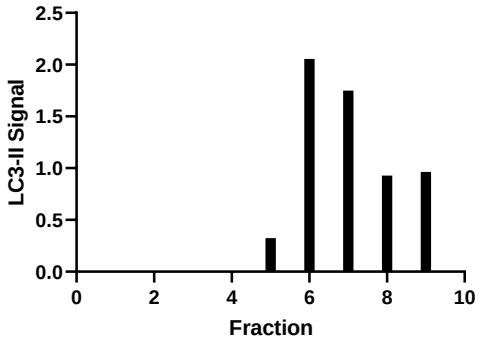

Ciii.

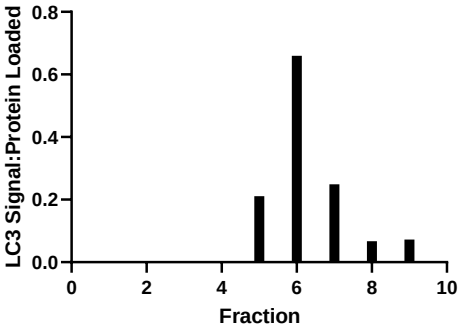

Civ.

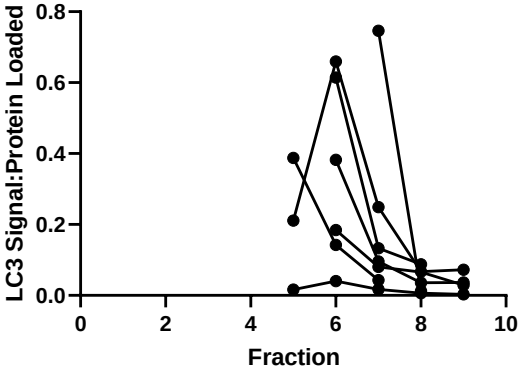

Di.

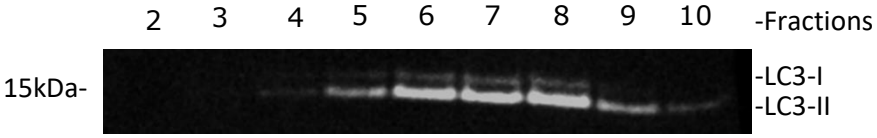

Dii.

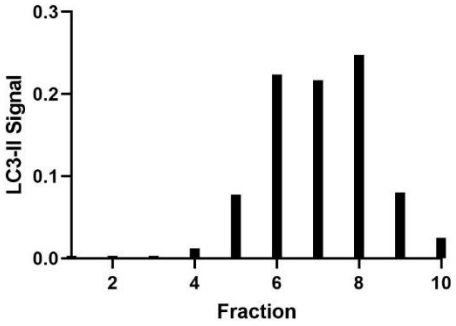

Diii.

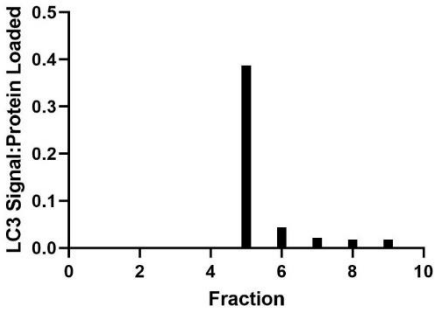

Figure 4.1. The analysis of tumour organelle fractions by western blot. A) Low-resolution organelle separation by differential centrifugation at 1,000, 3,000, 25,000, and 100,000g. Pellets were lysed and probed by western blot with anti-LC3 antibody. B) Western blot of MCF-7 organelle fractions (1-10). Primary antibodies for markers for the indicated organelle were used to characterise content. Bi) shows points of elution for the early endosome (EEA1), endoplasmic reticulum (calnexin), mitochondria (PHB1), and autophagosomes (LC3). The membrane was then stripped and reprobed in figure Bii, using primary antibodies for the golgi apparatus (GM130), lysosome (LAMP2), and peroxisome (PMP70). C) organelle separation from B16F1 cells, i) western blot of organelle fractions labelled with anti-LC3, ii) graphical representation of LC3 signal shown in Ci, iii) LC3 signal normalised to the amount of protein loaded into the western gel, iv) LC3 signal across fractions from multiple experiments (n=8). Connected dots show fractions isolated from the same tube after ultracentrifugation D) Organelle fractions isolated from ex-vivo B16 tumour, i) western blot of organelle fractions labelled with anti-LC3, ii) Graphical representation of LC3 signal show in i., iii) LC3 signal normalised to protein loading.

4.3.2. Characterisation of autophagosome content of organelle density fractions from B16F1 tumour, using small particle flow cytometry.

Biochemical characterisation of autophagosomes allows for detailed content analysis of each fraction, but is time consuming. We attempted to determine if these fractions could be analysed by flow cytometry, which would make analysis of sample preparation a simpler process. Initially benchtop flow cytometers for cellular FACS (Miltenyi MACSQuant 10) were used to investigate autophagosomes, however autophagosomes were too small to resolve. Therefore we sought a flow cytometer with higher resolution, the Beckman Coulter MoFlo Astrios EQ.

Nano sizing beads were used to set voltages and give an indication of where autophagosome events can be expected based on a size of 500-1500nm[372,373] (fig 4.2A). Calibrated sizing beads (100-800nm diameter) were referenced and populations of >500nm were found to localise to the upper right corner of the forward vs side scatter dot plot. Gating of autophagosomes in organelle fractions was therefore directed to this area, as shown in gate B in figure 4.2.B.

Doublets and aggregates were excluded by plotting side scatter area vs side scatter width and gating around the main

population (gate G in figure 4.2B). Autophagosomes were labelled with anti-LC3-AF647 and the gating strategy shown in figure 4.2B, using an isotype control antibody to gate out negative fluorescence, was used to determine the number of LC3+ (autophagosome) events in each fraction.

Fractions 2 and 3 had relatively few positive events for LC3 expression. This agreed with both the BCA and western blot analysis of organelle fractions, which shows low protein and minimal LC3 in early fractions. For fraction 2, the MFI for the anti-LC3 labelled population was lower than that of the isotype control and so cannot be taken as a positive signal for LC3. Events from fraction 3 showed early signs of LC3 positive events, with 42% positive for LC3, although the event count remained low at 18. The remaining events were LC3 negative and therefore are likely due to other organelles.

Higher fractions containing organelles of greater density showed increased total event numbers and LC3 positive events. This was in concordance with western blot data which shows LC3 positive populations in mid-density fractions. Fraction 4, 5, 6 and 7 showed majority LC3 positive populations through this gating strategy (91, 58, 87, and 87% positive, respectively), suggesting enrichment of autophagosomes. In fractions 4, 6, and 7, there were minimal

LC3 negative peaks, and therefore events at this size and granularity appear to be almost all autophagosomes. Fraction 5 showed a smaller AF647 negative peak suggesting more non-autophagosomal organelles in this fraction.

In fractions with the densest organelles (8 and 10), the peak for the isotype control partially overlapped with the LC3 positive peak and because of this, % positive events for LC3 were low. MFI of the isotype control increases relative to lower fractions and therefore it is likely that fluorescence is due to non-specific binding of antibodies in these fractions.

Figure 4.2

A.

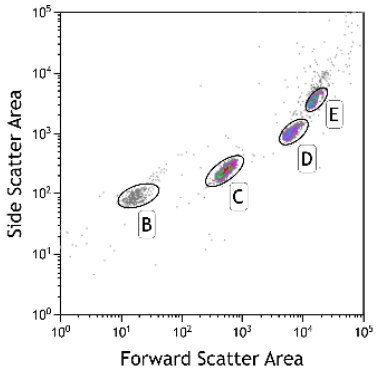
Side Scatter Area
Forward Scatter Area
B
C
D
E

B.

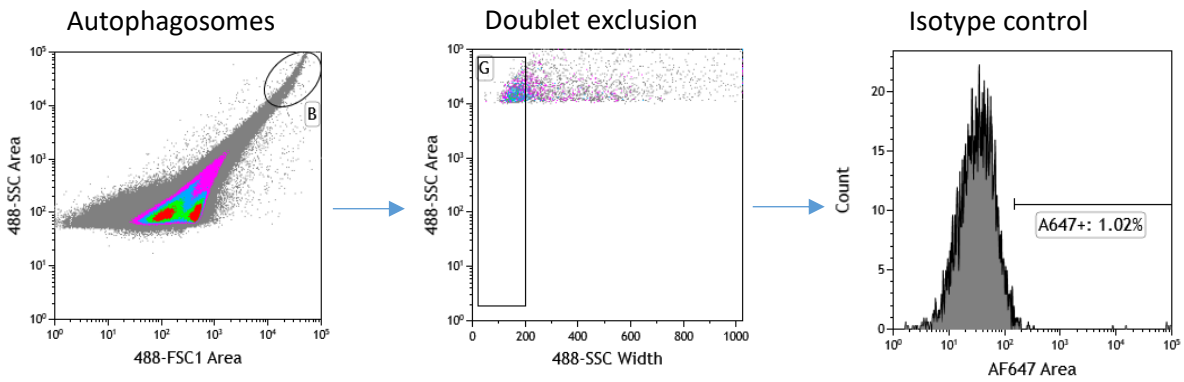
Autophagosomes
Doublet exclusion
Isotype control
488-SSC Area
488-FSC1 Area
B
G
488-SSC Width
Count
A647+: 1.02%
AF647 Area

C.

Fraction 2

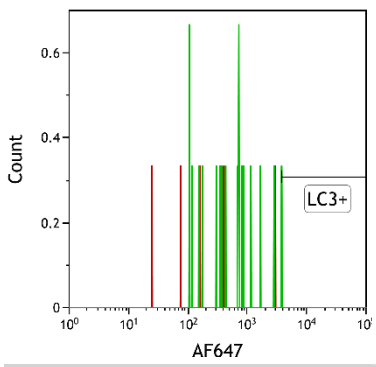

Marker	Number	%Gated	X-Med
All	18	100.00	686.93
All	5	100.00	158.38
LC3+	1	5.56	3,766.08
LC3+	0	0.00	N/A

Fraction 3

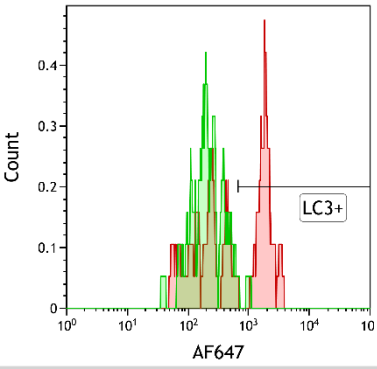

Marker	Number	%Gated	X-Med
All	37	100.00	207.44
All	42	100.00	463.46
LC3+	1	2.70	984.74
LC3+	18	42.86	1,976.51

Fraction 4

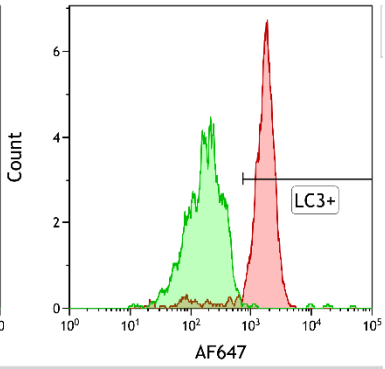

Marker	Number	%Gated	X-Med
All	568	100.00	180.24
All	471	100.00	1,692.72
LC3+	9	1.58	9,170.70
LC3+	430	91.30	1,750.95

Fraction 5

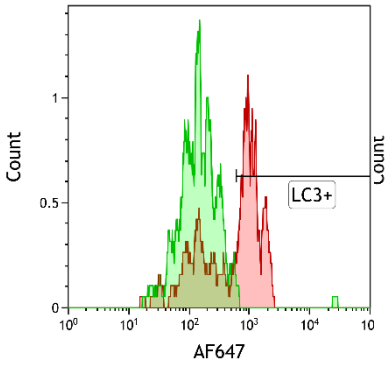

Marker	Number	%Gated	X-Med
All	144	100.00	141.81
All	118	100.00	768.67
LC3+	2	1.39	13,384.97
LC3+	68	57.63	1,026.77

Fraction 6

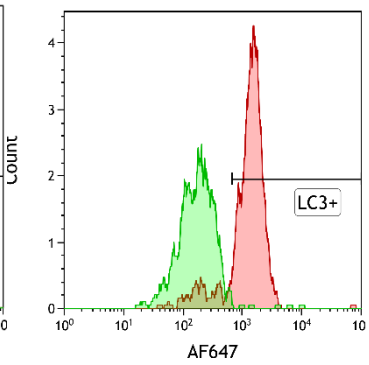

Marker	Number	%Gated	X-Med
All	313	100.00	179.49
All	366	100.00	1,401.15
LC3+	5	1.60	3,946.31
LC3+	317	86.61	1,495.80

Fraction 7

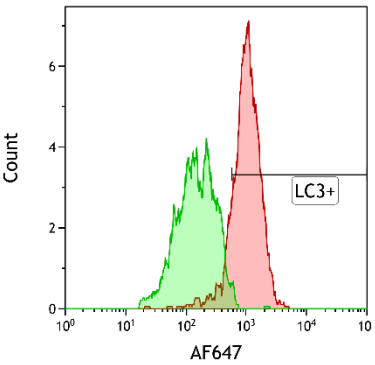

Marker	Number	%Gated	X-Med
All	622	100.00	147.22
All	671	100.00	1,024.85
LC3+	10	1.61	607.02
LC3+	585	87.18	1,090.74

Fraction 8

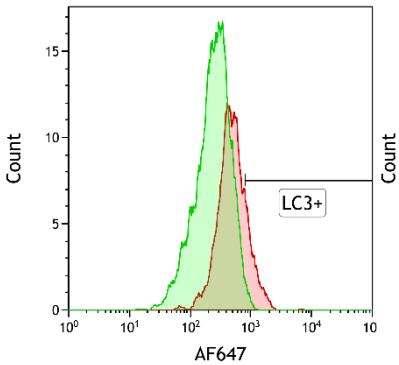

Marker	Number	%Gated	X-Med
All	2,175	100.00	254.42
All	1,257	100.00	487.94
LC3+	23	1.06	887.98
LC3+	223	17.74	1,023.89

Fraction 10

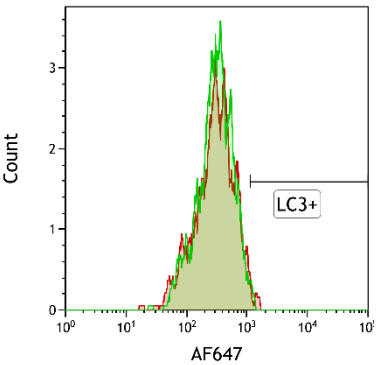

Marker	Number	%Gated	X-Med
All	434	100.00	316.23
All	400	100.00	309.20
LC3+	4	0.92	1,232.59
LC3+	5	1.25	1,467.25

Figure 4.2. Flow cytometry analysis of organelle fractions isolated from B16F1 cells, stained for LC3 with anti-LC3 alexafluor647. Figure A) forward vs side scatter of nano sizing beads at sizes 100, 200, 500, 800nm. B) Gating strategy for LC3 positive events gating firstly on events of the correct size using forward and side scatter (gate B), then doublet exclusion using side scatter width vs area (gate G), then positive AF647 fluorescence gate was placed, based on the binding of an isotype control antibody for the anti-LC3-AF647 antibody. Ci-viii) histogram of AF647 fluorescence of isotype control antibody (green) and anti-LC3-AF647 antibody (red) in each organelle fraction. Median fluorescence intensity (X-Med) and event number are given for each plot.

4.3.3 Citrullinated proteins coincide with autophagosome high organelle fractions

Autophagy and protein citrullination are interconnected processes[182], and autophagosomes are a potential site of protein citrullination. Therefore, the hypothesis that autophagosome high organelle fractions contain citrullinated proteins was investigated.

Protein lysates from a B16F1 organelle fractionation were fluorescently labelled, using a phenyl glyoxal based probe, for citrullinated residues and resolved by SDS-PAGE. Figure 4.3.A shows the presence of citrullinated proteins across all fractions with peak fluorescence in fractions 7 and 8. Normalisation of fluorescence signal to protein loading (fig 4.3.A.iii) showed fraction 6 had relatively the highest citrullinated protein content.

Quantification of the autophagosome content (fig 4.3.B) showed LC3 signals in fractions 4-8, with the highest amount found in fraction 6. When the signal in fractions 6-8 were normalised to amount of protein loaded, the highest amount of autophagosomes per µg loaded was also shown to be in fraction 6. Fractions with the highest amount of autophagosomes therefore coincide with fractions that have the highest amount of citrullinated residues.

Organelle fractionation of cells taken from ex-vivo B16 tumour samples permitted analysis of the LC3 content in a physiological setting (figure 4.1.D). An anti-citrullinated-HSP70 antibody was used to further aid in confirming the presence of citrullinated proteins, as this antibody has previously been shown to bind citrullinated proteins (unpublished). The antibody showed reactivity against proteins of estimated mass 21, 23, and 56kDa. The highest expression was found in fraction 6, 7, and 8 for the 21kDa protein, fraction 8 and 9 for the 23kDa protein, and fraction 6 and 7 for the 56kDa protein. Normalisation to protein content indicated that fraction 5 had the most concentrated amount of the 21 and 57kDa species. This corresponds with the fraction that has the highest concentration of LC3-II, as shown in figure 4.1.D.

Figure 4.3

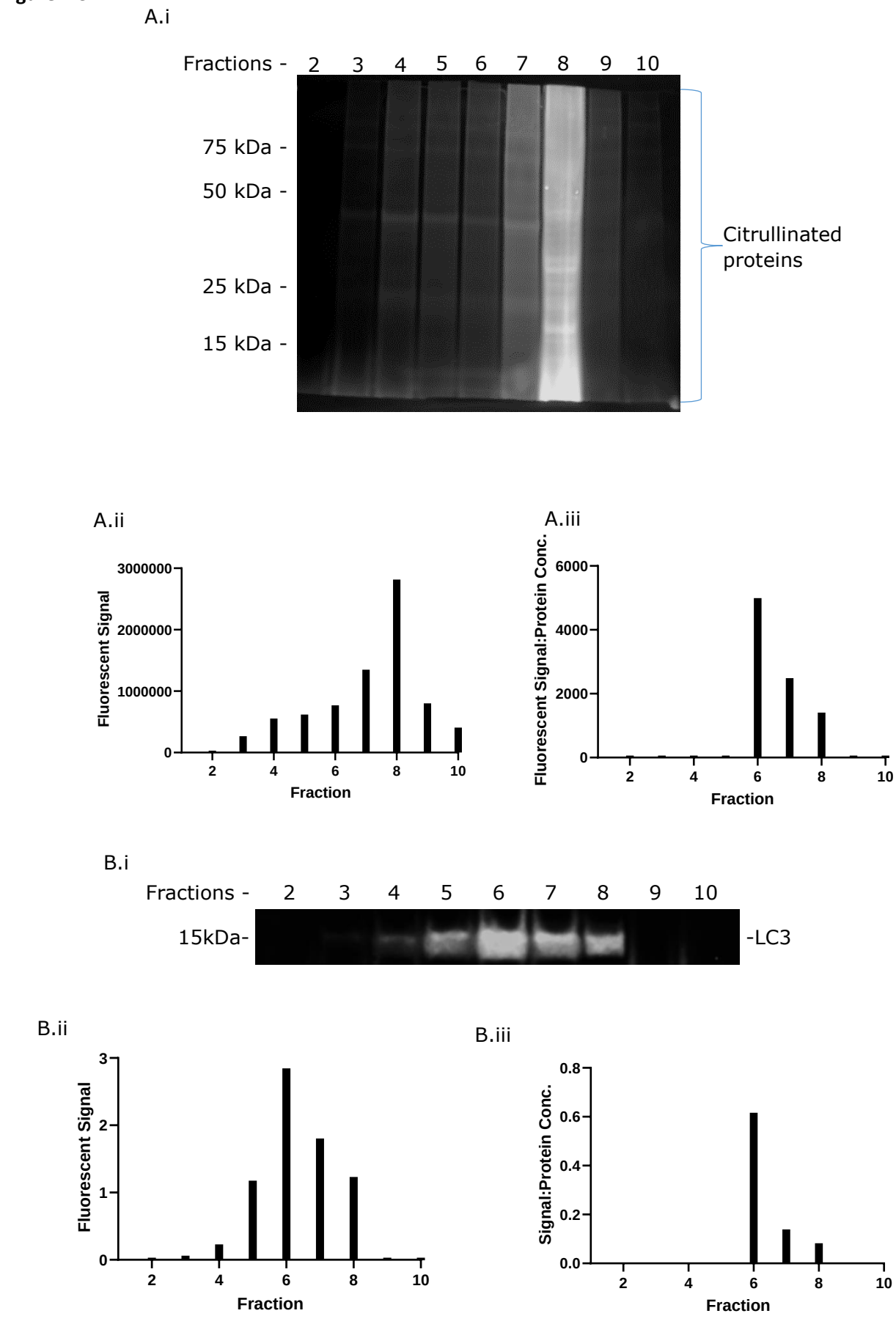
A.i
Fractions - 2 3 4 5 6 7 8 9 10
75 kDa -
50 kDa -
25 kDa -
15 kDa -
Citrullinated proteins
A.ii
Fluorescent Signal
3000000
2000000
1000000
0
2 4 6 8 10
Fraction
A.iii
Fluorescent Signal:Protein Conc.
6000
4000
2000
0
2 4 6 8 10
Fraction
B.i
Fractions - 2 3 4 5 6 7 8 9 10
15kDa-
-LC3
B.ii
Fluorescent Signal
3
2
1
0
2 4 6 8 10
Fraction
B.iii
Signal:Protein Conc.
0.8
0.6
0.4
0.2
0.0
2 4 6 8 10
Fraction

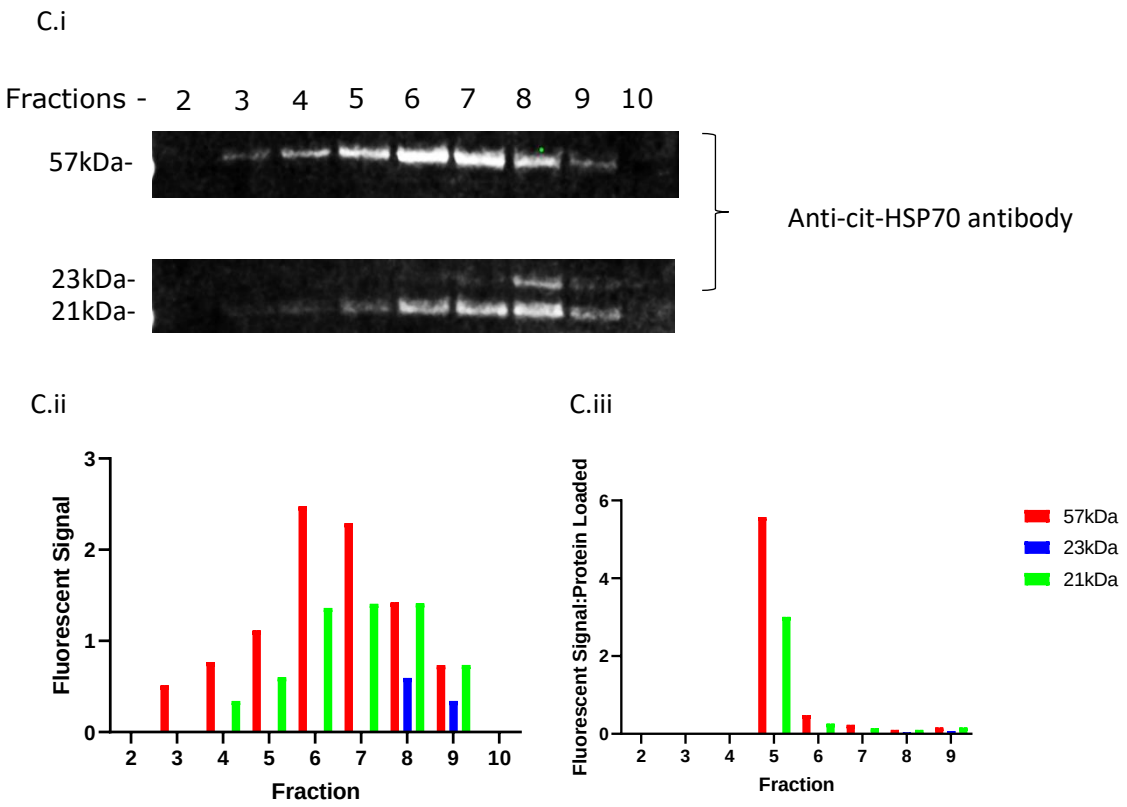

Figure 4.3. Western blot or organelle fractions to identify citrullinated proteins and autophagosomes. A) SDS-PAGE showing citrullinated proteins as shown by fluorescence of a phenylglyoxal-rhodamine probe conjugated to citrullinated epitopes. Aii) Graphical representation of fluorescence shown in Ai. Aiii) fluorescence signals normalised to the amount of protein loaded, as calculated using a BCA assay. B) Western blot of the same sample as in A, labelled with anti-LC3 antibodies (green). Bii) graphical representation of the fluorescence shown in Bi. Biii) LC3 fluorescence normalised to amount of protein loaded, as determined by BCA assay. C) Western blot of an independent ex-vivo B16 tumour organelle fraction preparation. Anti-citrullinated HSP70 antibodies were used for detection, showing bands at 57, 23, and 21 kDa. C(ii)) Graphical representation of the fluorescence signal seen in C(i). C(iii)) fluorescence signal normalised to amount of protein loaded, as determined by BCA assay.

4.3.4. Electron microscopy can be used to identify double membrane vesicles in organelle fractions.

Autophagosomes can be easily identified by their double membrane structure. To further confirm the presence of autophagosomes in the enriched organelle fractions, preliminary studies by electron microscopy was attempted, to identify vesicles with double membranes (figure 4.4). Not all organelles have a double membrane structure and therefore are made up of a mixed population of organelles. As indicated by the black arrows, some double membrane vesicles can be found, however the majority of these are electron sparse and smaller than the size given for autophagosomes in the literature[372,373] (figure 4.4.A). Autophagosomes are commonly found to be electron dense. Electron dense organelles are visible within the figure 4.4.A however image resolution does not allow for identification of a double membrane. Quantum dot labelled LC3 was used to further aid in the identification of autophagosomes. LC3 was found localised to double membrane structures however these were shown to be electron lucent (figure 4.4.B). A high proportion of single membrane/electron dense structures were shown to be LC3 positive as well (figure 4.4.B-C). No LC3 was detected extra-organelle.

Figure 4.4

A.

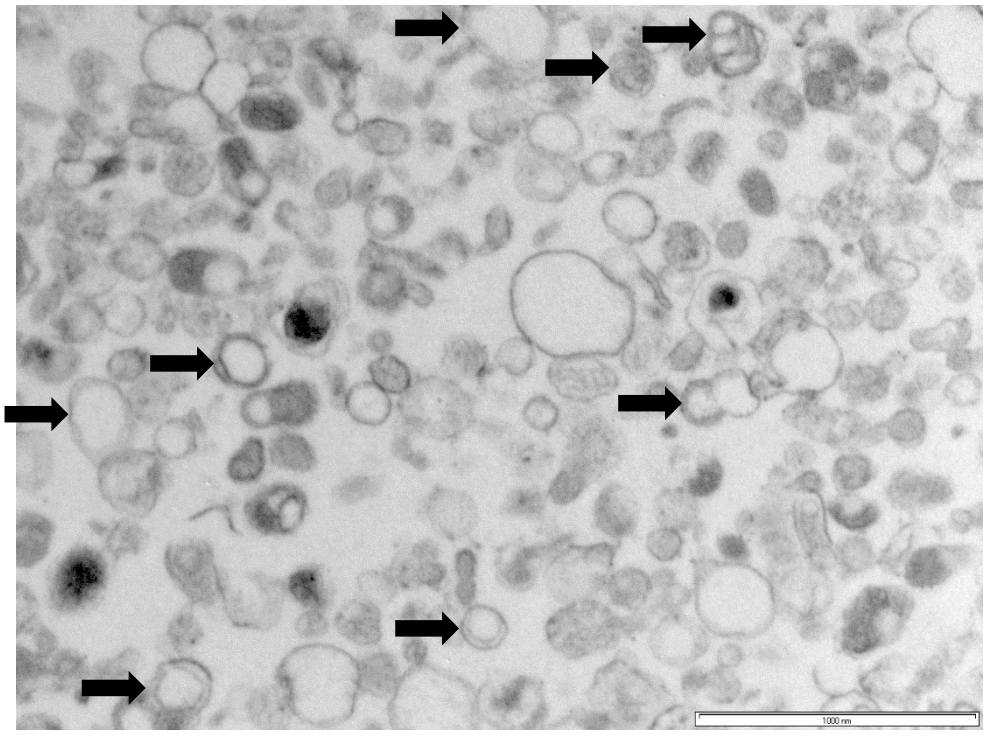

B.

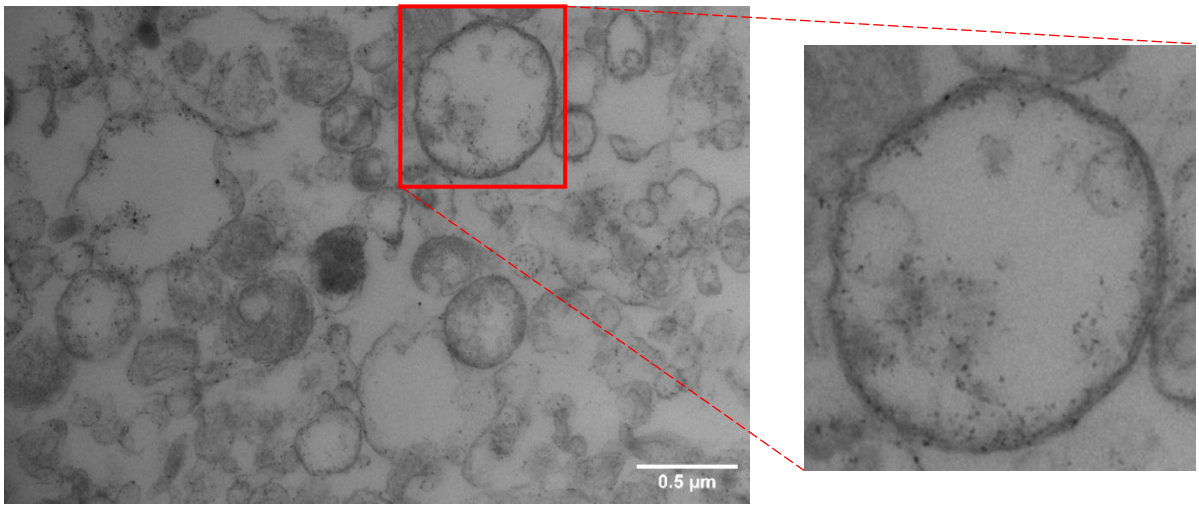

C.

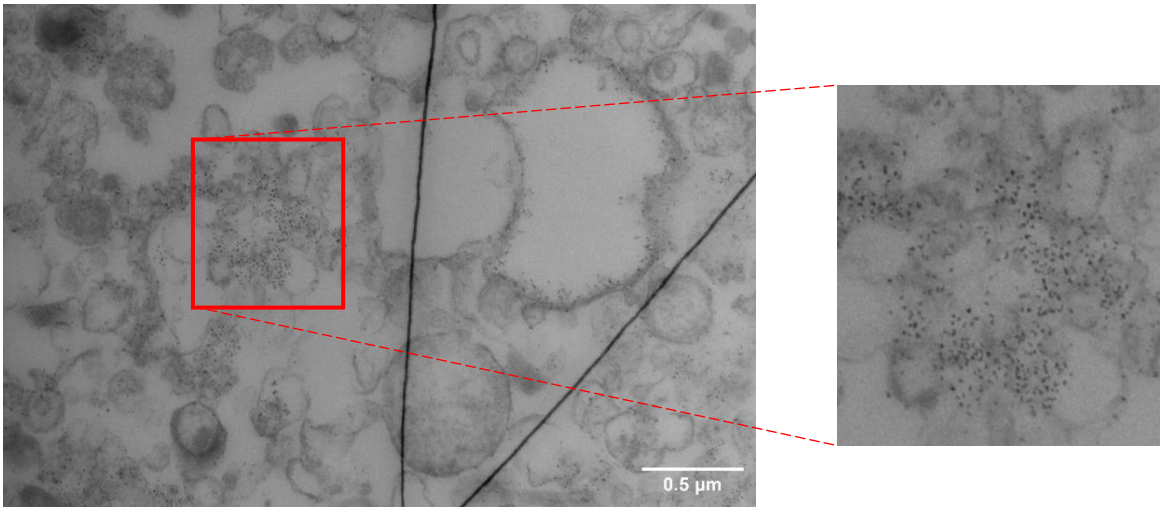

Figure 4.4 Electron micrographs of organelle fraction. Electron microscopy images of MCF-7 organelle fraction 7 and B16F1 organelle fraction 8 at resolutions of 1000 and 500nm. A) Double membrane structures are found (indicated by black arrows). B-C) Fraction 8 organelles harvested from B16F1 cells and labelled with quantum dots against LC3. B) LC3 is shown bound to double membrane structures as shown in magnified image. C) LC3 is shown also bound to many other structures.

4.4 Discussion

Isolating organelles by their density allows for enrichment of autophagosomes. Repeated isolations showed points of maximum enrichment to be reproducible in mid-density fractions, as shown by the presence of LC3-II signal in western blot. Different organelles showed particular density characteristics, as illuminated by the differences in fraction elution. As a technique for further examination of autophagosomes, co-isolated organelles need to be considered as contributors to protein content. All vesicular species have a range of densities, therefore isolation of a completely pure subcellular organelle in this way is impossible. Early endosomes, endoplasmic reticulum, mitochondria and lysosomes were shown to be co-isolated with autophagosomes, however peak fractions differed between organelles. Density fractions can therefore be selected in order to maximise autophagosome content while minimising the presence of other organelles. For example, mitochondria, endoplasmic reticulum, and lysosomes are the most populous organelles other than autophagosomes, however they all elute across heavier fractions. Therefore an earlier fraction (i.e. 5 or 6) will have a higher total number of autophagosomes compared to these other heavier organelles.

Further evidence for the use of fraction 6 for autophagosome investigation came from repeated isolation experiments. When band signal was normalised to the amount of protein loaded in each well, fraction 6 was repeatedly shown to be the most autophagosome dense.

Unlike whole cell lysate, LC3-I signal is often not visible in Western blots of isolated organelles. This gives evidence that organelles only are isolated through ultracentrifugation, and that smaller cytoplasmic-based proteins are washed out during the process. LC3-II is found ~15kDa on each blot, as it is in whole cell lysates where LC3-I is also present, giving confirmation that this band is due to LC3-II species only. On some occasions LC3-I does remain. It is possible that it could be sequestered within cytoplasm-containing organelles and therefore would co-isolate with these into fractions. Autophagosomes themselves sequester cytoplasm which could explain why LC3-I high fractions in are also LC3-II high. Other organelles that sequester cytoplasm include endosomes and endosomal markers could have been utilised in this case to see whether endosomes co-isolated with LC3-I high fractions.

LC3-II signal could also be effected by the presence of other organelles within each fraction. Endoplasmic reticulum is the site of protein synthesis and therefore would be involved in

the generation of pro-LC3. A paper by Wang et al. has described unprocessed pro-LC3 as having similar migration characteristics in western blot to LC3-II and therefore pro-LC3 contents in ER could contribute to the LC3-II signal in ER containing fractions. However, the pro-LC3 content of ER does not appear to be high as within fraction 8 and 9 where ER signal is high, LC3-II signal remains low and therefore the impact of pro-LC3 on the LC3-II signal appears to be minimal.

For organelle content of each fraction to be accurately determined, markers for each organelle need to be specific to each species. There is evidence that autophagosomes are created using the membranes of other organelles and therefore it is possible that markers of other organelles could be present. There is currently debate within the literature of the membrane source for autophagosomes. Hailey et al. showed LC3 localised with mitochondrial markers upon starvation of cells and that the membrane of LC3 positive organelles has been shown to be continuous with outer mitochondrial membranes[374]. This then allowed for the transfer of mitochondrial lipids and, to a lesser extent, protein to autophagosomes. Limited mitochondrial protein transfer was found, and although PHB1 (mitochondrial marker) was not studied, it is possible that the same selection of lipid/protein transfer occurred and that PHB1 remains

mitochondria specific, despite being a membrane source for autophagosomes. This would reduce the chance of mitochondria being incorrectly labelled in autophagosome high fractions. A more well-established theory is that autophagosomes are nucleated at the ER, at a side called the omegasome[375]. Here, scaffold proteins associate and nucleate the autophagosome, and the membrane gets elongated. As this region is high in phospholipid synthases, autophagosomes may be elongated from newly synthesised phospholipids[376,377], and not from ER associated phospholipids. There has not been any evidence of ER proteins being transferred to autophagosome membranes in this process. The golgi apparatus has also been investigated for its contribution to the formation of autophagosomes, as ATG9, a protein essential for autophagy, is found localised to the golgi membrane[345]. Further studies have shown that a subunit of the golgi apparatus, the conserved oligomeric golgi (COG) complex is involved in the early stages of autophagy[378], but appears to be through aiding localisation and signalling cascades rather than membrane contribution. Furthermore, freeze-fracture electron microscopy has been employed to show that autophagosomes membranes are protein-poor[379], giving less opportunity for other markers than LC3 to be present within the membrane.

Further evidence for the optimal density fraction for autophagosome content was found using small particle flow cytometry. Here, LC3 positive particles that were the correct size for autophagosomes (>500nM as determined by nano sizing beads) were found in fractions that correlate with fractions shown via western blot. The highest percentage for LC3 positive events were found in fraction 4 closely followed by fraction 6. Fraction 6 is repeatedly shown to be one of the highest LC3 containing fractions by western blot as well, showing concordance between techniques. Most LC3 containing fractions show a high percentage positive for LC3 (i.e. over 50%) which may be an over estimation of autophagosome purity, caused by the initial placing of B gate to give the highest LC3 signal. Ideally a gate would be placed around a single population that is distinct from the debris however due to the size of the events, this is not possible for this sample. This does however still allow for comparison between fractions. Fraction 5 shows an LC3+ percentage that is lower than expected, considering fractions are harvested from a continuous gradient and therefore should contain relatively similar contents to neighbouring fractions. Possible reasons for this include that the negative species elutes at a very precise density, or that the slight change in density in neighbouring fractions means that the negative fraction is

gated out using this gating strategy. Furthermore, as each fraction is labelled individually, it is possible that the amount of anti-LC3 antibody was saturated in this fraction, giving negative populations due to the unavailability of antibody. However this is unlikely to be true because counts of LC3 positive species are lower in this fraction than others with very small negative populations. This LC3 negative population could be identified by additional labelling of other organelles, similarly to the initial labelling carried out by western blot.

The localisation of citrullinated proteins in organelle fractions were also investigated, using a phenyl glyoxal based probe and anti-cit-HSP70 primary antibodies. Fractions with a high concentration of autophagosomes (i.e. fraction 6) correlated with fractions with a high concentration of citrullinated proteins, giving evidence that citrullinated proteins could be within these organelles. Other organelles have a peak concentration in different fractions suggesting that citrullinated proteins are not contained in these organelles as a main source. However, autophagosomes are known to interact with the endosomal compartment and early endosomes are shown to co-localise with autophagosomes in fractions. It is possible that endosomes are the source of citrullinated proteins however, this would allow loading of citrullinated epitopes to MHCII while autophagy is inhibited

and this was shown not to be the case in the study by Ireland et al[182].

Unfortunately, the specificity of the phenyl glyoxal probe was not fully characterised for this study. For future experiments, citrulline could be conjugated to a carrier protein of known molecular weight. This protein could be resolved by SDS-PAGE, alongside the carrier protein without conjugation and probed for with phenyl glyoxal. Binding to the citrulline-conjugated carrier protein only will indicate specificity.

As the phenyl glyoxal probe labels global citrullinated protein, cit-HSP70 would be expected to also be labelled by this method and therefore bands seen at similar points to the anti-cit-HSP70 antibody. Smears are visible on the phenyl-glyoxal treated western blot, which makes identification of particular bands more difficult, however bands in the early 20kDa and 50kDa region are visible and therefore could correspond to the proteins seen in the anti-cit-HSP70 treated western blot. This gives evidence that these are true citrullinated proteins being labelled in each individual experiment, as they corroborate.

HSP70 resolves at the 70kDa marker on western blots. Using the in-house anti-cit-HSP70 antibody, bands were seen at 21, 23, 56kDa. A band at 70kDa is not present suggesting that HSP70 is not present in these fractions and therefore would

not be found in autophagosomes in detectable amounts. The addition of citrulline is unlikely to change the position of the protein band within a western blot, as it only adds 1Da of weight. In any case, this would increase the size of the protein, not decrease as seen in this blot. The bands seen are therefore unlikely to be mature HSP70 protein. The anti-cit-HSP70 antibody is known to cross-react with other citrullinated proteins, therefore these bands could correspond to those different protein species. A peptide microarray study was carried out (unpublished) for crossreactivity. The antibody was shown to bind to 57kDa protein Vimentin which could correspond to the 57kDa protein on the western blot. No 23 or 21kDa proteins were found in this microarray study. Another possibility is that the antibody is detecting splice variants of cit-HSP70, although there isn't any evidence within the literature of HSP70 splice variants below the size of 62kDa[380]. As the antibody crossreacts, it's possible that the antibody could bind to splice variants of other protein species.

Further to the above work, organelle fractions were checked by electron microscopy to confirm whether autophagosomes can be identified. Autophagosomes have a characteristic double membrane vesicle structure which can be easily identified by electron microscopy, however they usually appear as electron dense organelles, both in whole cell and

isolated organelle imaging[371,381]. The isolated double membrane organelles in this study all appeared as electron lucent organelles. There is some evidence within the literature that autophagosomes can be electron lucent. In a study by Gao et al., LC3 positive, electron lucent, double membrane vesicles are identified and described as mature autophagosomes[382]. However mature autophagosomes will contain mostly cytoplasm which should cause some electron density. Other sources of double membrane organelles could be endosomes, or swollen mitochondria, although swollen mitochondria should have visible cristae which is not present in these images[344]. In LC3 labelled samples, LC3 is found localised to double membrane structures suggesting that these are autophagosomes or autophagosome-like structures. However LC3 was found at much of the other species within the sample. This corroborates with the flow cytometry data, which showed a high LC3-positive populations, but doesn't align with the known structural features of autophagosomes. It is possible that the processing of the organelle fractions may have caused changes in morphology. The process of fixing and embedding used for the sample is commonly used in autophagosome research[383], however alterations may have been caused in initial preparation of the organelle fractions. Firstly, the sample my not have been substantially washed

following the binding of quantum dots. This could lead to non-specific staining and the widespread staining seen amongst many organelle species. However not all staining appears to be non-specific as quantum dots are commonly seen at specific structures, such as membranes, and no dots are seen extra-organelle. It is possible that a mixture of specific and non-specific staining is seen. Furthermore, organelles are pelleted at high centrifugal speeds which could cause sheer stress and burst/fuse organelles, releasing organelle contents or changing morphology. This is one possible explanation for electron lucent and single membrane LC3 species.

Nevertheless, these data give indication of citrullinated proteins localised to autophagosomes, however further experimentation is required.

5. Using Autophagosomes as a Vaccine

5.1 Introduction

Autophagosomes are an established source of citrullinated proteins suitable for loading on to MHCII[182,384]. Therefore, in the setting of malignancy they could theoretically provide a source of novel epitopes for anti-cancer T-cell responses. This is particularly interesting as the stress responses, contributing to citrullination in the autophagosomal compartment, appears to be constitutively active in tumour cells, rather than the carefully regulated autophagy in normal cells, as indicated in previous chapters. As a consequence the continued production of citrullinated proteins in tumours and elevated levels of Cit-peptide epitopes presented by MHCII are an interesting therapeutic target.

Autophagosomes, as a source of citrullinated epitopes, should theoretically be able to induce a citrullinated specific response through vaccination. The intramuscular route favours adaptive T cell responses and therefore an autophagosome vaccine may benefit from this route to generate an anti-citrullinated epitope T cell response[385]. Autophagosomes, taken up by dendritic cells via phagocytosis due to their size[386], could enable citrullinated-epitopes to be processed and loaded onto both Class II and Class I, via cross presentation. The presence of activating signals could then activate DC to migrate to local

draining lymph nodes to encounter naïve T cell [387,388,389]. Accordingly, citrullinated epitope-specific T cells have been shown to be of the CD4 lineage. For this to take place, autophagosomes, phagocytosed by immature DC (iDC), are targeted to the MHCII loading compartment (MIIC) where citrullinated proteins are partially degraded, loaded on MHCII, then displayed on the membrane for specific T cell activation[390,391]. Activated CD4 T cells then migrate away from the lymph node to carry out their effector functions against tumour cells. Different subsets of DC may be better/worse for inducing an anti-tumour response due to slightly different effector functions, i.e. cDC2 cells are more specialised for CD4 activation[392]. BMDC have been used to induce anti-tumour responses in other studies, and provided they are activated, give robust anti-tumour activity[393]. BMDC have also been shown to have high expression of MHC-II[394] which is important for CD4 stimulation. Anti-citrullinated epitope specific T cell responses have previously been shown to be fulfilled by CD4 cells[183], therefore BMDC appear to be relevant to the experiments described in this chapter.

There is some evidence that subcellular organelles can be a source of anti-cancer epitopes that induce an immune responses. In a study by Twitty et al. isolated extracellular autophagosomes were used to activate tumour-specific T cells

that conferred protection against homologous and non-homologous tumour challenge *in-vivo*[395]. Extracellular LC3-II positive vesicles are generated through secretory autophagy which may have different cargo to classical autophagy[360]. In the study, autophagosomes were isolated by firstly treating tumour cells with proteasome inhibitor Bortezomib, the extracellular autophagosomes released were then purified using centrifugation. Antigen presenting cells (APC) were pulsed with autophagosomes and used to prime T cells against tumour targets. Autophagosome primed T cells showed anti-tumour response against homologous tumours, from which autophagosomes had been isolated, and non-homologous tumours, suggesting that autophagosomes also conferred a broader target specificity. This effectively translated *in-vivo* where autophagosome vaccination conferred protection from tumour challenge. The hypothesised mechanism of action was interference in proteasomal degradation causing short-lived protein (SLiPs) and defective ribosomal product (DRiPS) stabilisation with direction to autophagosomes as an alternative degradation path. DRiPS comprise a significant proportion of the proteins loaded onto MHCI, therefore APC activated against tumour specific DRiPs contained within tumour autophagosomes could elicit CD8 T cell responses.

Substantially more work has been done on the use of tumour exosomes as an anti-tumour vaccine. Exosomes are created when intracellular endosomes, or multivesicular bodies (MVBs) fuse with the cell membrane and are then released extracellularly[396]. They are comprised of cytosolic content, as well as membrane proteins and lipids, extracellular proteins, and nucleic acids. The contents are therefore similar to that of the parent cell and as such can contain multiple epitopes specific for the cell of origin. Multiple studies have successfully used exosomes to target the parent tumour cell from which it came from, both as a standalone vaccine[397–400], or as a exosome-fed dendritic cell vaccine[401]. Additional work has shown that exosomes taken from tumour antigen-experienced DC can also induce an anti-tumour T cell response[402,403].

Tumour exosomes have also been reported to be immunosuppressive against T lymphocytes, natural killer (NK) cells, monocytes, macrophages, and DC, and therefore would be an inferior choice for use as a cancer vaccine[404-405]. Their inhibitory action is mainly due to cell ligands on the surface of exosomes. For example, the presence of TGFβ both inhibits NK cells[404], and drives myeloid precursors to myeloid-derived suppressor cell (MDSC)[406]. Suppressive ligands such as MICA, MICB, and ULBP1/2, or FasL and PD1-L inhibit/cause apoptosis in NK cells and T cells respectively[407–409]. Furthermore, CD39

and CD73 found on the surface of endosomes cause suppressive T cell phenotypes through ectonucleotidase cascades[410]. With this in mind, if tumour exosomes are already in circulation, exosome vaccination may not overcome the suppressive effects that are already exerted[405].

Relating to the above highlighted research and the knowledge on how citrullinated proteins are formed, there is reason to believe that multiple citrullinated-tumour epitopes exist within autophagosomes, and autophagosomes or their contents be used to activate citrullinated epitope-specific T cells against tumour cells. This was primarily investigated using ELISpot assays to determine T cell activation of citrullinated epitope-specific T cells, in response to citrullinated epitope within B16 derived autophagosomes, as shown in figure 5.1.

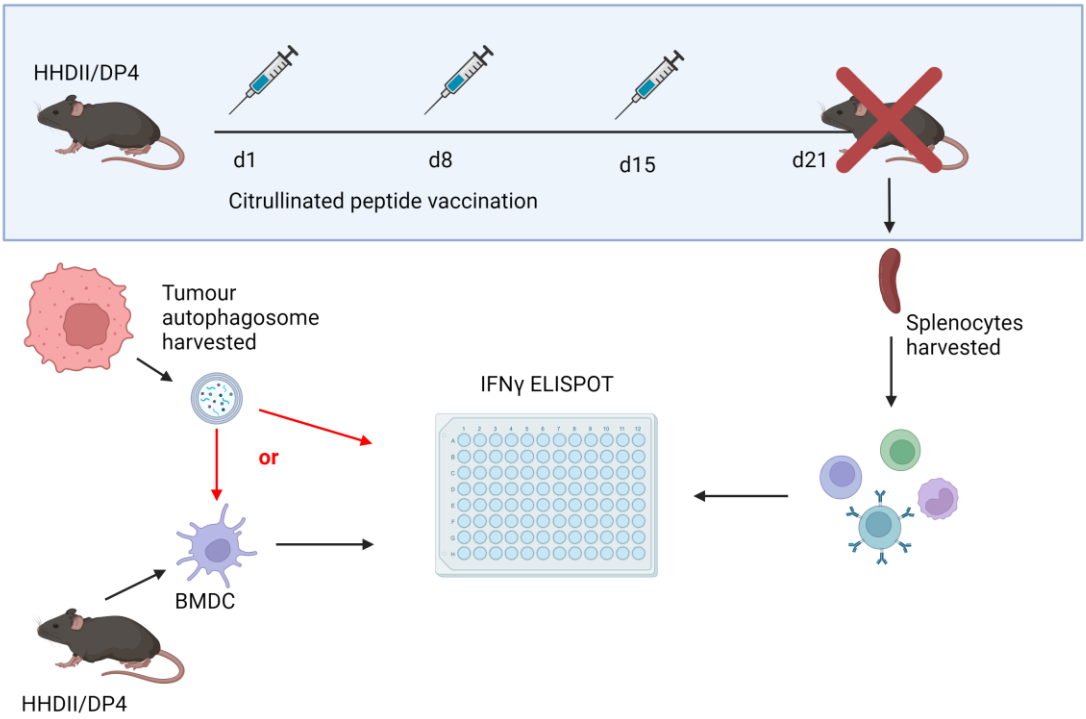

Figure 5.1 Schematic of IFNγ ELISpot for detection of citrullinated epitopes in tumour autophagosomes.

HHDII/DP4 mice were vaccinated on day 1, 8, and 15 with a citrullinated peptide vaccine. Mice were culled on day 21 and their splenocytes harvested. Splenocytes were then co-cultured for 40 hours with either B16 tumour derived autophagosomes, or HHDII/DP4 mouse bone marrow derived dendritic cells fed with B16 tumour derived autophagosomes (as detailed in the below figures). T cell activation was determined by IFNγ spot count. Created with BioRender.com.

5.2 Aims

This chapter seeks to confirm the presence of citrullinated proteins within autophagosomes through their ability to stimulate an anti-citrullinated epitope T cell response.

5.3 Results

5.2.1 Autophagosomes alone are not sufficient to generate immune responses

Splenocytes from cit-peptide plus CPG and MPLA immunised HHDII/DP4 mice were used to asses for cit-peptide specific T cell responses, following co-culture with B16F1 derived autophagosomes. Two mice out of three showed low levels of IFNγ positive cells (figure 5.2.A and B) following autophagosome treatment. There was little difference between test wells and negative control wells, and all were markedly below IFNγ produced by positive control.

The experiment was repeated with a 20-fold lower dose of the autophagosome preparation, (0.5ug/well) (figure 5.2.C and D). Again, there was no increase in IFNγ above the baseline for autophagome-fed splenocytes, irrespective of the treatment prior to harvesting autophagosomes. Differences between media controls and autophagosome treated splenocytes were non-significant.

Figure 5.2

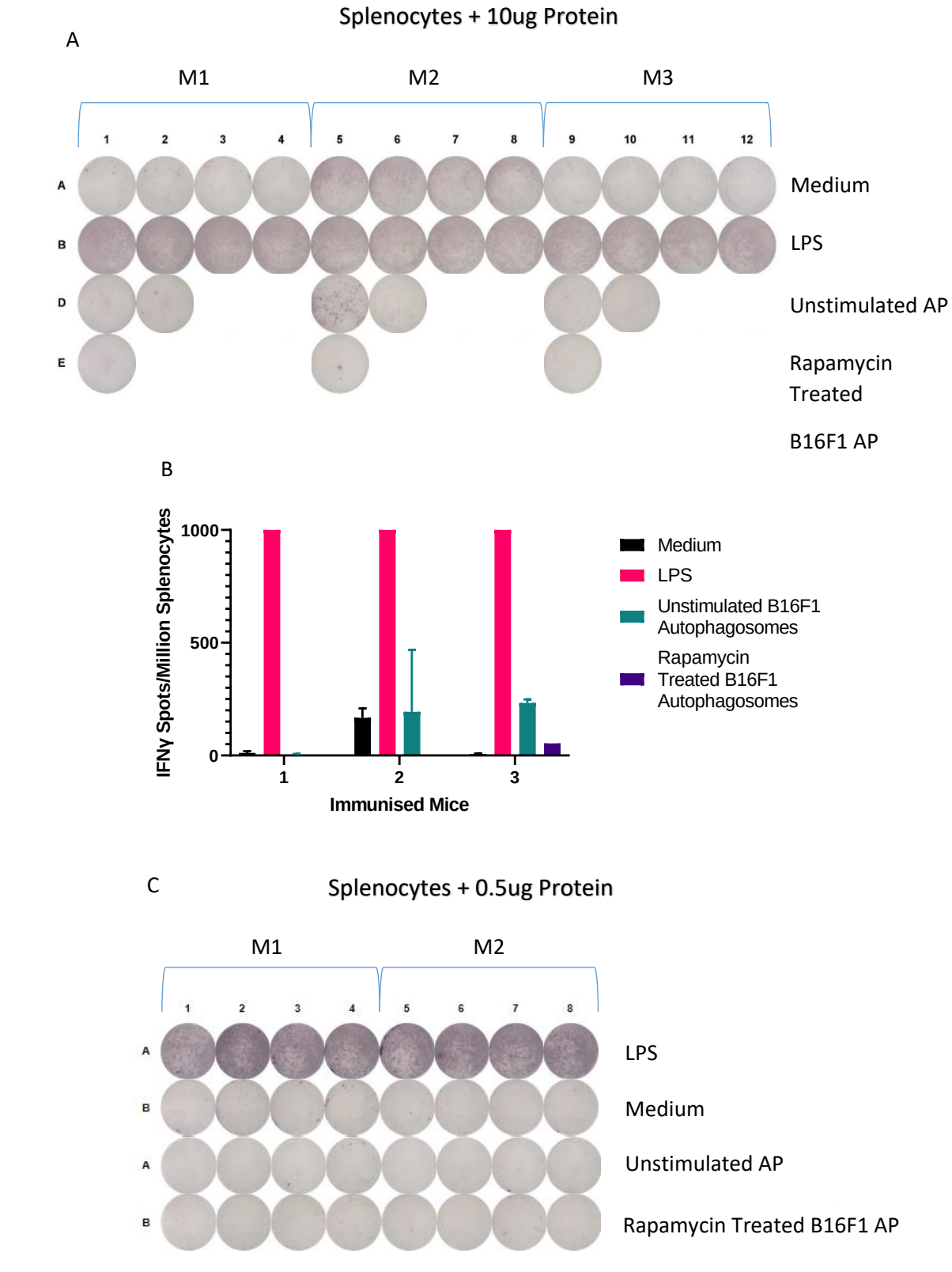
A
Splenocytes + 10ug Protein
M1
M2
M3
1
2
3
4
5
6
7
8
9
10
11
12
A
B
D
E
Medium
LPS
Unstimulated AP
Rapamycin Treated B16F1 AP
B
IFNγ Spots/Million Splenocytes
1000
500
0
1
2
3
Immunised Mice
Medium
LPS
Unstimulated B16F1 Autophagosomes
Rapamycin Treated B16F1 Autophagosomes
C
Splenocytes + 0.5ug Protein
M1
M2
1
2
3
4
5
6
7
8
A
B
A
B
LPS
Medium
Unstimulated AP
Rapamycin Treated B16F1 AP

D

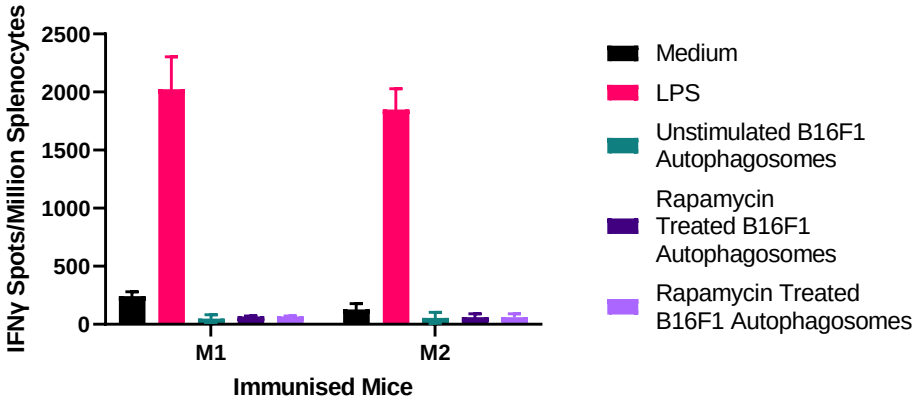

Figure 5.2 Activation of T cells after treatment with autophagosome preps. Splenocytes were harvested from mixed cit-peptides plus CPG and MPLA immunised mice for use in an IFNγ ELISPOT at $5x10^5$ cells per well. A) IFNγ production by splenocytes from three independent mice (M1, M2 and M3). A positive control of LPS treated and a negative control of media treated splenocytes were used. Autophagosome (AP) preps were given at 10µg/well in duplicate or singlicate and co-cultured with splenocytes for 40 hours to test for immunogenicity. Unstimulated AP refers to autophagosomes harvested from resting B16F1 cells cultured *in-vitro*. Rapamycin treated B16F1 AP refers to autophagosomes harvested from rapamycin treated B16F1 cells cultured *in-vitro* B) a graphical representation of the spot/millions splenocyte counts from the plate shown in A, n=3, statistical analysis carried out by two way ANOVA with Tukey's multiple comparison test. C) An IFNγ capture ELISpot of splenoctyes from two independent mixed cit-peptides plus CPG and MPLA immunised HHDII/DP4 mice (M1 and M2). LPS and media treated cells were used as a positive and negative control, respectively. AP preps were given at 0.5µg/well in quadruplet. D) A graphical representation of the IFNγ spot count/million splenocytes from the plate shown in figure C, n=2, statistical analysis carried out by two way ANOVA with Tukey's multiple comparison test.

5.3.2 Optimising bone marrow derived dendritic cells for autophagosome uptake and activation

Feeding autophagosomes in a 40hr culture with splenocytes failed to generate a T cell response. Splenocyte culture contain a mixture of APCs, not all of which are activated. As professional APC may be required for autophagosome peptide presentation for T cell activation, bone marrow cells were purified from HHDII/DP4 mice and differentiated to dendritic cells. Immature dendritic cells (iDC) were then treated with autophagosome preps and activated for use in a splenocyte co-culture for T cell activation.

In the first instance, BALB/c or HHDII/DP4 mice were used for optimisation bone marrow cell differentiation to dendritic cells, and for the uptake of autophagosomes by DC. The development of immature dendritic cells from bone marrow cells was first tested by determining the expression of CD11c from harvested cells. As shown in figure 5.3.B the cell population showed an increase in CD11c expression suggesting that cells had differentiated.

Mature DC (mDC) are required for full T cell activation and therefore the optimal concentration of LPS was determined in order to achieve this. CD80 was used as a marker for activation, as this co-stimulation molecule is upregulated when

dendritic cells are activated. As shown in figure 5.3.C, in all conditions, CD80 expression was increased. The addition of LPS to iDC increased CD80 expression ~1.6-fold and the differences in expression between each concentration of LPS were small. The addition of IFNγ did not appear to have an additive effect on CD80 expression, compared to LPS alone. In further experiments, 300ng/ml LPS was used to activate dendritic cells, unless otherwise stated, due to achieving the highest level of CD80 expression.

An uptake assay was used to determine the correct time point for the uptake of particles from within the media. 40kDa FITC-dextran was used to determine this (figure 5.3.D). A ~2-fold increase in FITC fluorescence between cells cultured at 4°C and 37°C was seen as early as 30 minutes in culture, suggesting energy dependent uptake of particulate antigen had taken place within this time point.

Figure 5.3

A

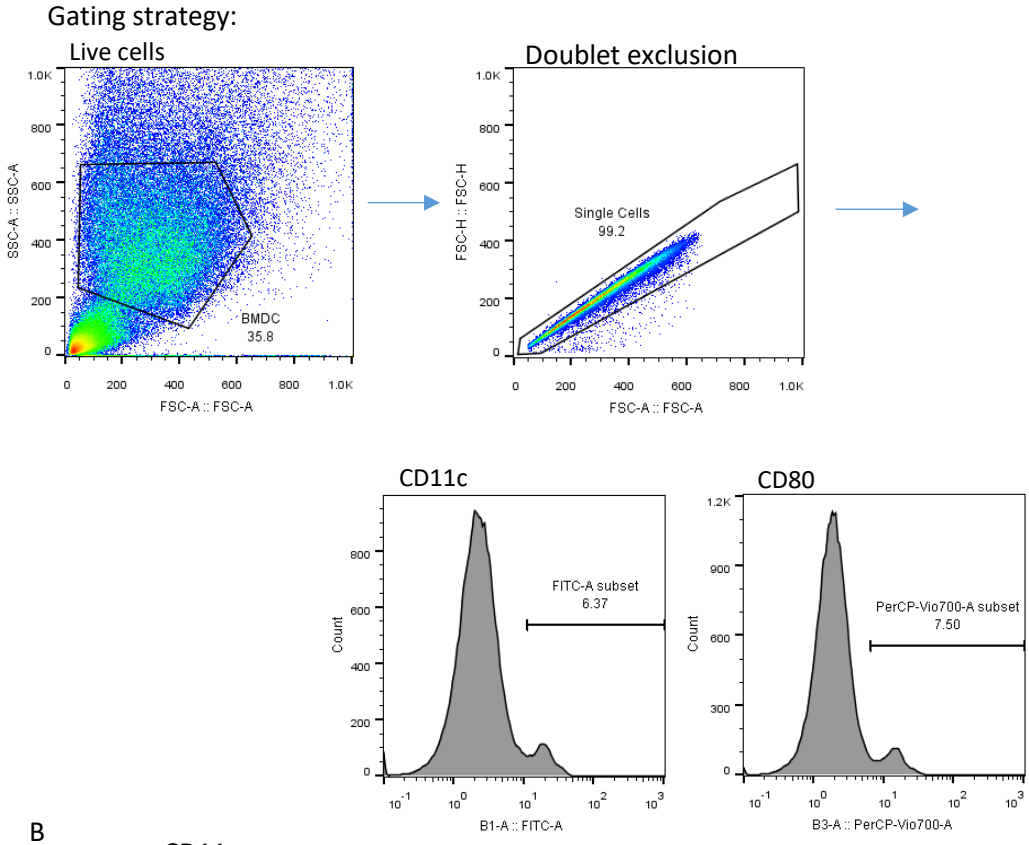

B

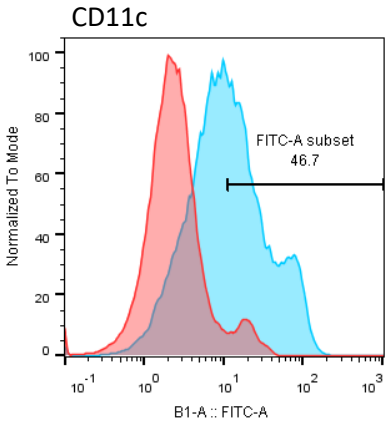

C

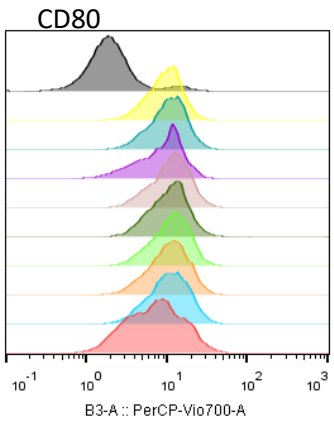

	Condition	MFI
	Isotype Control	1.91
	300ng/ml LPS + 100ng/ml IFNγ	10.1
	100ng/ml LPS + 100ng/ml IFNγ	11.1
	100ng/ml IFNγ	9.25
	1000ng/ml LPS	12.4
	500ng/ml LPS	11.9
	300ng/ml LPS	12.3
	100ng/ml LPS	11.3
	50ng/ml LPS	11.2
	iDC	7.16

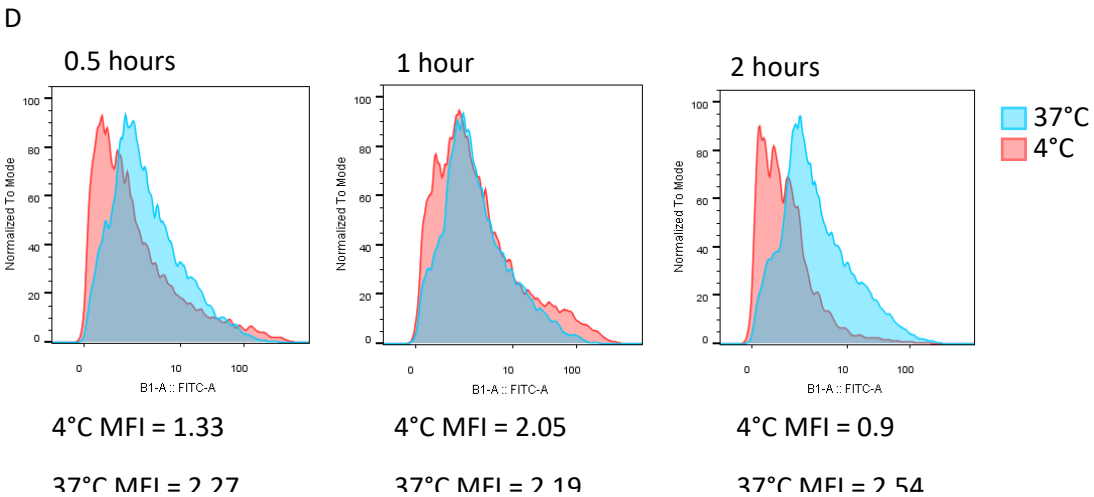

Figure 5.3 Differentiation and activation of dendritic cells from bone marrow cells and uptake of FITC-Dextran. A) gating strategy for the determination of positive fluorescence for FITC (anti-CD11c) and PerCP/Cy5.5 (anti-CD80) conjugated antibodies. Live cells are gated on initially, followed by a doublet exclusion, followed by gating for positive fluorescence using an isotype control antibody. B) The gating strategy in A) was applied to cells labelled with an IgG isotype control-FITC (red) and IgG anti-CD11c-FITC (blue), showing a histogram of FITC fluorescence for both populations. C) PerCP.Cy5.5 fluorescence of cells labelled with a PerCP/Cy5.5 control antibody (grey) or anti-CD80-PerCP/Cy5.5 (all other conditions), after treatment with LPS and/or IFNγ. Median fluorescence intensity (MFI) is given for each condition. D) histograms showing FITC fluorescence for bone marrow derived dendritic cells treated with FITC-Dextran for different time points at both 4°C (red) and 37°C (blue). Cell and doublet gating was applied as detailed in A.

5.3.3 Feeding Autophagosomes to bone marrow derived DC does not alter cell-viability or activation.

To account for any adverse impact of AP on the viability of DC, cell death and cell activation states were determined, following autophagosome treatment. Bone marrow derived dendritic were fed with 15µg of autophagosome-enriched organelle fraction and cell death determined (fig 5.4A-B). DC remained viable irrespective of exposure to autophagosomes, peptide, or negative control. In contrast exposure of DC to heat resulted in pronounced cell death. The autophagosomal preps could therefore be taken forward for further experimentation.

The expression of CD80 was investigated to determine the activation state of LPS and autophagosome-treated BMDC. As expected, resting immature DC had low expression of CD80 however on exposure to LPS CD80 expression was markedly increased suggesting successful maturation. On treatment with LPS alone, CD80 expression increased 2-fold compared to iDC control. Treatment with LPS and organelle preparations showed similar CD80 expression to LPS treatment alone and therefore maturation was unaffected by the addition of organelles.

Figure 5.4

A

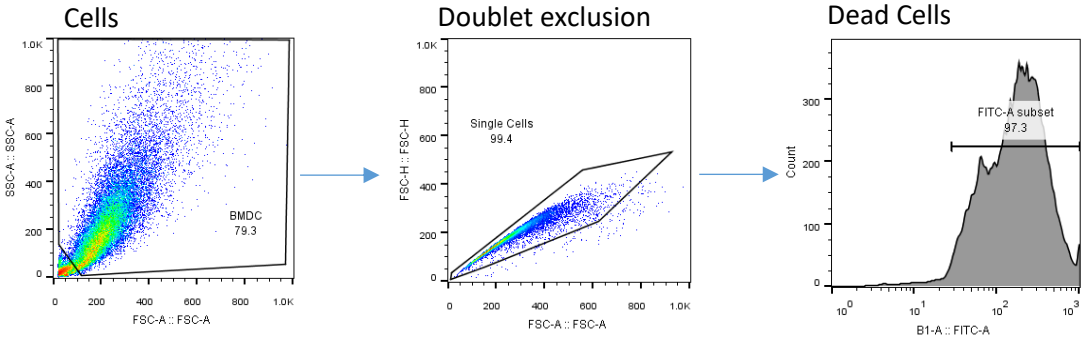

B

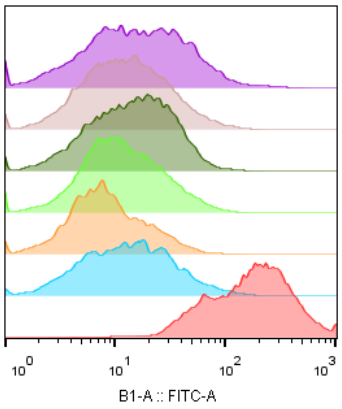

	Condition	MFI	% positive
	DC only	15.2	30
	DC + Stimulated B16F1 Fraction 7	12.1	17.9
	DC + Stimulated B16F1 Fraction 6	14.4	21.4
	DC + Unstimulated B16F1 Fraction 7	11	15
	DC + Unstimulated B16F1 Fraction 6	7.83	8.24
	DC + Peptide	13	21.1
	Dead Cells	175	97.3

C

CD11c+ and CD80+ isotype control gating of fed dendritic cells

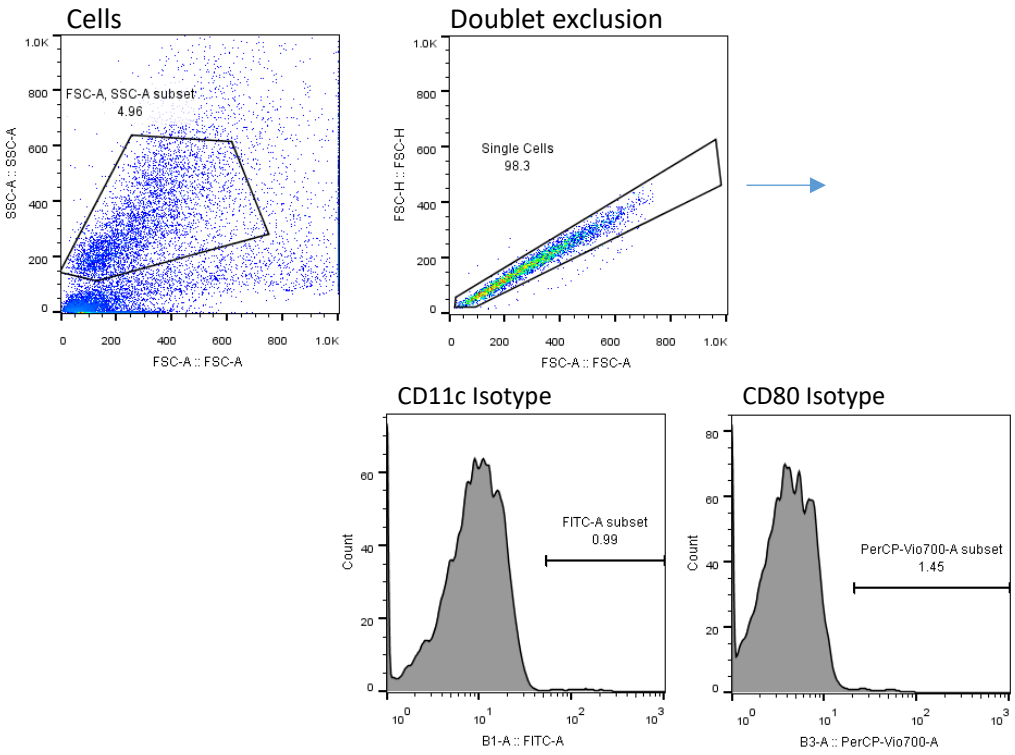

D

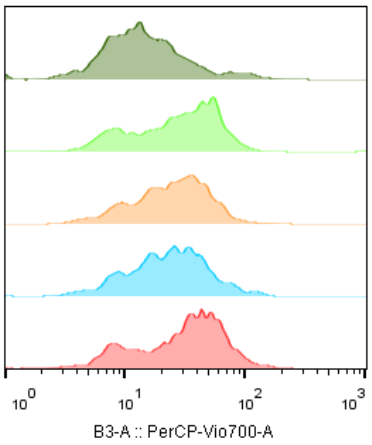

Sample	MFI for anti-CD80-FITC	% positive for CD80 expression
iDC	13.3	28.3
mDC	29.5	78.7
mDC + Stim B16 Fraction 6	25.2	82.3
mDC + Unstim B16 Fraction 6	23.7	80.7
mDC + Unstim B16 Fraction 4	33.9	81.3

Figure 5.4 Cell death assay using zombie green staining to determine the effects of autophagosome preps on cell viability. DCs fed with 15ug of organelle fractions from rapamycin and chloroquine stimulated or unstimulated B16F1 cells, or with 35ug of citrullinated peptide. A) A positive control of dendritic cells heated at 65°C for 10mins was used to determine the gating strategy for FITC negative (Live) cells, using zombie green stain. B) Zombie Green staining for dead cells for each DC condition. Median fluorescence intensity (MFI) and % of positive cells (as determined by the gating in A) for each condition is shown. C) Gating strategy for cells positive for FITC and PerCP/Cy5.5 fluorescence. Gating was placed using an isotype control antibody for negative fluorescence. D) CD80 expression in CD11c+ cells in each condition, as determined by flow cytometry and anti CD80-PerCP/Cy5.5 labelling. n=1

5.3.4 Autophagosomes uptake is not detectable by flow cytometry

To show that autophagosomes had been taken up by DC, an uptake assay was carried out using fluorescently labelled autophagosomes with flow cytometry and confocal microscopy.

Following culture of iDC with labelled autophagosomes, a marginal increase in LC3 positive species was seen in iDC cells and mDC cells showed a 4-fold increase in LC3 positive fluorescence suggesting that a fraction of cells may have taken up autophagosomes. However, following observation of cell images, no punctate areas of fluorescence were seen in iDC populations, as would be characteristic for autophagosomes. There was no clear difference in the amount of LC3 staining in DC fed with labelled vs unlabelled autophagosomes (Fig 5.5.D). Therefore, it was not possible to demonstrate whether autophagosomes had been phagocytosed by a small number of cells using imaging flow cytometry.

These techniques showed that autophagosomes may be taken up by DC but the numbers of autophagosomes available, the detection technique and/or the timing of the data collection may limit our ability to detect these events.

Figure 5.5

A.

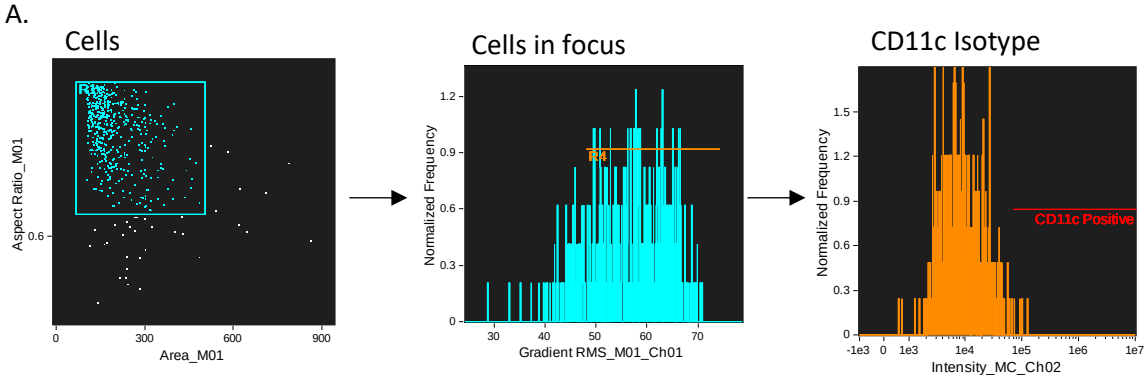

B.

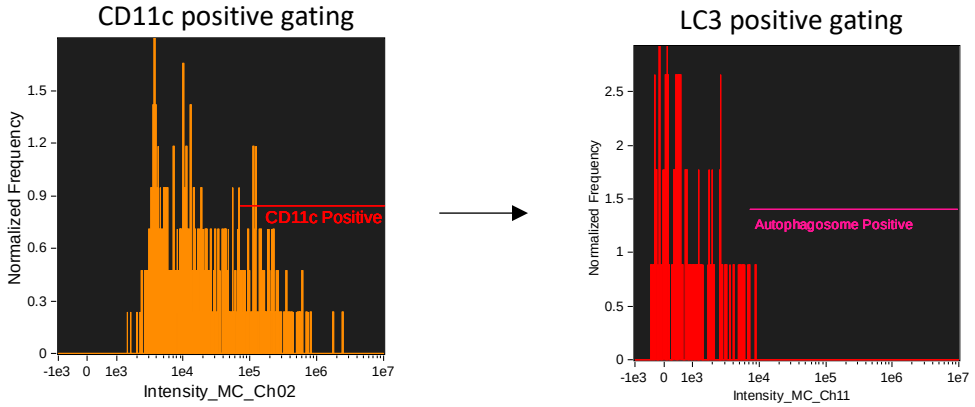

Intensity_MC_Ch02

Population	Count	%Gated	Mean	Std. Dev.
R4 & R1	423	100	79543.81	185629
CD11c Positive & R4 & R1	113	26.7	251715.66	297115.47

Intensity_MC_Ch11

Population	Count	%Gated
CD11c Positive & R4 & R1	113	100
Autophagosome Positive & C...	1	0.88

C. **iDC + Autophagosomes**

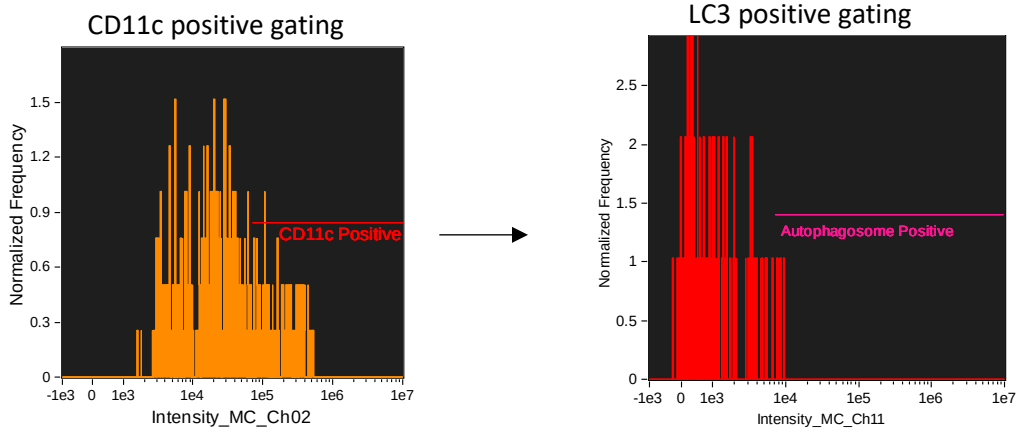

Intensity_MC_Ch02

Population	Count	%Gated	Mean	Std. Dev.
R4 & R1	396	100	65825.87	99701.97
CD11c Positive & R4 & R1	97	24.5	203969.55	120528.47

Intensity_MC_Ch11

Population	Count	%Gated	Median
CD11c Positive & R4 & R1	97	100	929.82
Autophagosome Positive & C...	4	4.12	8327.11

D. **mDC + Autophagosomes**

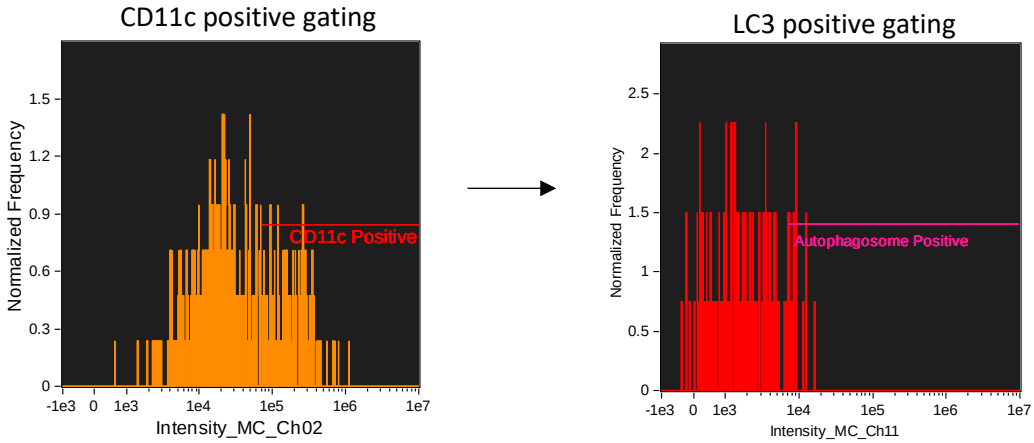

Intensity_MC_Ch02

Population	Count	%Gated	Mean	Std. Dev.
R4 & R1	422	100	81185.17	121477.76
CD11c Positive & R4 & R1	133	31.5	208455.51	150249.01

Intensity_MC_Ch11

Population	Count	%Gated	Median
CD11c Positive & R4 & R1	133	100	1705.29
Autophagosome Positive & C...	16	12	8929.48

Figure 5.5 Flow cytometry data of autophagosome uptake by dendritic cells. A) Gating strategy for CD11c positive single cells, using FITC isotype control antibodies for gating out the negative population. B) Gating strategy for LC3 positive fluorescence (autophagosomes), using dendritic cells fed with autophagosomes labelled with an AF647 isotype control antibody as negative fluorescence. C) iDC cells fed with anti-LC3-AF647 labelled autophagosomes, gated on CD11c and autophagosome positive events. D) mDC cells fed with anti-LC3-AF647 labelled autophagosomes, gated on CD11c and autophagosome positive events.

5.3.5 Fluorescent puncta evident following treatment of BMDC with fluorescently labelled autophagosomes and detection by confocal microscopy

Events positive for LC3, as determined by the gating described in figure 5.5, can be viewed as an image to determine the subcellular locality of the fluorescent signal. Figure 5.6 shows cells that were positive for CD11c and LC3 fluorescence.

iDC fed with labelled autophagosomes showed similar fluorescence to the isotype control, with only four events found to be both CD11c and LC3 positive (fig 5.6.B). No punctate fluorescence were evident, therefore there was inconclusive evidence for autophagosome uptake.

In fed mDC cells, punctate LC3 fluorescence was seen in cell images 37, 137, 157, 195, and 559 (fig 5.6.C). This represents 3.8% of the CD11c positive events and therefore found at very low frequencies within the population. Due to the punctate nature of the fluorescence, this could be due to the uptake of fluorescently labelled LC3-II on autophagosomes.

Phagocytosed autophagosomes were observed in the cytoplasm of iDC by confocal microscopy, however fluorescent puncta were relatively rare events (figure 5.6.E). When DC were treated with autophagosome low organelle fraction 4,

cells showed no LC3 positive species within the cell. Organelle fraction 7 (autophagosome high) treated dendritic cells showed LC3 puncta (irrespective of treatment prior to harvesting autophagosomes), suggesting that autophagosomes had been phagocytosed by these cells, however cells positive for LC3 fluorescence were rare within the population.

Figure 5.6

A.

Isotype-Labelled Autophagosome-fed iDC

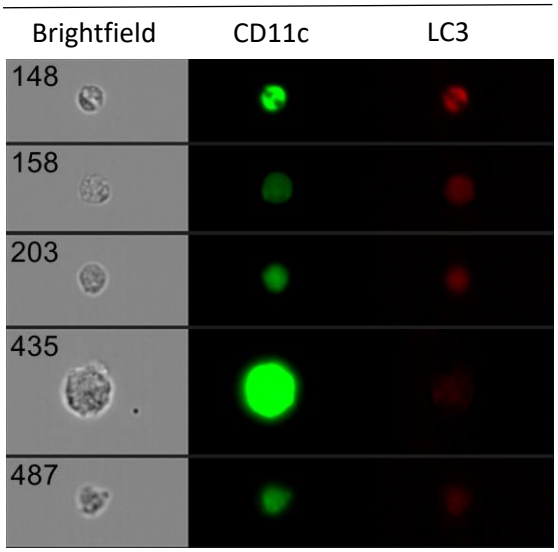

B.

Autophagosome fed iDC

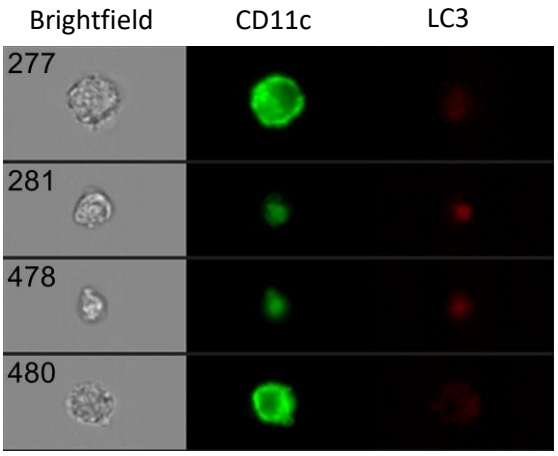

C.

Autophagosome fed mDC

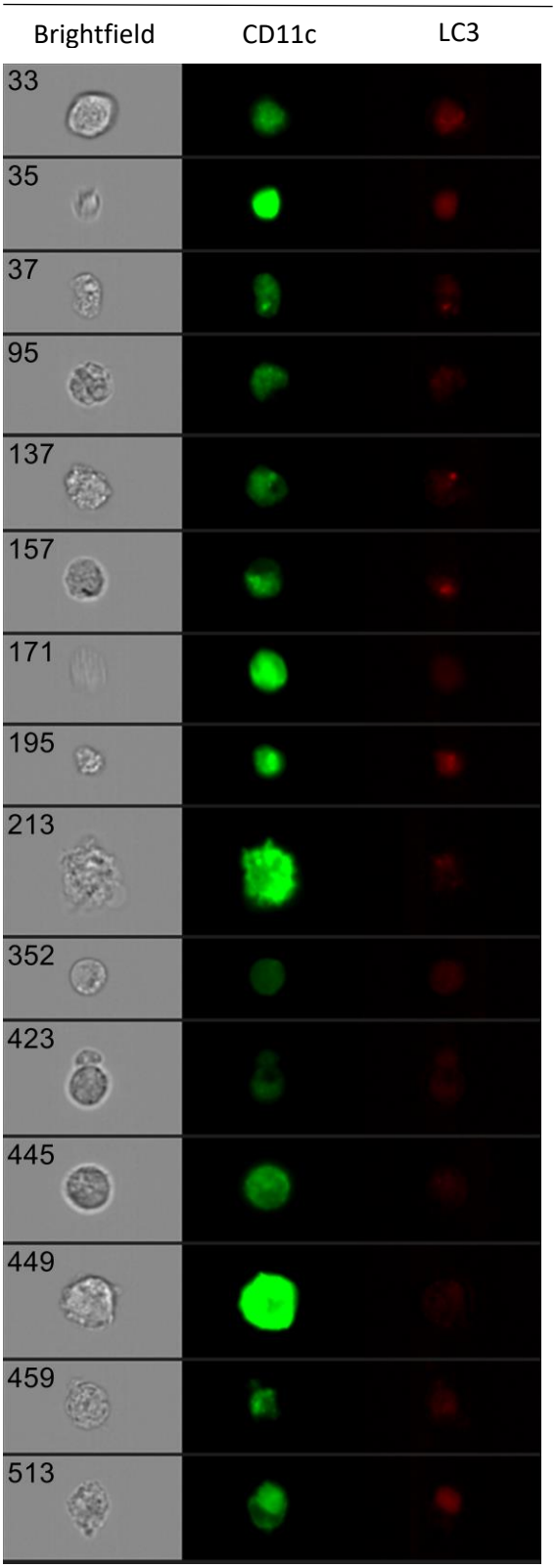

D.

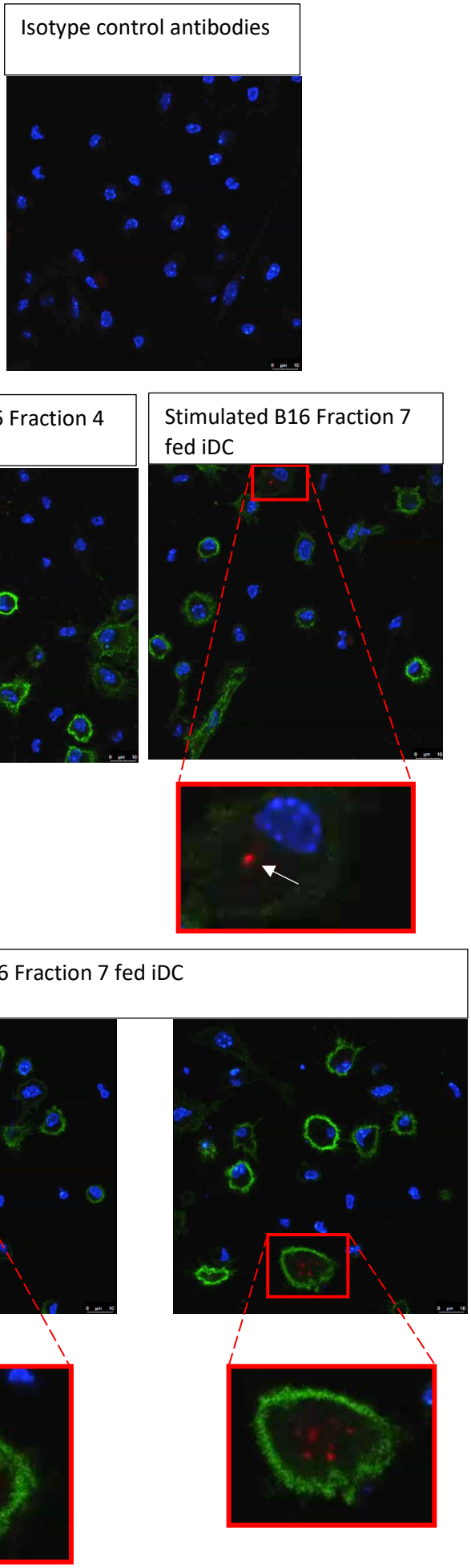
Isotype control antibodies
Stimulated B16 Fraction 4 fed iDC
Stimulated B16 Fraction 7 fed iDC
Unstimulated B16 Fraction 7 fed iDC

Figure 5.6. Cell images of autophagosome fed BMDC. A-C) BMDC positive for CD11c and LC3 fluorescence, as determined by the gating strategy in figure 5.5. A) iDC fed with autophagosomes labelled with isotype control antibody. B) iDC fed with autophagosomes labelled with anti-LC3 antibody. C) mDC fed with autophagosomes labelled with anti-LC3 antibody D) Confocal images of organelle fraction fed iDC preps with labelled nuclei (blue), CD11c (green) and LC3 (Autophagosomes) (red). Isotype control antibodies for FITC and AF647 were used as a control for non-specific binding.

5.3.6 Careful processing of BMDC is required for observing differences from controls

Autophagosome uptake experiments were largely inconclusive. Autophagosome treated dendritic cells were therefore used to induce citrullinated peptide-specific T cell response to confirm the presence of citrullinated peptide uptake from autophagosome treatment.

Bone marrow was harvested from HHDII/DP4 mice and differentiated to iDC. Expression of CD11c was shown to be 26.8% positive (figure 5.7.B), which is lower than previously seen. However, CD11c antigen did increase 2.5 fold suggesting differentiation to BMDC. Detection voltages were not optimal and therefore events from debris may be included in cellular events, decreasing CD11c positive percentages.

Autophagosome treated DCs were co-cultured with splenocytes harvested from HHDII/DP4 mice, immunised with mixed cit-peptides (SNAPvax formulation) and T cell activation determined (figure 5.7.C and D). Robust T cell activation was seen in all DC treatment conditions, which was similar to or exceeding that of positive control. DC treated with unstimulated B16 fraction 7 showed a lower IFNγ spot count, however the well images show a high level of activation, which has caused individual spots to merge together, and therefore

spot count is an underestimation of activation. However, the negative control group also generated a high level of T cell activity, suggesting that the activity from fed dendritic cells was not due to antigen specific T cell activation. All treated mDC groups were not significantly different to mDC only.

iDC and mDC populations alone, differentiated from bone marrow of HHDII/DP4 mice, were tested to see if dendritic cell LPS treatment increases T cell activation (figure 5.7.G-H). mDC populations, again, were shown to cause high levels of T cell activation, similar to that of the positive control, suggesting that DC LPS treatment alone had caused non-specific T cell activation. iDC populations were expected to show activity similar to the negative control however an increase in T cell activation was observed. Nevertheless, mDC caused a significant increase of activated T cells compared to iDC ($p<0.0001$). Based on these data, extra washing steps were added to future protocols in an attempt to reduce the non-specific activation of T cells through trace amounts of LPS.

Figure 5.7

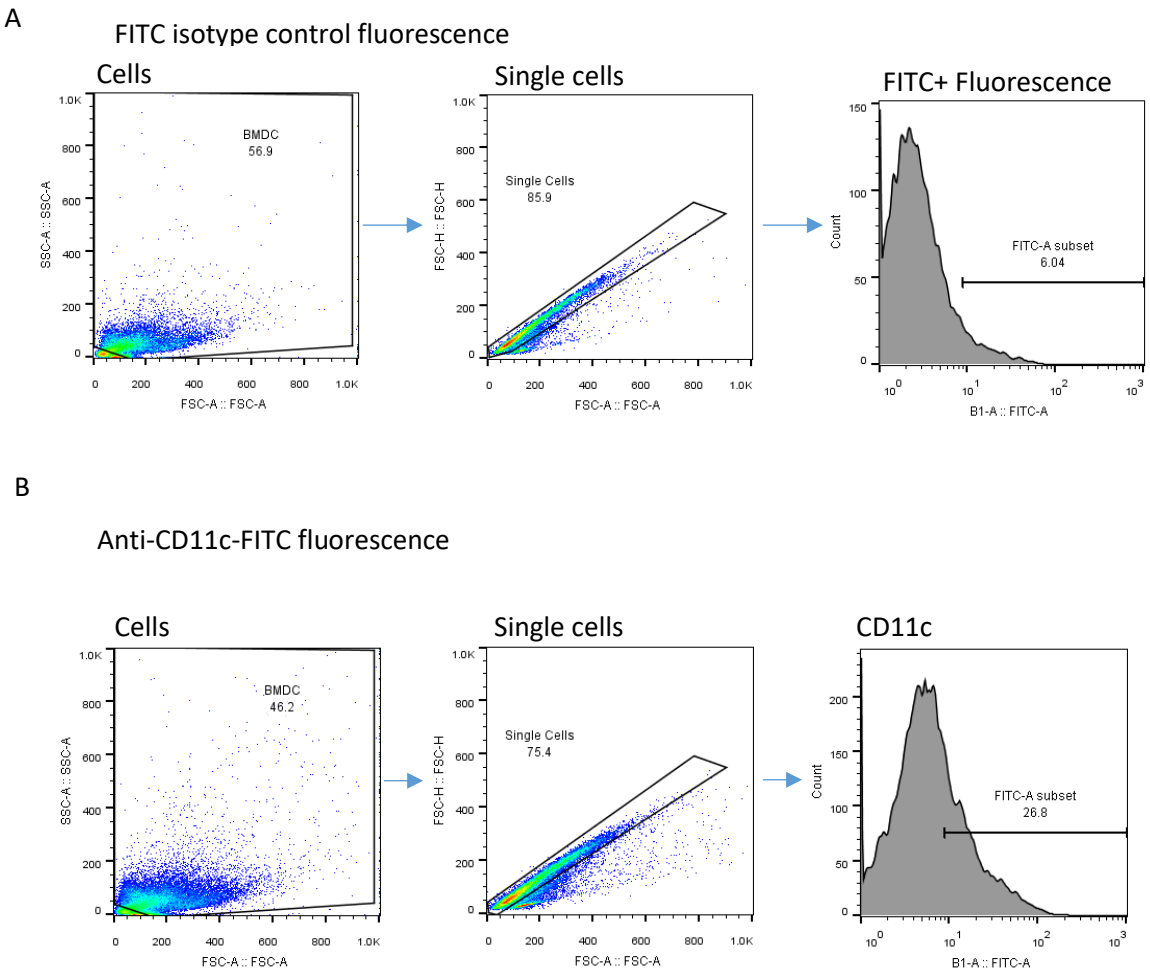
A
FITC isotype control fluorescence
Cells
Single cells
FITC+ Fluorescence
BMDC
56.9
Single Cells
85.9
FITC-A subset
6.04
SSC-A :: SSC-A
FSC-A :: FSC-A
FSC-H :: FSC-H
Count
B1-A :: FITC-A
B
Anti-CD11c-FITC fluorescence
Cells
Single cells
CD11c
BMDC
46.2
Single Cells
75.4
FITC-A subset
26.8

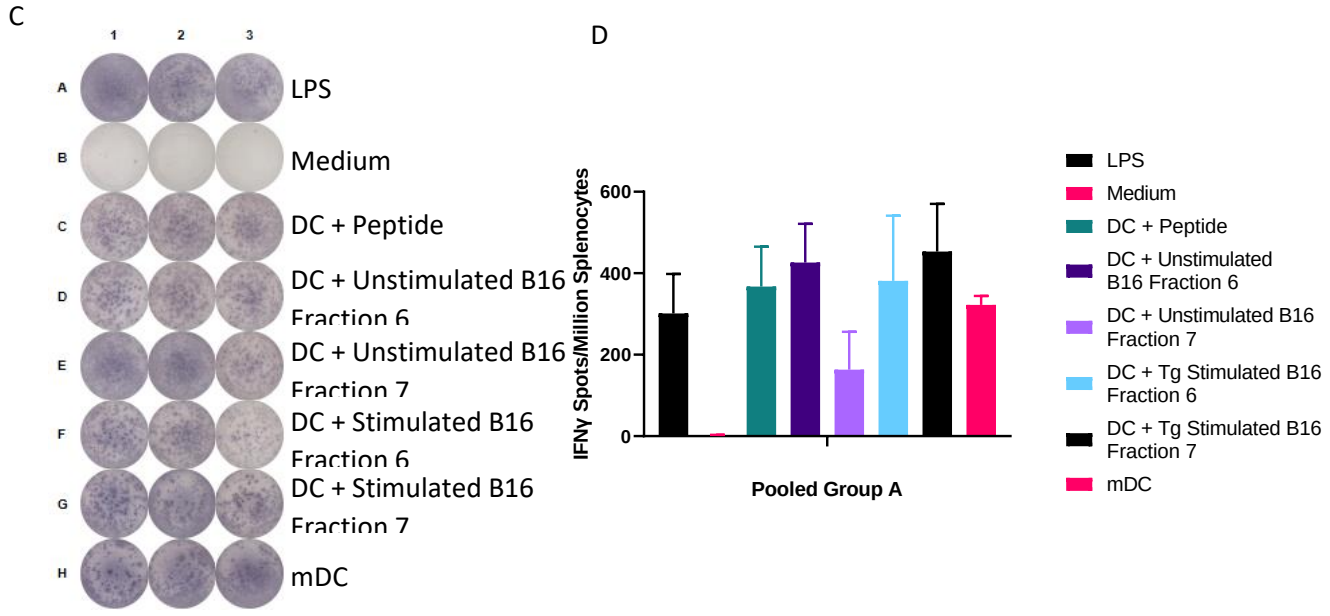
C
1
2
3
A
LPS
B
Medium
C
DC + Peptide
D
DC + Unstimulated B16 Fraction 6
E
DC + Unstimulated B16 Fraction 7
F
DC + Stimulated B16 Fraction 6
G
DC + Stimulated B16 Fraction 7
H
mDC
D
IFNγ Spots/Million Splenocytes
600
400
200
0
Pooled Group A
LPS
Medium
DC + Peptide
DC + Unstimulated B16 Fraction 6
DC + Unstimulated B16 Fraction 7
DC + Tg Stimulated B16 Fraction 6
DC + Tg Stimulated B16 Fraction 7
mDC

E

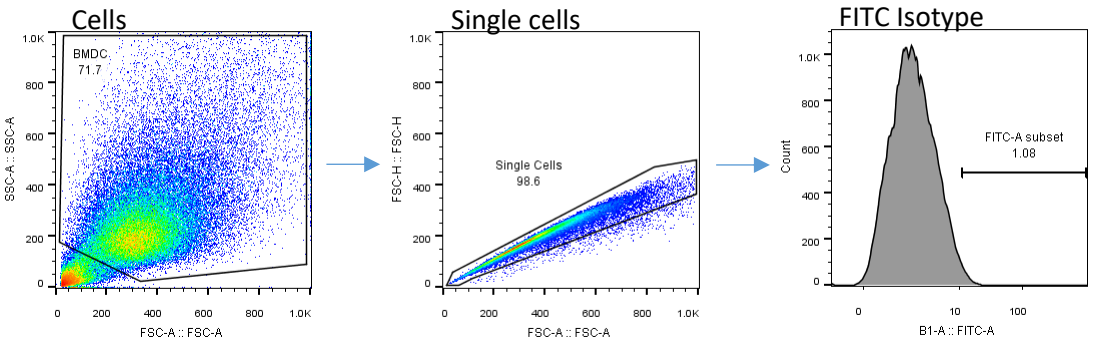
Cells
BMDC
71.7
SSC-A :: SSC-A
FSC-A :: FSC-A
Single cells
Single Cells
98.6
FSC-H :: FSC-H
FSC-A :: FSC-A
FITC Isotype
FITC-A subset
1.08
Count
B1-A :: FITC-A

F

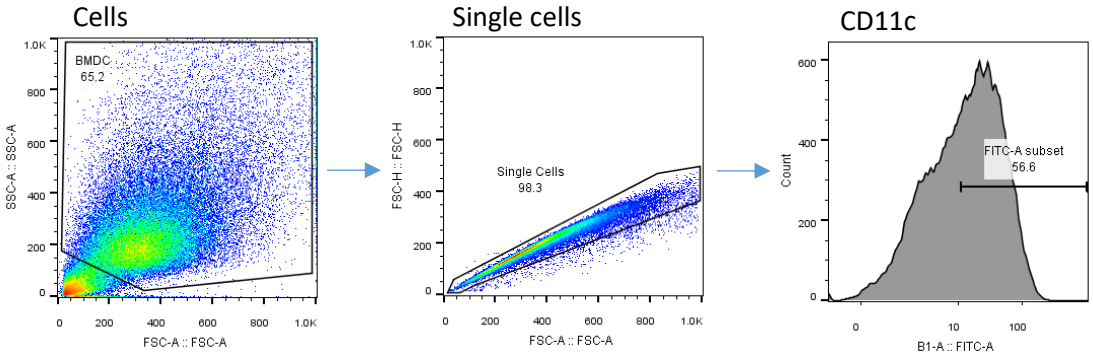
Cells
BMDC
65.2
SSC-A :: SSC-A
FSC-A :: FSC-A
Single cells
Single Cells
98.3
FSC-H :: FSC-H
FSC-A :: FSC-A
CD11c
FITC-A subset
56.6
Count
B1-A :: FITC-A

G.

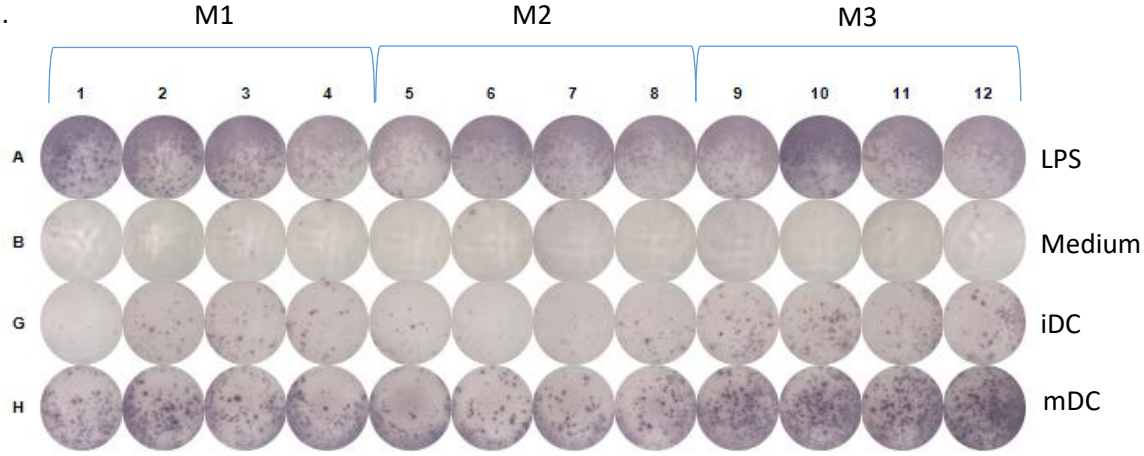
M1
M2
M3
1
2
3
4
5
6
7
8
9
10
11
12
A
B
G
H
LPS
Medium
iDC
mDC

H.

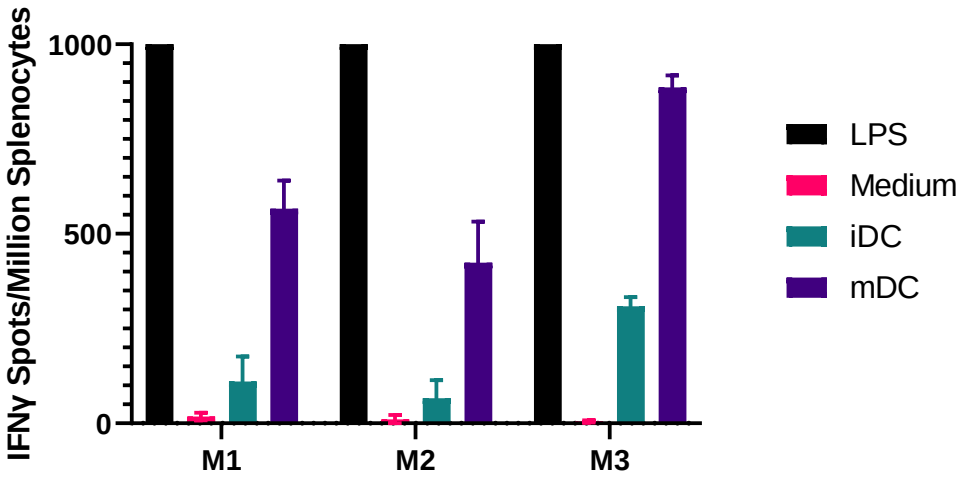
IFNγ Spots/Million Splenocytes
1000
500
0
M1
M2
M3
LPS
Medium
iDC
mDC

Figure 5.7 immature dendritic cells (iDC) and mature dendritic cells (mDC) (both AP treated and untreated) were tested by flow cytometry and ELISPOT for their capacity for T cell activation. A) FITC positive event gating strategy based on an antibody isotype control conjugated to FITC. Gating is placed around cells, then single cells, then positive events for FITC fluorescence. B) BMDC cells labelled with anti-CD11c-FITC. The gating strategy shown in A is applied to determine percentage positive events for CD11c expression. C) IFNγ capture ELISPOT for T cell activation after co-culture of splenocytes from HHDII/DP4 mice, immunised with mixed cit-peptide (SNAPvax formulation), with AP fed and unfed BMDC from naïve HHDII/DP4 mice or LPS and media controls. DC + peptide refers to BMDC pre-treated with the immunising cit-peptides. Unstimulated B16 fraction 6 or 7 refers to fraction 6 or 7 (AP high) of a gradient harvest of organelles from resting B16F1 cells. Tg stimulated B16 fraction 6/7 refers to fraction 6 or 7 (AP high) of a gradient harvest of organelles from thapsigargin stimulated B16F1 cells. D) Graphical representation of C, n=3, statistics were determined by one way ANOVA with Tukey's multiple comparison test E) Gating strategy for CD11c placed using a FITC isotype control antibody, gating on cells, then single cells, then positive events for FITC. F) the same gating strategy in E applied to cells treated with anti-CD11c-FITC antibody, to determine percentage positive cells for CD11c expression. G) IFNγ capture ELISPOT using splenocytes from three independent naïve HHDII/DP4 mice (M1, M2, M3), co-cultured with iDC and mDC populations, differentiated from bone marrow of HHDII/DP4 mice, or with LPS and media as positive and negative controls, respectively. H) a graphical representation of the spot count/million splenocytes in F., n=3, statistics were determined by two way ANOVA, with Tukey's multiple comparisons test.

5.3.7 Autophagosome fed DC induce T cell responses

Following confirmation that the addition of LPS may non-specifically activate T cells, it was decided to repeat the experiment with additional washing steps to further dilute residual LPS.

Dendritic cells from naïve HHDII/DP4 mice were co-cultured with splenocytes pooled from mixed cit-peptide (SNAPvax formulation) immunised (group A) or naïve (group B) HHDII/DP4 mice. Co-culture with iDC increased T-cell activation compared to negative control, with naïve groups giving a mean spot count that was 3-fold higher than immunised. Despite additional washing steps, mDC populations showed increased activation of T cells when compared with iDC populations, a ~2-fold increase in both immunised naïve groups. Comparable activity was seen across all mDC co-cultures in both mouse groups, regardless of pre-treatment with autophagosome preps. In both naive and immunised mice, the largest T-cell activation was seen with mDC treated with unstimulated B16, fraction 4. This was a significant difference to mDC only ($p=0.0126$).

Figure 5.8

A

Isotype control gating for FITC+ cells

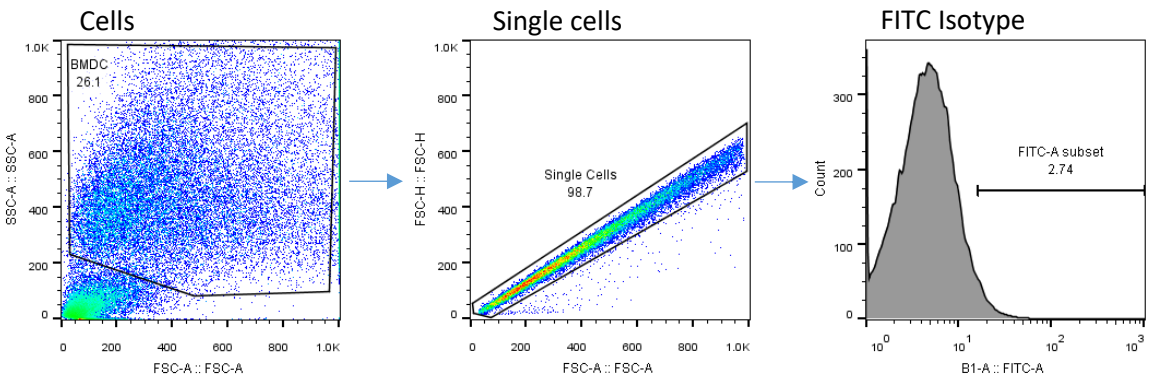

B

CD11c (FITC) Positive Gating on Harvested BMDC

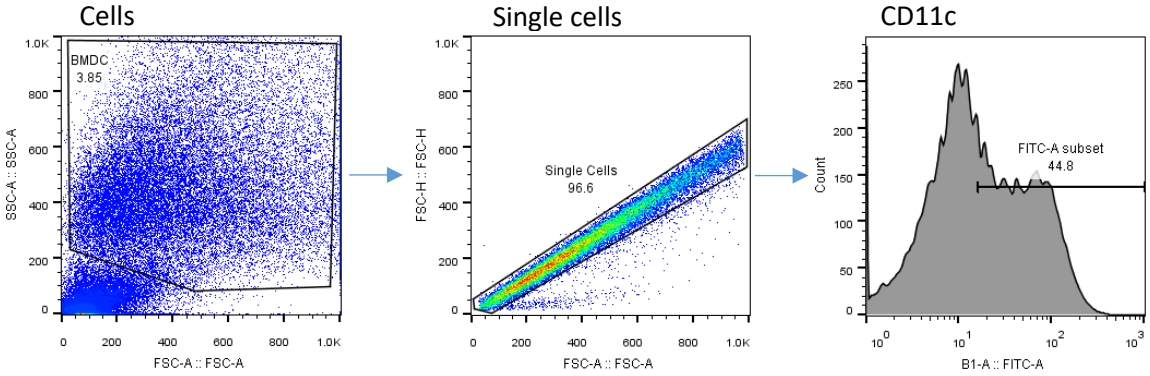

C

LPS and Media control ELISPOT

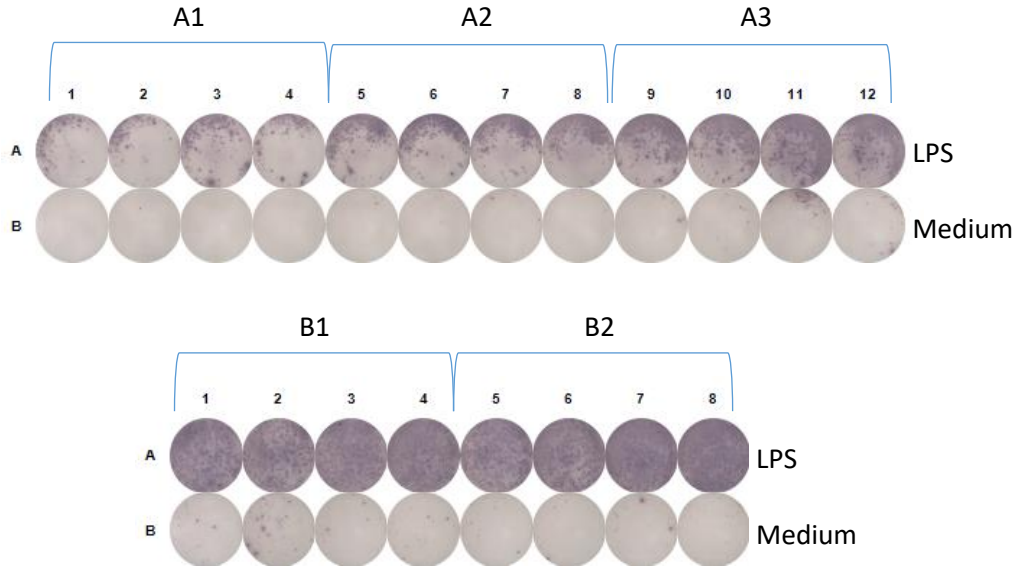

D

Dendritic cell/splenocyte co-culture

Pooled Immunised Mice Splenocytes (A group)

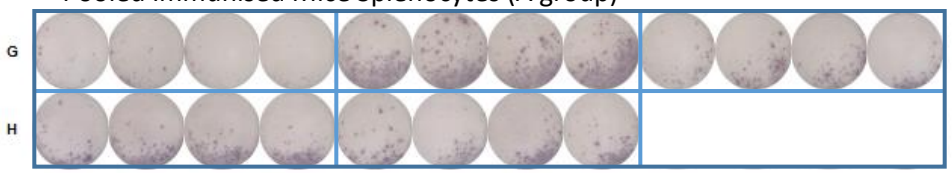

Pooled Naïve Mice Splenocytes (B group)

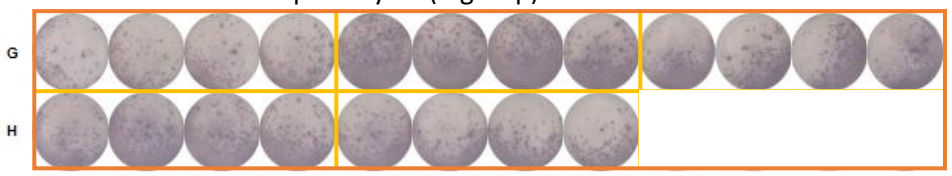

Pooled A group mouse splenocytes		
iDC	Unstimulated B16 Fraction 4	Stimulated B16 Fraction 6
mDC	Unstimulated B16 Fraction 6	
Pooled B group mouse splenocytes		
iDC	Unstimulated B16 Fraction 4	Stimulated B16 Fraction 6
mDC	Unstimulated B16 Fraction 6	

E.

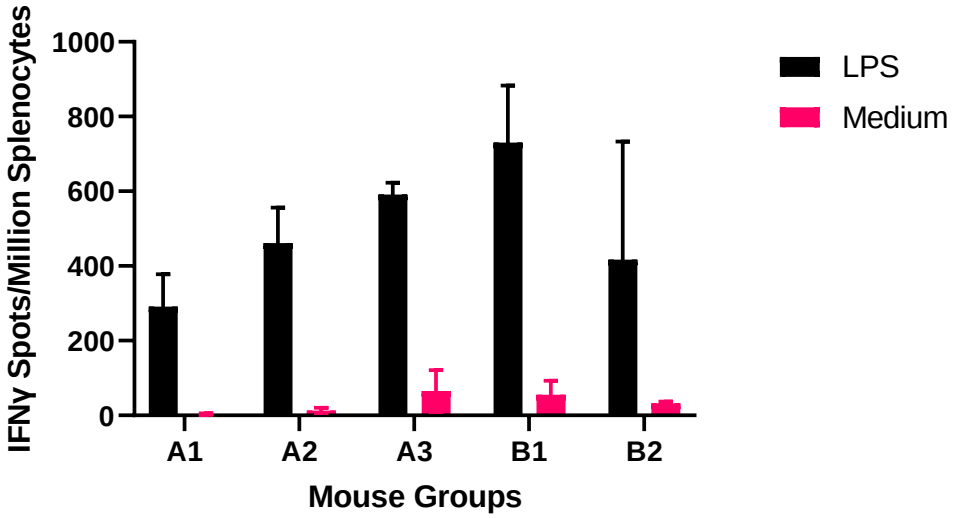

F.

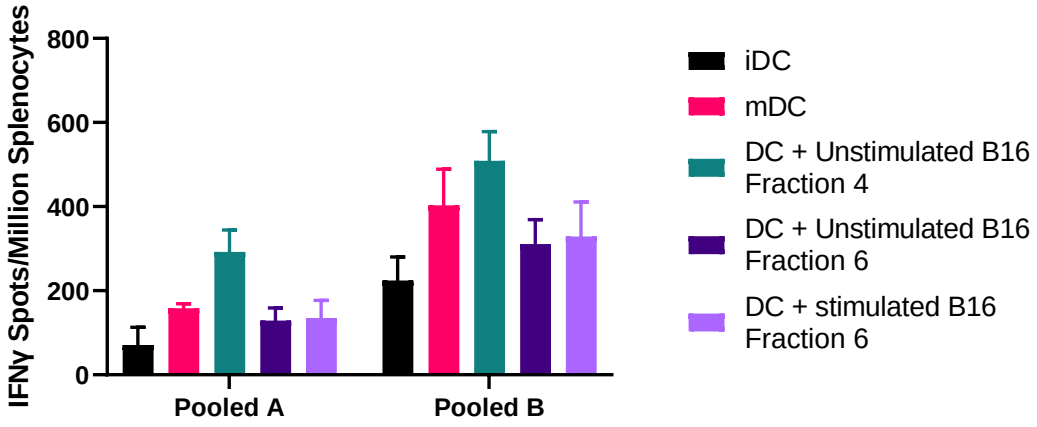

Figure 5.8 iDC or autophagosome pre-treated mDC are tested for their ability to induce citrullinated epitope specific T cell activation, by ELISPOT and flow cytometry. A) Gating strategy for FITC positive events, based on an antibody isotype control conjugated to FITC. Gating is placed around cells, then single cells, then positive events for FITC fluorescence. B) BMDC cells labelled with anti-CD11c-FITC. The gating strategy shown in A. is applied to determine percentage positive events for CD11c expression. C-F) Splenocytes, taken from HHDII/DP4 mice which were either immunised with mixed cit-peptides (SNAPvax formulayion) (Group A, n=3) or naïve (group B, n=2), were pooled and co-cultured with bone marrow derived dendritic cells from naïve HHDII/DP4 mice for 40 hours. BMDC groups included iDC, mDC, and mDC pre-treated with organelle fractionation preps before activation (D and H). Fraction 4 refers to an autophagosome low organelle fraction, and fraction 6 refers to an autophagosome high fraction. Un-pooled splenocytes cultured with LPS or media were used as positive or negative controls respectively (C and E). An IFNγ capture ELISPOT was used to detect T cell activation through IFNY release. C and D show images of ELISpot plates. E and F show graphical representation of spot counts from these plates. Statistics were carried out using two way ANOVA with Tukey's multiple comparisons test.

5.4 Discussion

Previous work using phenyl glyoxal based probes and evidence within the literature[182,411] suggests that autophagosomes may be a source of citrullinated proteins. Uptake of autophagosomes by APC and the resultant presentation of citrullinated epitopes on MHC could therefore activate citrullinated epitope specific T cells, potentially driving an immune response against multiple tumour specific epitopes. This chapter sought to investigate this.

Little to no activity was seen from citrullinated-peptide specific T cells, following the addition of autophagosome-rich organelle fractions. It was hypothesised that APC would phagocytose autophagosomes and process and present the associated citrullinated proteins. Citrulline specific T cells that were present from previous immunisation would then become activated. There are a number of reasons why this may not have occurred. Firstly, assay length may have been too minimal for APCs to effectively phagocytose, process, and present citrullinated epitopes. This assay has been used previously to successfully show T cell activation due to the addition of citrullinated peptides[183]. The peptides require no processing before presentation and can combine directly with the MHCII loading compartment (MIIC). Furthermore, it is possible that free peptides in the media can bind directly to

MHCII on the surface of antigen presenting cells, bypassing the MIIC entirely. The phagocytosis and processing of an organelle could take longer than the scope of the assay and it is difficult to predict without optimisation. This process could have been optimised through repeating the assay at different time points.

Dendritic cells require a "danger signal" for full activation and presentation of co-stimulatory molecules for T cell activation. Danger signals may not be present when using autophagosomes that may immunologically appear as "self". Without full activation of dendritic cells, any citrulline specific T cells that engage with DC MHC-II presenting citrullinated epitopes would become anergic and therefore production of IFNγ would not be seen. Due to the mixed cell lineage of splenocytes, the addition of an adjuvant (a danger signal) would lead to robust activation of immune cells and production of IFNγ regardless of antigen specificity. For this reason, allogeneic DC were isolated to feed with autophagosomes, and activate using LPS, before combining with splenocytes. This would allow for signal 1 and signal 2 to be present for full T cell activation.

An enriched population of 40% and above CD11c positive dendritic cells were achieved throughout BMDC maturation

however there was one instance where purity was substantially lower. Suboptimal voltage settings on the flow cytometer meant that cells were not able to be gated out of the debris, giving a falsely low percentage of cell events positive for CD11c. This population of cells were still activated by LPS effectively as shown by a shift in fluorescence for CD80 labelling, corresponding to an increase in expression in these cells, giving further evidence that these were the correct cell type and 27% was an underestimation of the true content of CD11c cells. However, the protocol for generation of BMDC has been shown to develop granulocytes and CD11c+ macrophages, each with differing effector functions that may not be specialised for T cell activation[412]. This could lead to inferior activation of citrullinated specific CD4 T cells. While macrophages should be removed due to their adherent phenotype, the BMDC population could have benefitted from further enrichment, such as immunoaffinity isolation.

The increase in CD80 expression upon activation led to the assumption that MHCII was presented on mDC however this was not proven. To give confidence that MHCII was available for T cell stimulation, anti-DP4 antibodies could have been used to detect this.

Further to phenotyping BMDC, their viability post-autophagosome treatment was investigated. Autophagosome preps are made up of intact subcellular organelles and particles from cells of the same species, therefore toxicity would not be expected. A cell death assay was carried out to investigate this. Cell death after addition of autophagosome preparations was minimal. The highest amount of cell death outside of the positive control was found in unfed DCs suggesting that 30% is baseline and that cell viability was not affected by the addition of autophagosomes.

Uptake of high molecular weight dextran serves as a standard assay for endocytosis by phagocytic cells such as DC[413] and is therefore a likely candidate route for the internalisation of autophagosomes. This typically can be observed within 30 minutes-1 hour however, to our surprise, there was no strong indication of such endocytosis/phagocytosis occurring, irrespective of the time-frame studied. The largest size of FITC dextran, at 40kDa, was used in order to be comparable to the phagocytosis of organelles. However the hydrodynamic radius of 40kDa FITC-Dextran is 6.6nm[414] whereas the radius of an autophagosome is much larger at 150-750nm[415]. The difference in size may limit the applicability of the FITC-Dextran assay for determining autophagosome uptake speed. FITC-Dextran is however taken up via the DC-SIGN

receptor[416] which binds to fucosylated and mannose rich glycans[417]. Provided autophagosomes have these modifications within their membrane, the uptake of these two species could be comparable. However, due to the size of autophagosomes, it was assumed that uptake was through phagocytosis. It is possible however that different routes of endocytosis are used for the uptake of autophagosomes. This can be examined by observing uptake whilst inhibiting other routes, such as clathrin-mediated endocytosis inhibition with monensin[418].

There was inconclusive evidence that autophagosomes had been phagocytosed by dendritic cells in imaging flow cytometry experiments, due to low increases in LC3 puncta, however puncta was present in mDC cells. As iDC scavenge their surroundings in order to seek out pathogens, it is expected that phagocytosis will be increased in this subset of cells compared to mDC however this was not observed. A study by Platt et al.[419] shows that mature DC are still able to phagocytose efficiently after activation and that it is only their ability to process and present peptides on MHCII that is reduced. This may explain why puncta can be seen in mDC populations, as phagocytosis by these cells is still functional but processing of phagosomes is decreased, allowing autophagosomes to persist in the cytoplasm. iDC are able to

process and present more efficiently and autophagosomes may have already been degraded in the MIIC compartment and therefore undetectable within this population. This could be investigated in future work by detecting LC3 uptake at earlier time points.

Imaging flow cytometry has the caveat of high background fluorescence due to cytoplasmic LC3-I which makes detection of puncta more difficult. For this reason confocal microscopy was used to limit fluorescence from outside the focal plane. LC3+ puncta, detected by confocal microscopy, were present in low cell numbers in iDC fed with fraction 7 from both resting and stimulated B16F1 cells, suggesting phagocytosis by these cells. The rarity of LC3+ signal may be due to assay timing. A 1hr incubation may allow autophagosomes to move into the latter stage of processing i.e. fusion with the lysosome for degradation. Nevertheless, the presence of fluorescence puncta in some cells is evidence that autophagosomes had been phagocytosed by iDC and the use of a 1hr time point for the phagocytosis of autophagosomes was further justified. The absence of LC3+ puncta in images of fraction 4 fed DC is in concordance with this being a low or negative fraction for LC3-II.

An additional experiment to analyse the timing of phagocytosis and degradation in the lysosome could have been investigated by observing the formation of the phagolysosome with GFP/RFP labelled LC3-II over time. Uptake of autophagosomes labelled with anti-LC3-GFP/RFP can be observed, followed by fusion with the lysosome where GFP, but not RFP is quenched.

Co-culture of fed dendritic cells with citrullinated epitope experienced splenocytes showed high T cell activation throughout all conditions, mostly exceeding that of LPS positive control. mDC alone also showed high levels of T cell activation therefore activation is likely to be non-specific and a high background may be masking citrullinated specific responses. LPS has been shown to activate T cells, generating Th1 responses which includes IFNγ release[420,421]. High background in mDC control could therefore be caused by residual LPS. Following multiple washes, the mDC background was reduced, however was still higher than iDC populations. As shown in the literature, LPS activated mDC are able to induce IFNγ release from T cells without full activation[422]. In a study by Kamath et al., this was shown to be mediated by IFNαβ release by activated CD11c DC[423]. For this reason, mDC conditions would always induce a higher IFNγ response than iDC or media only control. However, with the exception of DCs

fed with unstimulated fraction 7, there is increased T cell activation compared to mDC control. This suggests possible activation of citrullinated epitope-specific T cells, which is non-significant due to high background.

Following washing of residual LPS, background was reduced. However, no autophagosome treated groups showed a significant difference to mDC only, suggesting T cell activation was not citrullinated epitope specific. This was further evidenced by higher T cell activation in splenocytes from naïve mice rather than immunised. One possible reason for the absence of specific T cell responses is that the epitopes used for immunisation of mice are not present in autophagosomes, or are not generated through the processing of autophagosomes. Epitopes used for immunisation have been found within whole cell B16F1 samples (unpublished) however their location within autophaosomes has yet to be confirmed. Following the phagocytosis of autophagosomes, it is assumed that the autophagosome and peptides within will be partially degraded within the phagosome/phagolysosome. This will generate the peptides for loading into MHC-II. Depending on the proteins present in autophagosomes, the affinity of peptides for MHC-II, where proteases will cleave, and the extent of protein degradation, peptides used for immunisation may not be presented through this process and no citrullinated

epitope specific T cell activation will take place. Analysis of autophagosomes by mass spectrometry could be used to confirm the presence of immunogen peptides.

Autophagosomes from murine tumours may appear as immunologically self in murine models. To avoid autoimmunity, dendritic cells are able to distinguish between self (such as apoptotic bodies) and antigenic material when both are phagocytosed concomitantly[424,425]. TLR ligands are required within the phagosome cargo for efficient fusion of endosomal and lysosomal compartments[424] and processing of MHC class II–associated invariant chain (Ii) to class II–associated invariant chain derived peptide (CLIP), ready for peptide loading of MHC-II[425]. It is possible that autophagosomes do not contain the relevant TLR ligand for phagosome maturation and Ii processing. However, this would be expected in other studies where dendritic cells had been pulsed with autophagosomes[395]. Furthermore, as citrullinated epitopes could be considered self and therefore subject to tolerance, increased presentation on MHCII may be required to induce activation of T cells. If low presence of LC3 puncta in fed DC is indicative of low uptake, there may not be enough MHCII:peptide complexes to overcome tolerance and citrullinated epitope specific T cells may become anergic.

Despite the potential for autophagosomes to induce a tolerogenic response, T cell activation was occasionally increased compared to mDC control, although this was not isolated to autophagosome high fed DCs. This suggests that T cell activation was due to an antigen other than the immunogen. Due to the constraints of organelle processing, fractions were not kept sterile and therefore may have contaminants. T cell responses may have been raised against antigens of microorganisms within the autophagosome sample. In future work, alternative methods of isolation could be used to keep autophagosome samples sterile, such as immunoaffinity isolation.

IFNγ production by T cells is an indication that an inflammatory response has been activated, and will influence the immune system towards cell-mediated immunity. However, presented autophagosomal epitopes could have induced a regulatory response instead, with activation of T cells such as Th2 or Th17 phenotypes. This could be investigated further by testing alternative cytokines such as IL-4 and IL-13 for Th2 or IL-17 for Th17 activation.

Many experiments within this chapter were not repeated which decreases the confidence in results and reduces that chances of being statistically relevant. For more conclusive answers,

experiments should be repeated and further work, as outlined above, should be carried out.

6. Final Discussion

An effective cancer therapy will capitalise on differences between cancerous and physiological cells. One component that appears to display this is the constitutive presence of autophagy in cancer cells lines. The high presence of autophagosomes was due to activation of autophagy and not due to problems with fusion or turnover within the lysosome within tumour cell lines, as shown by the large increase in LC3-II upon treatment with chloroquine. Autophagosomes were shown to be significantly increased in tumour cells, compared to primary cells, potentially leading to significantly higher presentation of citrullinated peptides on MHCII. Activation of the immune system against citrullinated epitopes could therefore be selective against tumour cells only, due to the number of epitopes exceeding threshold levels for T cell activation. The reduced autophagy in primary cells may protect from T cell activity against them, as immunological threshold for activation may never be met. Furthermore, in a basal state, cells outside of the immune system do not express MHC-II unless it is induced through inflammation. Normal cells do not experience inflammation, unless infected, whereas inflammation is often present at the tumour microenvironment and MHCII presentation has been

reported[426–431]. This therefore gives another selection pressure against tumour cells, reducing toxicities in physiological cells.

Common activators (such as nutrient deprivation) or autophagosomal turnover events (such as degradation of p62) did not always occur as expected in tumour cell lines, possibly due to dysregulated signalling. Further evidence for autophagy dysregulation could be found by carrying out RNA-seq to give detailed information on the expression of autophagy associated genes. Autophagy-related genes (ATG) proteins may be expected to have increased transcription, as well as activating proteins such as Beclin1[432]. RNA-seq would not account for protein regulation due to PTM (and therefore would not observe lipidation of LC3 or activating phosphorylation of AMPK), however can give further evidence for autophagy dysregulation when compared with primary cells. The benefits of RNA-seq over western blot are that a wider range of proteins can be investigated simultaneously and therefore changes in expression at multiple nodes within the autophagy signalling pathway can be observed. Furthermore, protein transcription in response to autophagy inducers/inhibitors can be observed and compared against physiological cells to give evidence for dysregulated signalling.

A small selection of cancer cell lines were chosen in this work to aid in selecting a line for further experimentation. For a more in depth analysis of autophagy in cancer as a whole, and for analysis that may be more applicable to cancer in patients, in silico analysis can be carried out using available large databases such as the Cancer Genome Atlas. Similar changes in genetic expression to the ones outlined for RNA-Seq above can be investigated. Furthermore, tools such as the HAPTRIG R tool[433], developed by UCSD, can be used. This genetic analysis tool is able to look at genetic changes in the context of molecular pathways to identify positive or negative changes in processes such as autophagy.

Within this study, flow cytometry, western blots, and electron microscopy were used in conjunction with each other to determine the presence of autophagosomes within organelle preps. It is a strength that each technique largely agreed with each other, giving evidence that autophagosomes were positively selected through density gradient centrifugation. However isolating autophagosomes by their density gave a heterogeneous population, and any conclusions made may not be definitively due to the autophagosomes present in the sample. Enrichments using a discontinuous OptiPrep gradient were chosen due to the convenience of using a single gradient for isolation, and the likelihood of getting a good recovery of

autophagosomes after processing. More extensive gradient separation protocols are available however, such as the protocol used by Strømhaug et al when isolating autophagosomes from rat hepatocytes[371]. This used differential centrifugation, Nycodenz, Percoll, and OptiPrep gradients to sequentially remove contaminating organelles. Despite a laborious protocol, recovery of autophagosomal markers were only 11.8%, possibly due to loss at each step within the recovery protocol, and preparations are subject to the same problems experienced in this study – where separations based on density do not give a pure preparation due to organelles having variable and overlapping densities to each other. Immunoaffinity isolation[434] can also be used to generate a purer autophagosomal preparation and allows for a faster and gentler isolation of organelles compared to multi-step ultracentrifugation, potentially keeping the integrity of organelles and reducing processing. Furthermore, immunoaffinity isolation allows for purification via markers, rather than physical characteristics, and as LC3-II is largely localised to classical autophagosomes, will likely lead to an isolation preparation with less contaminants. Antibodies against LC3 can be immobilised onto magnetic beads in order to achieve this. Alternatively, GFP-LC3 transgenic cell lines have been generated and autophagosomes can be isolated

using anti-GFP magnetic beads, which are readily available to purchase, allowing for limited variability between batches and experiments. Furthermore, GFP-LC3 transgenic cells can be used to aid imaging and tracking of autophagosomes intracellularly, adding further benefits than aiding isolation. Within this study, an attempt was made to create GFP-LC3 transgenic cell lines using pEGFP-C1+LC3 plasmids however after transfection, expression of GFP-LC3 was lost over a short period of time (data not shown). It was hypothesised that this was due to either a lack of stable integration or the result of expression being under the CMV promotor which is highly susceptible to silencing by methylation[435]. A potential caveat to GFP-LC3 overexpression is that, due to the large amounts of protein generated, aggregates can form. However, as autophagy is a key process for the elimination of protein aggregates, it may be that GFP-LC3 puncta due to aggregates is indirectly labelling autophagosomes at the same time. Nevertheless, this would add a further complication to analysis of results.

This study sought to identify citrullinated proteins within isolated autophagosome preps, which is a difficult feat when the modified protein has a difference in weight of 1Da. Nonetheless phenyl glyoxal (PG) was used to specifically react with citrulline residues and identify the presence of

citrullinated proteins. However, without further analysis, it is unknown what these proteins are. Antibodies against known citrullinated proteins can be used in conjunction with a phenyl glyoxal probe in SDS PAGE and Western blot to identify their presence at the same molecular weight but this limits the assay to proteins that are known to be citrullinated and proteins for which antibodies have been acquired. A much more detailed and broad approach would be to test autophagosome preps by mass spectrometry. This allows for sensitive identification of citrullinated proteins with high resolution and for the identification of known proteins as well as the potential for previously undiscovered citrullinated proteins. Using autophagosome enriched preparations should enhance protein identification, due to the removal of other cellular components. This would increase the possibility of citrullinated protein identification. To further increase signal to noise, phenyl glyoxal could be used to enrich citrullinated proteins. Lewallen et al. developed a protocol using Biotin-PG to enrich proteins via streptavidin-agarose, for mass spectrometry after elution using on-bead tryptic digestion[435]. The same protocol could be used to enrich citrullinated proteins following autophagosome isolation. Importantly, mass spectrometry can also give information on the precise residue within the polypeptide chain which is citrullinated, which would

be required when finding epitopes to target for cancer therapy.

The efficacy of citrullinated epitope targeted therapy will depend upon the presentation of the epitopes on MHC-II. Despite getting information on citrullinated proteins contain in autophagosomes through mass spec, further analysis into their presentation on MHCII will be required. This could be done through the elution of proteins from MHC-II on cancer cells[436]. Firstly, tumour cells will need to be treated with IFNγ to induce MHC-II expression[437]. Alternatively, a transgenic tumour cell line that constitutively expresses MHC-II can be used. If this route is taken, common HLA haplotypes within the population can be used which would increase applicability to a wider population, for example HLA-DP4 is one of the most common haplotypes at 20-60% worldwide[438]. Further common haplotypes can be found using databases such as the Immuno Polymorphism Database[439] (to find genes with lower polymorphisms) or IPD-IMGT/HLA Database (for information on HLA allele prevalence)[440]. Following lysis of cells, MHC-II can be isolated by affinity purification, and peptides can be eluted by acid elution. This would give a heterogenous population of MHC-II bound peptides.

Citrullinated peptides could be further enriched using the PG probe highlighted above and these enriched proteins could be identified by mass spectrometry. Spectra from tumour autophagosomes and MHC-II can be aligned to find citrullinated species that are in both compartments, giving further evidence of the loading of MHC-II via autophagy. The epitopes that are found in both compartments can be used in an anti-cancer therapy and this method may uncover novel epitopes than can be targeted independently or in conjunction with already known epitopes such as citrullinated vimentin[183]. Repeating this work with other widely expressed HLA alleles or other tumour types may uncover a broader array of novel citrullinated epitopes that could be included in therapies to broaden the efficacy of cancer immunotherapy to a wider population.

Once novel citrullinated epitopes have been identified they need to be characterised for their ability to induce a CD4 T cell response and an anti-tumour response. Peptide vaccination with adjuvant is a proven route for T cell induction against citrullinated epitopes. Much of the work that has been done on previously identified citrullinated peptides[183,9] are useful as a reference when characterising novel epitopes. This could include PBMC and target tumour co-culture with/without citrullinated peptides plus adjuvant, using T cell activation and

proliferation as an indication of efficacy. Further work using mouse models could then be carried out, by immunisation of mice and re-challenge of splenocytes with citrullinated epitopes, and immunisation of tumour inoculated mice to determine anti-tumour efficacy in vivo.

Autophagosomes were used as a potential source of target epitopes for CD4 stimulation. ELISPOT assays were used for convenience, as they were already routinely performed for citrullinated epitope assays, however they were optimised for peptide stimulation. Results were inconclusive and techniques described above may be more suitable for confirmation of the presence of citrullinated proteins. Furthermore the use of autophagosomes as a vaccine would pose challenges if administered clinically. Firstly, the isolation of autophagosomes is laborious and time consuming, and it is possible that a high number of autophagosomes across multiple doses will be required for full regression of the tumour, making this treatment potentially very expensive. Allogeneic autophagosomes would be easier to achieve, as these could be harvested from relevant cell lines that are easier to produce in high numbers, but introduces the risk of activating immunity against foreign, non-tumour specific epitopes. Despite this, autophagosomes could be a promising source for novel citrullinated epitopes for the generation of

novel peptide vaccines. Peptide vaccines are better characterised and therefore no unwanted epitope targeting should take place and are also relatively cost effective and can be mass produced, allowing for a more off the shelf treatment. Provided that multiple citrullinated epitopes are included in a vaccine, it can be potentially used against multiple cancers in multiple patients.

Overall this study indicated that autophagy is increased in tumour cells, giving selectivity over non-tumour cells, and that tumour autophagosomes contain citrullinated proteins and therefore could be harvested as a potential source of novel, tumour specific epitopes. As indicated above, further work is required to confirm the potential of these findings.

7. References

1. Wang, R. F. & Wang, H. Y. Immune targets and neoantigens for cancer immunotherapy and precision medicine. *Cell Res. 2017 271* **27**, 11–37 (2016).

2. Cluff, C. W. Monophosphoryl lipid a (MPL) as an adjuvant for anti-cancer vaccines: Clinical results. *Adv. Exp. Med. Biol.* **667**, 111–123 (2009).

3. Flavell, R. A., Sanjabi, S., Wrzesinski, S. H. & Licona-Limón, P. The polarization of immune cells in the tumour environment by TGFβ. *Nat. Rev. Immunol. 2010 108* **10**, 554–567 (2010).

4. Dredge, K., Marriott, B. J., Todryk, S. M. & Dalgleish, A. G. Adjuvants and the promotion of Th1-type cytokines in tumour immunotherapy. *Cancer Immunol. Immunother.* **51**, 521–531 (2002).

5. Farhood, B., Najafi, M. & Mortezaee, K. CD8+ cytotoxic T lymphocytes in cancer immunotherapy: A review. *J. Cell. Physiol.* **234**, 8509–8521 (2019).

6. Bachmann, M. F. *et al.* T cell responses are governed by avidity and co-stimulatory thresholds. *Eur. J. Immunol.* **26**, 2017–2022 (1996).

7. WANG, S. HER2 overexpression and cancer targeting.

Semin. Oncol. **28**, 115–124 (2001).

8. Dagogo-Jack, I. & Shaw, A. T. Tumour heterogeneity and resistance to cancer therapies. *Nat. Rev. Clin. Oncol. 2017 152* **15**, 81–94 (2017).

9. Brentville, V. A. *et al.* Original research: Combination vaccine based on citrullinated vimentin and enolase peptides induces potent CD4-mediated anti-tumor responses. *J. Immunother. Cancer* **8**, 560 (2020).

10. Nezafat, N., Ghasemi, Y., Javadi, G., Khoshnoud, M. J. & Omidinia, E. A novel multi-epitope peptide vaccine against cancer: An in silico approach. *J. Theor. Biol.* **349**, 121–134 (2014).

11. Liu, J. *et al.* Cancer vaccines as promising immuno-therapeutics: platforms and current progress. *J. Hematol. Oncol. 2022 151* **15**, 1–26 (2022).

12. Beck, S. & Trowsdale, J. The human major histocompatability complex: lessons from the DNA sequence. *Annu. Rev. Genomics Hum. Genet.* **1**, 117–137 (2000).

13. Bodmer, W. F. The HLA system: structure and function. *J Clin Pathol* **40**, 948–958 (1987).

14. Little, A. M. & Parham, P. Polymorphism and evolution of

HLA class I and II genes and molecules. *Rev. Immunogenet.* **1**, 105–123 (1999).

15. Hedrick, P. W., Whittam, T. S. & Parham, P. Heterozygosity at individual amino acid sites: extremely high levels for HLA-A and -B genes. *Proc. Natl. Acad. Sci.* **88**, 5897–5901 (1991).

16. Charles A Janeway, J., Travers, P., Walport, M. & Shlomchik, M. J. The major histocompatibility complex and its functions. (2001).

17. Wysocki, T., Olesinska, M. & Paradowska-Gorycka, A. Current Understanding of an Emerging Role of HLA-DRB1 Gene in Rheumatoid Arthritis–From Research to Clinical Practice. *Curr. Underst. an Emerg. Role HLA-DRB1 Gene Rheum. Arthritis–From Res. to Clin. Pract.* 1–31 (2020).

18. Koopmann, J. O., Hämmerling, G. J. & Momburg, F. Generation, intracellular transport and loading of peptides associated with MHC class I molecules. *Curr. Opin. Immunol.* **9**, 80–88 (1997).

19. Garcia, K. C. *et al.* CD8 enhances formation of stable T-cell receptor/MHC class I molecule complexes. *Nat. 1996 3846609* **384**, 577–581 (1996).

20. Burgdorf, S., Kautz, A., Böhnert, V., Knolle, P. A. &

Kurts, C. Distinct pathways of antigen uptake and intracellular routing in CD4 and CD8 T cell activation. *Science (80-.).* **316**, 612–616 (2007).

21. Drozina, G., Kohoutek, J., Jabrane-Ferrat, N. & Peterlin, B. M. Expression of MHC II genes. *Curr. Top. Microbiol. Immunol.* **290**, 147–170 (2005).

22. Stern, L. J. & Wiley, D. C. Antigenic peptide binding by class I and class II histocompatibility proteins. *Structure* **2**, 245–251 (1994).

23. Brown, J. H. *et al.* Three-dimensional structure of the human class II histocompatibility antigen HLA-DR1. *Nature* **364**, 33–39 (1993).

24. Nguyen, A. T., Szeto, C. & Gras, S. The pockets guide to HLA class I molecules. *Biochem. Soc. Trans.* **49**, 2319 (2021).

25. Stern, L. J. *et al.* Crystal structure of the human class II MHC protein HLA-DR1 complexed with an influenza virus peptide. *Nature* **368**, 215–221 (1994).

26. Germain, R. N. & Margulies, D. H. The Biochemistry and Cell Biology of Antigen Processing and Presentation. *https://doi.org/10.1146/annurev.iy.11.040193.002155* **11**, 403–450 (2003).

27. Vizcaíno, J. A. *et al.* The Human Immunopeptidome Project: A Roadmap to Predict and Treat Immune Diseases. *Mol. Cell. Proteomics* **19**, 31 (2020).

28. Dubey, P. *et al.* The Immunodominant Antigen of an Ultraviolet-induced Regressor Tumor Is Generated by a Somatic Point Mutation in the DEAD Box Helicase p68. *J. Exp. Med.* **185**, 695 (1997).

29. Zarling, A. L. *et al.* From the Cover: Identification of class I MHC-associated phosphopeptides as targets for cancer immunotherapy. *Proc. Natl. Acad. Sci. U. S. A.* **103**, 14889 (2006).

30. Inaba, K., Metlay, J. P., Crowley, M. T., Witmer-Pack, M. & Steinman, R. M. Dendritic Cells as Antigen Presenting Cells in Vivo. *http://dx.doi.org/10.3109/08830189009056630* **6**, 197–206 (2009).

31. Reis E Sousa, C. Activation of dendritic cells: translating innate into adaptive immunity. *Curr. Opin. Immunol.* **16**, 21–25 (2004).

32. Kim, M. K. & Kim, J. Properties of immature and mature dendritic cells: phenotype, morphology, phagocytosis, and migration. *RSC Adv.* **9**, 11230–11238 (2019).

33. Sallusto, F., Cella, M., Danieli, C. & Lanzavecchia, A. Dendritic cells use macropinocytosis and the mannose receptor to concentrate macromolecules in the major histocompatibility complex class II compartment. *rupress.org*

34. Sozzani, S. *et al.* Migration of dendritic cells in response to formyl peptides, C5a, and a distinct set of chemokines. *J. Immunol.* **155**, 3292–3295 (1995).

35. S Sozzani 1, P Allavena, G D'Amico, W Luini, G Bianchi, M Kataura, T Imai, O Yoshie, R Bonecchi, A. M. Differential regulation of chemokine receptors during dendritic cell maturation: a model for their trafficking properties. *The Journal of Immunology* 161(3):1083–6. (1998). Available at: https://pubmed.ncbi.nlm.nih.gov/9686565/. (Accessed: 24th March 2023)

36. Blanco, P., Palucka, A. K., Pascual, V. & Banchereau, J. Dendritic cells and cytokines in human inflammatory and autoimmune diseases. *Cytokine Growth Factor Rev.* **19**, 41 (2008).

37. Fitzgerald-Bocarsly, P. Human natural interferon-α producing cells. *Pharmacol. Ther.* **60**, 39 (1993).

38. Siegal, F. P. *et al.* The nature of the principal type 1

interferon-producing cells in human blood. *Science* **284**, 1835–1837 (1999).

39. Kadowaki, N. *et al.* Subsets of human dendritic cell precursors express different toll-like receptors and respond to different microbial antigens. *J. Exp. Med.* **194**, 863–869 (2001).

40. Dzionek, A. *et al.* BDCA-2, a Novel Plasmacytoid Dendritic Cell–specific Type II C-type Lectin, Mediates Antigen Capture and Is a Potent Inhibitor of Interferon α/β Induction. *J. Exp. Med.* **194**, 1823–1834 (2001).

41. Cohn, L. *et al.* Antigen delivery to early endosomes eliminates the superiority of human blood BDCA3+ dendritic cells at cross presentation. *J. Exp. Med.* **210**, 1049–1063 (2013).

42. Poulin, L. F. *et al.* Characterization of human DNGR-1+ BDCA3+ leukocytes as putative equivalents of mouse CD8α+ dendritic cells. *J. Exp. Med.* **207**, 1261–1271 (2010).

43. Haniffa, M. *et al.* Human Tissues Contain CD141hi Cross-Presenting Dendritic Cells with Functional Homology to Mouse CD103+ Nonlymphoid Dendritic Cells. *Immunity* **37**, 60–73 (2012).

44. Dzionek, A. *et al.* BDCA-2, BDCA-3, and BDCA-4: Three Markers for Distinct Subsets of Dendritic Cells in Human Peripheral Blood. *J. Immunol.* **165**, 6037–6046 (2000).

45. Zhang, J. G. *et al.* The Dendritic Cell Receptor Clec9A Binds Damaged Cells via Exposed Actin Filaments. *Immunity* **36**, 646–657 (2012).

46. Cabeza-Cabrerizo, M., Cardoso, A., Minutti, C. M., Pereira Da Costa, M. & Reis E Sousa, C. Dendritic Cells Revisited. *https://doi.org/10.1146/annurev-immunol-061020-053707* **39**, 131–166 (2021).

47. Guilliams, M. *et al.* Unsupervised High-Dimensional Analysis Aligns Dendritic Cells across Tissues and Species Resource Unsupervised High-Dimensional Analysis Aligns Dendritic Cells across Tissues and Species. *Immunity* **45**, 669–684 (2016).

48. Heidkamp, G. F. *et al.* Human lymphoid organ dendritic cell identity is predominantly dictated by ontogeny, not tissue microenvironment. *Sci. Immunol.* **1**, (2016).

49. Vu Manh, T. P., Bertho, N., Hosmalin, A., Schwartz-Cornil, I. & Dalod, M. Investigating evolutionary conservation of dendritic cell subset identity and functions. *Front. Immunol.* **6**, 140220 (2015).

50. Inba, K. *et al.* Generation of large numbers of dendritic cells from mouse bone marrow cultures supplemented with granulocyte/macrophage colony-stimulating factor. *J. Exp. Med.* **176**, 1693–1702 (1992).

51. Rock, K. L. & Goldberg, A. L. Degradation of cell proteins and the generation of MHC class I-presented peptides. *Annu. Rev. Immunol.* **17**, 739–779 (1999).

52. Hinz, A. & Tampé, R. ABC transporters and immunity: Mechanism of self-defense. *Biochemistry* **51**, 4981–4989 (2012).

53. Sadasivan, B., Lehner, P. J., Ortmann, B., Spies, T. & Cresswell, P. Roles for Calreticulin and a Novel Glycoprotein, Tapasin, in the Interaction of MHC Class I Molecules with TAP. *Immunity* **5**, 103–114 (1996).

54. Blees, A. *et al.* Structure of the human MHC-I peptide-loading complex. *Nat. 2017 5517681* **551**, 525–528 (2017).

55. Ortmann, B., Androlewicz, M. J. & Cresswell, P. MHC class l/β2-microglobulin complexes associate with TAP transporters before peptide binding. *Nat. 1994 3686474* **368**, 864–867 (1994).

56. Rajagopalan, S. & Brenner, M. B. Calnexin retains

unassembled major histocompatibility complex class I free heavy chains in the endoplasmic reticulum. *J. Exp. Med.* **180**, 407–412 (1994).

57. Saric, T. *et al.* An IFN-γ–induced aminopeptidase in the ER, ERAP1, trims precursors to MHC class I–presented peptides. *nature.com*

58. Cresswell, P. Invariant Chain Structure and MHC Class II Function. *Cell* **84**, 505–507 (1996).

59. Roche, P. A., Teletski, C. L., Stang, E., Bakke, O. & Long, E. O. Cell surface HLA-DR-invariant chain complexes are targeted to endosomes by rapid internalization. *Proc. Natl. Acad. Sci.* **90**, 8581–8585 (1993).

60. McCormick, P. J., Martina, J. A. & Bonifacino, J. S. Involvement of clathrin and AP-2 in the trafficking of MHC class II molecules to antigen-processing compartments. *Proc. Natl. Acad. Sci. U. S. A.* **102**, 7910–7915 (2005).

61. Warmerdam, P. A. M., Long, E. O. & Roche, P. A. Isoforms of the invariant chain regulate transport of MHC class II molecules to antigen processing compartments. *J. Cell Biol.* **133**, 281–291 (1996).

62. Riese, R. J. *et al.* Cathepsin S activity regulates antigen

presentation and immunity. *J. Clin. Invest.* **101**, 2351–2363 (1998).

63. Riese, R. J. *et al.* Essential role for cathepsin S in MHC class II-associated invariant chain processing and peptide loading. *Immunity* **4**, 357–366 (1996).

64. Hsieh, C.-S., deRoos, P., Honey, K., Beers, C. & Rudensky, A. Y. A role for cathepsin L and cathepsin S in peptide generation for MHC class II presentation. *J. Immunol.* **168**, 2618–2625 (2002).

65. Villadangos, J. A. *et al.* Proteases involved in MHC class II antigen presentation. *Immunol. Rev.* **172**, 109–120 (1999).

66. Sloan, V. S. *et al.* Mediation by HLA-DM of dissociation of peptides from HLA-DR. *Nature* **375**, 802–806 (1995).

67. Pond', L. & Watts, C. Characterization of transport of newly assembled, T cell-stimulatory MHC class II-peptide complexes from MHC class II compartments to the cell surface. *J. Immunol.* **159**, 543–553 (1997).

68. Vyas, J. M. *et al.* Tubulation of Class II MHC Compartments Is Microtubule Dependent and Involves Multiple Endolysosomal Membrane Proteins in Primary Dendritic Cells. *J. Immunol.* **178**, 7199–7210 (2007).

69. Kornfeld, S. STRUCTURE AND FUNCTION OF THE MANNOSE 6-PHOSPHA TE/INSULINLIKE GROWTH FACTOR II RECEPTORS.

70. Pastan, I. H. & Willingham, M. C. RECEPTOR-MEDIATED ENDOCYTOSIS OF HORMONES IN CULTURED CELLS. *Ann. Rev. Physiol* **43**, 239–50 (1981).

71. Morton$$, P. A., Owensbytiii, D. A., Sobelq, B. E. & Schwartz$, A. L. Catabolism of tissue-type plasminogen activator by the human hepatoma cell line Hep G2: Modulation by plasminogen activator inhibitor type 1. *J. Biol. Chem.* **264**, 7228–7235 (1989).

72. Hanover, J. A. & Dickson, R. B. Transferrin: Receptor-Mediated Endocytosis and Iron Delivery. *Endocytosis* 131–161 (1985). doi:10.1007/978-1-4615-6904-6_5

73. Ashwell, G. & Harford, J. Carbohydrate-specific receptors of the liver. *Annu. Rev. Biochem.* **51**, 531–554 (1982).

74. Brown, M. S. & Goldstein, J. L. Receptor-mediated endocytosis: insights from the lipoprotein receptor system. *Proc. Natl. Acad. Sci.* **76**, 3330–3337 (1979).

75. McMahon, H. T. & Boucrot, E. Molecular mechanism and physiological functions of clathrin-mediated endocytosis. *Nat. Rev. Mol. Cell Biol. 2011 128* **12**, 517–533 (2011).

76. Osaki, F., Kanamori, T., Sando, S., Sera, T. & Aoyama, Y. A quantum dot conjugated sugar ball and its cellular uptake. On the size effects of endocytosis in the subviral region. *J. Am. Chem. Soc.* **126**, 6520–6521 (2004).

77. Grant, B. D. & Donaldson, J. G. Pathways and mechanisms of endocytic recycling. *Nat. Rev. Mol. Cell Biol. 2009 109* **10**, 597–608 (2009).

78. Swanson, J. A. & Watts, C. Macropinocytosis. *Trends Cell Biol.* **5**, 424–428 (1995).

79. Greenberg, S. Signal transduction of phagocytosis. *Trends Cell Biol.* **5**, 93–99 (1995).

80. Ramachandra, L. & Harding, C. V. Phagosomes Acquire Nascent and Recycling Class II MHC Molecules but Primarily Use Nascent Molecules in Phagocytic Antigen Processing. *J. Immunol.* **164**, 5103–5112 (2000).

81. Mantegazza, A. R. *et al.* Adaptor Protein-3 in Dendritic Cells Facilitates Phagosomal Toll-like Receptor Signaling and Antigen Presentation to CD4+ T Cells. *Immunity* **36**, 782–794 (2012).

82. Kovacsovics-Bankowski, M. & Rock, K. L. A Phagosome-to-Cytosol Pathway for Exogenous Antigens Presented on MHC Class I Molecules. *Science (80-.).* **267**, 243–246

(1995).

83. Ackerman, A. L., Giodini, A. & Cresswell, P. A Role for the Endoplasmic Reticulum Protein Retrotranslocation Machinery during Crosspresentation by Dendritic Cells. *Immunity* **25**, 607–617 (2006).

84. Ackerman, A. L., Kyritsis, C., Tampé, R. & Cresswell, P. Early phagosomes in dendritic cells form a cellular compartment sufficient for cross presentation of exogenous antigens. *Proc. Natl. Acad. Sci.* **100**, 12889–12894 (2003).

85. Bertholet, S. *et al.* Leishmania Antigens Are Presented to CD8+ T Cells by a Transporter Associated with Antigen Processing-Independent Pathway In Vitro and In Vivo. *J. Immunol.* **177**, 3525–3533 (2006).

86. Shen, L., Sigal, L. J., Boes, M. & Rock, K. L. Important Role of Cathepsin S in Generating Peptides for TAP-Independent MHC Class I Crosspresentation In Vivo. *Immunity* **21**, 155–165 (2004).

87. Schmid, D., Pypaert, M. & Münz, C. MHC class II antigen loading compartments continuously receive input from autophagosomes. *Immunity* **26**, 79 (2007).

88. Jin, Y. *et al.* Regulation of SIV Antigen-Specific CD4+ T

Cellular Immunity via Autophagosome-Mediated MHC II Molecule-Targeting Antigen Presentation in Mice. *PLoS One* **9**, e93143 (2014).

89. Fonteneau, J. F., Brilot, F., Münz, C. & Gannagé, M. The Tumor Antigen NY-ESO-1 Mediates Direct Recognition of Melanoma Cells by CD4+ T Cells after Intercellular Antigen Transfer. *J. Immunol.* **196**, 64–71 (2016).

90. Kasai, M., Tanida, I., Ueno, T., … E. K.-T. J. of & 2009, undefined. Autophagic compartments gain access to the MHC class II compartments in thymic epithelium. *journals.aai.org*

91. Avtonomov, D. M., Kong, A. & Nesvizhskii, A. I. DeltaMass: Automated detection and visualization of mass shifts in proteomic open-search results. *J. Proteome Res.* **18**, 715 (2019).

92. Jimenez-Morales, D., Adamian, L., Shi, D. & Liang, J. Lysine carboxylation: unveiling a spontaneous post-translational modification. *Acta Crystallogr. Sect. D Biol. Crystallogr.* **70**, 48–57 (2014).

93. Nawale, R. B., Mourya, V. K. & Bhise, S. B. Non-enzymatic glycation of proteins: a cause for complications in diabetes. *Indian J. Biochem. Biophys.* **43**, 337–44 (2006).

94. Delanghe, S., Delanghe, J. R., Speeckaert, R., Van Biesen, W. & Speeckaert, M. M. Mechanisms and consequences of carbamoylation. *Nat. Rev. Nephrol.* **13**, 580–593 (2017).

95. Weng, S.-L. *et al.* Investigation and identification of protein carbonylation sites based on position-specific amino acid composition and physicochemical features. *BMC Bioinformatics* **18**, 66 (2017).

96. Raposo, B. *et al.* T cells specific for post-translational modifications escape intrathymic tolerance induction. *Nat. Commun.* **9**, 353 (2018).

97. Engelhard, V. H., Altrich-Vanlith, M., Ostankovitch, M. & Zarling, A. L. Post-translational modifications of naturally processed MHC-binding epitopes. *Curr. Opin. Immunol.* **18**, 92–97 (2006).

98. Doyle, H. A. & Mamula, M. J. Post-translational protein modifications in antigen recognition and autoimmunity. *Trends Immunol.* **22**, 443–449 (2001).

99. Burkhardt, H. *et al.* Humoral immune response to citrullinated collagen type II determinants in early rheumatoid arthritis. *Eur. J. Immunol.* **35**, 1643–1652 (2005).

100. Roep, B. O., Kracht, M. J., van Lummel, M. & Zaldumbide, A. A roadmap of the generation of neoantigens as targets of the immune system in type 1 diabetes. *Curr. Opin. Immunol.* **43**, 67–73 (2016).

101. Srivastava, A. K., Guadagnin, G., Cappello, P. & Novelli, F. Post-Translational Modifications in Tumor-Associated Antigens as a Platform for Novel Immuno-Oncology Therapies. *Cancers (Basel).* **15**, (2023).

102. Thomas, D., Rathinavel, A. K. & Radhakrishnan, P. Altered glycosylation in cancer: A promising target for biomarkers and therapeutics. *Biochim. Biophys. Acta - Rev. Cancer* **1875**, 188464 (2021).

103. Stowell, S. R., Ju, T. & Cummings, R. D. Protein glycosylation in cancer. *Annu. Rev. Pathol.* **10**, 473–510 (2015).

104. Stowell, S. R., Ju, T. & Cummings, R. D. Protein glycosylation in cancer. *Annu. Rev. Pathol.* **10**, 473–510 (2015).

105. Haurum', J. S. *et al. Peptide anchor residue glycosylation: effect on class I major histocompatibility complex binding and cytotoxic T lymphocyte recognition*. *Eur. J. Immunol* **25**, (1995).

106. Michaëlsson, E. *et al.* T cell recognition of carbohydrates on type II collagen. *J. Exp. Med.* **180**, 745–9 (1994).

107. Haurum, J. S. *et al.* Recognition of carbohydrate by major histocompatibility complex class I-restricted, glycopeptide-specific cytotoxic T lymphocytes. *J. Exp. Med.* **180**, 739–44 (1994).

108. G Y Ishioka, A G Lamont, D Thomson, N Bulbow, F C Gaeta, A Sette, H. M. G. *MHC INTERACTION AND T CELL RECOGNITION AND GLYCOPEPTIDES OF CARBOHYDRATES Downloaded from*. (1992).

109. Harding, U. C. V, Kihlberg, J., Elofsson, M. & Magnusson, G. *Glycopeptides Bind MHC Molecules and Elicit Specific T Cell Responses*. (1993).

110. Deck, B., Elofsson, M., Kihlberg, J. & Unanue, E. R. Specificity of glycopeptide-specific T cells. *J. Immunol.* **155**, 1074–8 (1995).

111. Kario, E., Tirosh, B., Ploegh, H. L. & Navon, A. N-Linked Glycosylation Does Not Impair Proteasomal Degradation but Affects Class I Major Histocompatibility Complex Presentation. *J. Biol. Chem.* **283**, 244–254 (2008).

112. Apostolopoulos, V., Stojanovska, L. & Gargosky, S. E. MUC1 (CD227): a multi-tasked molecule. *Cell. Mol. Life*

Sci. 2015 7223 **72**, 4475–4500 (2015).

113. Ressing, M. E. *et al.* Human CTL epitopes encoded by human papillomavirus type 16 E6 and E7 identified through in vivo and in vitro immunogenicity studies of HLA-A*0201-binding peptides. *J. Immunol.* **154**, 5934–43 (1995).

114. Tabarés, G. *et al.* Different glycan structures in prostate-specific antigen from prostate cancer sera in relation to seminal plasma PSA. *Glycobiology* **16**, 132–145 (2006).

115. Ju, T. *et al.* Human Tumor Antigens Tn and Sialyl Tn Arise from Mutations in Cosmc. *Cancer Res.* **68**, 1636–1646 (2008).

116. Dorsett, K. A. *et al.* Regulation of ST6GAL1 sialyltransferase expression in cancer cells. *Glycobiology* **31**, 530 (2021).

117. Napoletano, C., Rughetti, A., research, M. A. T.-C. & 2007, undefined. Tumor-associated Tn-MUC1 glycoform is internalized through the macrophage galactose-type C-type lectin and delivered to the HLA class I and II compartments in. *AACRC Napoletano, A Rughetti, MP Agervig Tarp, J Coleman, EP Bennett, G Picco, P SaleCancer Res. 2007•AACR*

118. Napoletano, C. *et al.* Targeting of macrophage galactose-type C-type lectin (MGL) induces DC signaling and activation. *Wiley Online Libr. Napoletano, IG Zizzari, A Rughetti, H Rahimi, T Irimura, H Clausen, HH WandallEuropean J. Immunol. 2012•Wiley Online Libr.* **42**, 936–945 (2012).

119. Mohammed, F. *et al.* Phosphorylation-dependent interaction between antigenic peptides and MHC class I: a molecular basis for the presentation of transformed self. *Nat. Immunol.* **9**, 1236–43 (2008).

120. Zarling, A. L. *et al.* Identification of class I MHC-associated phosphopeptides as targets for cancer immunotherapy. *Proc. Natl. Acad. Sci. U. S. A.* **103**, 14889–94 (2006).

121. Andersen, M. H. *et al.* Phosphorylated peptides can be transported by TAP molecules, presented by class I MHC molecules, and recognized by phosphopeptide-specific CTL. *J. Immunol.* **163**, 3812–8 (1999).

122. Li, Y. *et al.* Structural Basis for the Presentation of Tumor-Associated MHC Class II-Restricted Phosphopeptides to CD4+ T Cells. *J. Mol. Biol.* **399**, 596–603 (2010).

123. Zarour, H. M. *et al.* Identification of tumor-associated,

MHC class II-restricted phosphopeptides as targets for immunotherapy. *Proc. Natl. Acad. Sci.* **97**, 400–405 (2009).

124. Abello, N., Kerstjens, H. A. M., Postma, D. S. & Bischoff, R. Protein tyrosine nitration: Selectivity, physicochemical and biological consequences, denitration, and proteomics methods for the identification of tyrosine-nitrated proteins. *J. Proteome Res.* **8**, 3222–3238 (2009).

125. Pignatelli, B. *et al.* Nitrated and Oxidized Plasma Proteins in Smokers and Lung Cancer Patients. *Cancer Res.* **61**, 778–784 (2001).

126. Masri, F. A. *et al.* Abnormalities in Nitric Oxide and Its Derivatives in Lung Cancer. *Am. J. Respir. Crit. Care Med.* **172**, 597–605 (2005).

127. Radi, R. Protein tyrosine nitration: biochemical mechanisms and structural basis of functional effects. *Acc. Chem. Res.* **46**, 550–9 (2013).

128. Benner, E. J. *et al.* Nitrated α–Synuclein Immunity Accelerates Degeneration of Nigral Dopaminergic Neurons. *PLoS One* **3**, e1376 (2008).

129. Gaubaa, V. *et al.* Loss of CD4 T-cell–dependent tolerance to proteins with modified amino acids. *Proc. Natl. Acad.*

Sci. **108**, 12821–12826 (2011).

130. Goldstein, R., Webb H Chaim Birnboim, J. R., Lemay, A.-M. & Ka Yee, D. Cutting Edge: MHC Class II-Restricted Peptides Containing the Inflammation-Associated Marker 3-Nitrotyrosine Evade Central Tolerance and Elicit a Robust Cell-Mediated Immune Response. *J Immunol Ref.* **171**, 528–532 (2003).

131. Herzog, J., Maekawa, Y., Cirrito, T. P., Illian, B. S. & Unanue, E. R. Activated antigen-presenting cells select and present chemically modified peptides recognized by unique CD4 T cells. *PNAS* **102**, 7928–7933 (2005).

132. Ohmori, H. *et al.* Immunogenicity of autologous IgG bearing the inflammation-associated marker 3-nitrotyrosine. *Immunol. Lett.* **96**, 47–54 (2005).

133. Hardy, L. L., Wick, D. A. & Webb, J. R. Conversion of tyrosine to the inflammation-associated analog 3'-nitrotyrosine at either TCR- or MHC-contact positions can profoundly affect recognition of the MHC class I-restricted epitope of lymphocytic choriomeningitis virus glycoprotein 33 by CD8 T ce. *J. Immunol.* **180**, 5956–62 (2008).

134. Nagaraj, S. *et al.* Altered recognition of antigen is a mechanism of CD8+ T cell tolerance in cancer. *Nat. Med.*

13, 828–835 (2007).

135. Kumagai, H. & Urade, R. Deamidation of Gluten Proteins as a Tool for Improving the Properties of Bread. *Flour Breads Their Fortif. Heal. Dis. Prev.* 3–11 (2019). doi:10.1016/B978-0-12-814639-2.00001-0

136. Jabri, B. & Sollid, L. M. T Cells in Celiac Disease. *J. Immunol.* **198**, 3005–3014 (2017).

137. Jonathan A Skipper, B. C. *et al.* An HLA-A2-restricted Tyrosinase Antigen on Melanoma Cells Results from Posttranslational Modification and Suggests a Novel Pathway for Processing of Membrane Proteins. doi:10.1084/jem.183.2.527

138. Dalet, A. *et al.* An antigenic peptide produced by reverse splicing and double asparagine deamidation. doi:10.1073/pnas.1101892108

139. Moss, C. X., Matthews, S. P., Lamont, D. J. & Watts, C. Asparagine deamidation perturbs antigen presentation on class II major histocompatibility complex molecules. *J. Biol. Chem.* **280**, 18498–503 (2005).

140. Fernandes, C., Medronho, B., Alves, L. & Rasteiro, M. G. On Hair Care Physicochemistry: From Structure and Degradation to Novel Biobased Conditioning Agents.

Polymers (Basel). **15**, (2023).

141. Chen, W., Yewdell, J. W., Levine, R. L. & Bennink, J. R. Modification of cysteine residues in vitro and in vivo affects the immunogenicity and antigenicity of major histocompatibility complex class I-restricted viral determinants. *J. Exp. Med.* **189**, 1757–64 (1999).

142. Meadows, L. *et al.* The HLA-A*0201-Restricted H-Y Antigen Contains a Posttranslationally Modified Cysteine That Significantly Affects T Cell Recognition. *Immunity* **6**, 273–281 (1997).

143. Haque, M. A., Hawes, J. W. & Blum, J. S. Cysteinylation of MHC class II ligands: peptide endocytosis and reduction within APC influences T cell recognition. *J. Immunol.* **166**, 4543–51 (2001).

144. Simizu, S. *et al.* Involvement of Disulfide Bond Formation in the Activation of Heparanase. *Cancer Res.* **67**, 7841–7849 (2007).

145. Arif, M. *et al.* Nitric Oxide-Mediated Histone Hyperacetylation in Oral Cancer: Target for a Water-Soluble HAT Inhibitor, CTK7A. *Chem. Biol.* **17**, 903–913 (2010).

146. Bai, X. *et al.* Overexpression of myocyte enhancer factor

2 and histone hyperacetylation in hepatocellular carcinoma. *J Cancer Res Clin Oncol* **134**, 83–91 (2008).

147. Rye, P. T., Frick, L. E., Ozbal, C. C. & Lamarr, W. A. Advances in label-free screening approaches for studying histone acetyltransferases. *J. Biomol. Screen.* **16**, 1186–1195 (2011).

148. Fu, M. *et al.* Acetylation of androgen receptor enhances coactivator binding and promotes prostate cancer cell growth. *Mol. Cell. Biol.* **23**, 8563–75 (2003).

149. Sun, M. *et al.* Nα-terminal acetylation for T cell recognition: molecular basis of MHC class I-restricted nα-acetylpeptide presentation. *J. Immunol.* **192**, 5509–19 (2014).

150. Yagüe, J. *et al.* An N-acetylated natural ligand of human histocompatibility leukocyte antigen (HLA)-B39. Classical major histocompatibility complex class I proteins bind peptides with a blocked NH(2) terminus in vivo. *J. Exp. Med.* **191**, 2083–92 (2000).

151. Yagüe, J. *et al.* An N-acetylated Natural Ligand of Human Histocompatibility Leukocyte Antigen (HLA)-B39: Classical Major Histocompatibility Complex Class I Proteins Bind Peptides with a Blocked NH 2 Terminus In Vivo. *J. Exp. Med* **191**, (2000).

152. He, X. *et al.* Structural Snapshot of Aberrant Antigen Presentation Linked to Autoimmunity: The Immunodominant Epitope of MBP Complexed with I-Au. *Immunity* **17**, 83–94 (2002).

153. Kumai, T. *et al.* Induction of tumor-reactive T helper responses by a posttranslational modified epitope from tumor protein p53. *Cancer Immunol. Immunother.* **63**, 469–478 (2014).

154. Seligson, D. B. *et al.* Global histone modification patterns predict risk of prostate cancer recurrence. *Nature* **435**, 1262–1266 (2005).

155. Wang, H. *et al.* Methylation of Histone H4 at Arginine 3 Facilitating Transcriptional Activation by Nuclear Hormone Receptor. *Science (80-.).* **293**, 853–857 (2001).

156. Le Romancer, M., Treilleux, I., Bouchekioua-Bouzaghou, K., Sentis, S. & Corbo, L. Methylation, a key step for nongenomic estrogen signaling in breast tumors. *Steroids* **75**, 560–564 (2010).

157. Gu, H. *et al.* Identification of highly methylated arginine residues in an endogenous 20-kDa polypeptide in cancer cells. *Life Sci.* **65**, 737–745 (1999).

158. Zhang, Y. & Reinberg, D. Transcription regulation by histone methylation: Interplay between different covalent modifications of the core histone tails. *Genes Dev.* **15**, 2343–2360 (2001).

159. Marino, F. *et al.* Arginine (Di)methylated Human Leukocyte Antigen Class I Peptides Are Favorably Presented by HLA-B*07. (2016). doi:10.1021/acs.jproteome.6b00528

160. Jarmalavicius, S., Trefzer, U. & Walden, P. Differential arginine methylation of the G-protein pathway suppressor GPS-2 recognized by tumor-specific T cells in melanoma. *FASEB J.* **24**, 937–946 (2010).

161. Nadolski, M. J. & Linder, M. E. Protein lipidation. *FEBS J.* **274**, 5202–5210 (2007).

162. Zhang, F. & Du, G. Dysregulated lipid metabolism in cancer. *World J. Biol. Chem.* **3**, 167–74 (2012).

163. Yamamoto, Y. *et al.* Identification and Structure of an MHC Class I-Encoded Protein with the Potential to Present N-Myristoylated 4-mer Peptides to T Cells. *J. Immunol.* **202**, 3349–3358 (2019).

164. Morita, D. & Sugita, M. Lipopeptides: a novel antigen repertoire presented by major histocompatibility complex

class I molecules. *Immunology* **149**, 139–45 (2016).

165. Gahéry-Ségard, H. *et al.* Multiepitopic B- and T-cell responses induced in humans by a human immunodeficiency virus type 1 lipopeptide vaccine. *J. Virol.* **74**, 1694–703 (2000).

166. Deres, K., Schild, H., Wiesmüller, K.-H., Jung, G. & Rammensee, H.-G. In vivo priming of virus-specific cytotoxic T lymphocytes with synthetic lipopeptide vaccine. *Nature* **342**, 561–564 (1989).

167. Stittelaar, K. J. *et al.* In vitro processing and presentation of a lipidated cytotoxic T-cell epitope derived from measles virus fusion protein. *Vaccine* **20**, 249–261 (2001).

168. Srebrow, A. & Kornblihtt, A. R. The connection between splicing and cancer. *J. Cell Sci.* **119**, 2635–2641 (2006).

169. Singh, B. & Eyras, E. The role of alternative splicing in cancer. *Transcription* **8**, 91–98 (2017).

170. Kahles, A., Lehmann, K.-V., Toussaint, N. C. & Sander, C. Comprehensive Analysis of Alternative Splicing Across Tumors from 8,705 Patients. (2018). doi:10.1016/j.ccell.2018.07.001

171. Smart, A. C. *et al.* Intron retention is a source of

neoepitopes in cancer. *Nat. Biotechnol.* **36**, 1056–1058 (2018).

172. Jayasinghe, R. G. *et al.* Systematic Analysis of Splice-Site-Creating Mutations in Cancer. *Cell Rep.* **23**, 270-281.e3 (2018).

173. Guerrin, M. *et al.* cDNA cloning, gene organization and expression analysis of human peptidylarginine deiminase type I. *Biochem. J.* **370**, 167–174 (2003).

174. Zhang, Y. *et al.* PADs in cancer: Current and future. *Biochim. Biophys. Acta - Rev. Cancer* **1875**, 188492 (2021).

175. Nachat, R. *et al.* Peptidylarginine Deiminase Isoforms Are Differentially Expressed in the Anagen Hair Follicles and Other Human Skin Appendages. *J. Invest. Dermatol.* **125**, 34–41 (2005).

176. Chang, X. *et al.* Increased PADI4 expression in blood and tissues of patients with malignant tumors. *BMC Cancer* **9**, 1–11 (2009).

177. Horibata, S., Coonrod, S. A. & Cherrington, B. D. Role for Peptidylarginine Deiminase Enzymes in Disease and Female Reproduction. *J. Reprod. Dev.* **58**, 274–282 (2012).

178. Nguyen, H. & James, E. A. Immune recognition of citrullinated epitopes. *Immunology* **149**, 131–8 (2016).

179. Brentville, V. A., Vankemmelbeke, M., Metheringham, R. L. & Durrant, L. G. Post-translational modifications such as citrullination are excellent targets for cancer therapy. *Semin. Immunol.* **47**, 101393 (2020).

180. Takahara, H., Okamoto, H. & Sugawara, K. Calcium-dependent Properties of Peptidylarginine Deiminase from Rabbit Skeletal Muscle. *Agric. Biol. Chem.* **50**, 2899–2904 (1986).

181. Chang, X. *et al.* Increased PADI4 expression in blood and tissues of patients with malignant tumors. *BMC Cancer* **9**, 40 (2009).

182. Ireland, J. M. & Unanue, E. R. Autophagy in antigen-presenting cells results in presentation of citrullinated peptides to CD4 T cells. *J. Exp. Med.* **208**, 2625–32 (2011).

183. Brentville, V. A. *et al.* Citrullinated Vimentin Presented on MHC-II in Tumor Cells Is a Target for CD4 þ T-Cell-Mediated Antitumor Immunity. (2016). doi:10.1158/0008-5472.CAN-15-1085

184. Brentville, V. A. *et al.* T cell repertoire to citrullinated

self-peptides in healthy humans is not confined to the HLA-DR SE alleles; Targeting of citrullinated self-peptides presented by HLA-DP4 for tumour therapy. *Oncoimmunology* **8**, e1576490 (2019).

185. Lee, C.-Y. *et al. Mining the human tissue proteome for protein citrullination*. (MCP Papers in Press, 2018).

186. Hill, J. A. *et al.* Cutting edge: the conversion of arginine to citrulline allows for a high-affinity peptide interaction with the rheumatoid arthritis-associated HLA-DRB1*0401 MHC class II molecule. *J. Immunol.* **171**, 538–41 (2003).

187. Law, S. C. *et al.* T-cell autoreactivity to citrullinated autoantigenic peptides in rheumatoid arthritis patients carrying HLA-DRB1 shared epitope alleles. *Arthritis Res. Ther.* **14**, R118 (2012).

188. Ting, Y. T. *et al.* The interplay between citrullination and HLA-DRB1 polymorphism in shaping peptide binding hierarchies in rheumatoid arthritis. *J. Biol. Chem.* **293**, 3236–3251 (2018).

189. Tarcsa, E. *et al.* Protein unfolding by peptidylarginine deiminase: Substrate specificity and structural relationships of the natural substrates trichohyalin and filaggrin. *J. Biol. Chem.* **271**, 30709–30716 (1996).

190. György, B., Tóth, E., Tarcsa, E., Falus, A. & Buzás, E. I. Citrullination: A posttranslational modification in health and disease. *International Journal of Biochemistry and Cell Biology* **38**, 1662–1677 (2006).

191. Pritzker, L. B., Joshi, S., Gowan, J. J., Harauz, G. & Moscarello, M. A. Deimination of Myelin Basic Protein. 1. Effect of Deimination of Arginyl Residues of Myelin Basic Protein on Its Structure and Susceptibility to Digestion by Cathepsin D †. *Biochemistry* **39**, 5374–5381 (2000).

192. Nakashima, K., Hagiwara, T. & Yamada, M. Nuclear localization of peptidylarginine deiminase V and histone deimination in granulocytes. *J. Biol. Chem.* **277**, 49562–49568 (2002).

193. Wang, Y. *et al.* Human PAD4 regulates histone arginine methylation levels via demethylimination. *Science (80-.).* **306**, 279–283 (2004).

194. Mizoguchi, M. *et al.* Deimination of 70-kD Nuclear Protein During Epidermal Apoptotic Events In Vitro. *J. Histochem. Cytochem.* **46**, 1303–1309 (1998).

195. Neeli, I., Khan, S. N. & Radic, M. Histone deimination as a response to inflammatory stimuli in neutrophils. *J. Immunol.* **180**, 1895–902 (2008).

196. Li, P. *et al.* PAD4 is essential for antibacterial innate immunity mediated by neutrophil extracellular traps. *J. Exp. Med.* **207**, 1853–1862 (2010).

197. Christophorou, M. A. *et al.* Citrullination regulates pluripotency and histone H1 binding to chromatin. *Nature* **507**, 104–108 (2014).

198. Struyf, S. *et al.* Citrullination of CXCL12 Differentially Reduces CXCR4 and CXCR7 Binding with Loss of Inflammatory and Anti-HIV-1 Activity via CXCR4. *J. Immunol.* **182**, 666–674 (2009).

199. Baka, Z. *et al.* Citrullination under physiological and pathological conditions. *Joint Bone Spine* **79**, 431–436 (2012).

200. Loos, T., Opdenakker, G., Van Damme, J. & Proost, P. Citrullination of CXCL8 increases this chemokine's ability to mobilize neutrophils into the blood circulation. *Haematologica* **94**, 1346–1353 (2009).

201. Tanikawa, C. *et al.* Regulation of protein citrullination through p53/PADI4Network in DNA damage response. *Cancer Res.* **69**, 8761–8769 (2009).

202. Yao, H. *et al.* Histone Arg modifications and p53 regulate the expression of OKL38, a mediator of apoptosis. *J. Biol.*

Chem. **283**, 20060–20068 (2008).

203. Li, P. *et al.* Regulation of p53 Target Gene Expression by Peptidylarginine Deiminase 4. *Mol. Cell. Biol.* **28**, 4745–4758 (2008).

204. Guo, Q. & Fast, W. Citrullination of Inhibitor of Growth 4 (ING4) by Peptidylarginine Deminase 4 (PAD4) disrupts the interaction between ING4 and p53. *J. Biol. Chem.* **286**, 17069–17078 (2011).

205. Zhou, Y. *et al.* Spontaneous secretion of the citrullination enzyme PAD2 and cell surface exposure of PAD4 by neutrophils. *Front. Immunol.* **8**, (2017).

206. Padyukov, L., Silva, C., Stolt, P., Alfredsson, L. & Klareskog, L. A gene-environment interaction between smoking and shared epitope genes in HLA-DR provides a high risk of seropositive rheumatoid arthritis. *Arthritis Rheum.* **50**, 3085–3092 (2004).

207. Klareskog, L., Rönnelid, J., Lundberg, K., Padyukov, L. & Alfredsson, L. Immunity to Citrullinated Proteins in Rheumatoid Arthritis. *Annu. Rev. Immunol.* **26**, 651–675 (2008).

208. Marotte, H. *et al.* The association between periodontal disease and joint destruction in rheumatoid arthritis

extends the link between the HLA-DR shared epitope and severity of bone destruction. *Ann. Rheum. Dis.* **65**, 905–909 (2006).

209. Zhou, Y. *et al.* Spontaneous Secretion of the Citrullination Enzyme PAD2 and Cell Surface Exposure of PAD4 by Neutrophils. *Front. Immunol.* **8**, 1200 (2017).

210. Chang, X. & Han, J. Expression of peptidylarginine deiminase type 4 (PAD4) in various tumors. *Mol. Carcinog.* **45**, 183–196 (2006).

211. Chang, X. *et al.* Increased PADI4 expression in blood and tissues of patients with malignant tumors. *BMC Cancer* **9**, (2009).

212. Ordóñez, A. *et al.* Effect of citrullination on the function and conformation of antithrombin. *FEBS J.* **276**, 6763–6772 (2009).

213. Zhang, X. *et al.* Genome-Wide analysis reveals PADI4 cooperates with Elk-1 to activate C-Fos expression in breast cancer cells. *PLoS Genet.* **7**, (2011).

214. Katayama, H. *et al.* Protein citrullination as a source of cancer neoantigens. *J. Immunother. Cancer* **9**, e002549 (2021).

215. Jiang, Z. *et al.* Investigating citrullinated proteins in

tumour cell lines. *World J. Surg. Oncol.* **11**, (2013).

216. Ylä-Anttila, P., Vihinen, H., Jokitalo, E. & Eskelinen, E. L. Chapter 10 Monitoring Autophagy by Electron Microscopy in Mammalian Cells. *Methods Enzymol.* **452**, 143–164 (2009).

217. Dou, Z. *et al.* Autophagy mediates degradation of nuclear lamina. *Nat. 2015 5277576* **527**, 105–109 (2015).

218. Ganley, I. G. *et al.* ULK1·ATG13·FIP200 complex mediates mTOR signaling and is essential for autophagy. *J. Biol. Chem.* **284**, 12297–12305 (2009).

219. Bach, M., Larance, M., James, D. E. & Ramm, G. The serine/threonine kinase ULK1 is a target of multiple phosphorylation events. *Biochem. J.* **440**, 283–291 (2011).

220. Kamber, R. A., Shoemaker, C. J. & Denic, V. Receptor-Bound Targets of Selective Autophagy Use a Scaffold Protein to Activate the Atg1 Kinase. *Mol. Cell* **59**, 372–381 (2015).

221. Yeh, Y. Y., Wrasman, K. & Herman, P. K. Autophosphorylation Within the Atg1 Activation Loop Is Required for Both Kinase Activity and the Induction of Autophagy in Saccharomyces cerevisiae. *Genetics* **185**,

871–882 (2010).

222. Bar-Peled, L. & Sabatini, D. M. Regulation of mTORC1 by amino acids. *Trends Cell Biol.* **24**, 400–406 (2014).

223. Egan, D. F. *et al.* Phosphorylation of ULK1 (hATG1) by AMP-activated protein kinase connects energy sensing to mitophagy. *Science (80-.).* **331**, 456–461 (2011).

224. Chan, E. Y. W., Longatti, A., McKnight, N. C. & Tooze, S. A. Kinase-Inactivated ULK Proteins Inhibit Autophagy via Their Conserved C-Terminal Domains Using an Atg13-Independent Mechanism. *https://doi.org/10.1128/MCB.01082-08* **29**, 157–171 (2023).

225. Alemu, E. A. *et al.* ATG8 family proteins act as scaffolds for assembly of the ULK complex: Sequence requirements for LC3-interacting region (LIR) motifs. *J. Biol. Chem.* **287**, 39275–39290 (2012).

226. Di Bartolomeo, S. *et al.* The dynamic interaction of AMBRA1 with the dynein motor complex regulates mammalian autophagy. *J. Cell Biol.* **191**, 155–168 (2010).

227. Egan, D. F. *et al.* Small Molecule Inhibition of the Autophagy Kinase ULK1 and Identification of ULK1

Substrates. *Mol. Cell* **59**, 285–297 (2015).

228. Russell, R. C. *et al.* ULK1 induces autophagy by phosphorylating Beclin-1 and activating VPS34 lipid kinase. *Nat. Cell Biol. 2013 157* **15**, 741–750 (2013).

229. Kumar, S. *et al.* Mammalian hybrid pre-autophagosomal structure HyPAS generates autophagosomes. *Cell* **184**, 5950-5969.e22 (2021).

230. Mari, M. *et al.* An Atg9-containing compartment that functions in the early steps of autophagosome biogenesis. *J. Cell Biol.* **190**, 1005–1022 (2010).

231. Ravikumar, B., Moreau, K., Jahreiss, L., Puri, C. & Rubinsztein, D. C. Plasma membrane contributes to the formation of pre-autophagosomal structures. *Nat. Cell Biol.* **12**, 747–757 (2010).

232. Kumar, S. *et al.* Phosphorylation of Syntaxin 17 by TBK1 Controls Autophagy Initiation. *Dev. Cell* **49**, 130-144.e6 (2019).

233. Zhao, Y. G. *et al.* The ER Contact Proteins VAPA/B Interact with Multiple Autophagy Proteins to Modulate Autophagosome Biogenesis. *Curr. Biol.* **28**, 1234-1245.e4 (2018).

234. Puri, C., Renna, M., Bento, C. F., Moreau, K. &

Rubinsztein, D. C. Diverse autophagosome membrane sources coalesce in recycling endosomes. *Cell* **154**, (2013).

235. Itakura, E., Kishi, C., Inoue, K. & Mizushima, N. Beclin 1 forms two distinct phosphatidylinositol 3-kinase complexes with mammalian Atg14 and UVRAG. *Mol. Biol. Cell* **19**, 5360–5372 (2008).

236. Kametaka, S., Okano, T., Ohsumi, M. & Ohsumi, Y. Apg14p and Apg6/Vps30p form a protein complex essential for autophagy in the yeast, Saccharomyces cerevisiae. *J. Biol. Chem.* **273**, 22284–22291 (1998).

237. Obara, K., Sekito, T. & Ohsumi, Y. Assortment of phosphatidylinositol 3-kinase complexes-Atg14p directs association of complex I to the pre-autophagosomal structure in Saccharomyces cerevisiae. *Mol. Biol. Cell* **17**, 1527–1539 (2006).

238. Zhong, Y. *et al.* Distinct regulation of autophagic activity by Atg14L and Rubicon associated with Beclin 1–phosphatidylinositol-3-kinase complex. *Nat. Cell Biol. 2009 114* **11**, 468–476 (2009).

239. Young, L. N., Cho, K., Lawrence, R., Zoncu, R. & Hurley, J. H. Dynamics and architecture of the NRBF2-containing phosphatidylinositol 3-kinase complex I of autophagy.

Proc. Natl. Acad. Sci. U. S. A. **113**, 8224–8229 (2016).

240. Wei, Y. *et al.* The stress-responsive kinases MAPKAPK2/MAPKAPK3 activate starvation-induced autophagy through Beclin 1 phosphorylation. *Elife* **2015**, (2015).

241. Kim, J. *et al.* Differential regulation of distinct Vps34 complexes by AMPK in nutrient stress and autophagy. *Cell* **152**, 290–303 (2013).

242. Fujiwara, N., Usui, T., Ohama, T. & Sato, K. Regulation of beclin 1 protein phosphorylation and autophagy by protein phosphatase 2A (PP2A) and death-associated protein kinase 3 (DAPK3). *J. Biol. Chem.* **291**, 10858–10866 (2016).

243. Hu, Y. & Reggiori, F. Molecular regulation of autophagosome formation. *Biochem. Soc. Trans.* **50**, 55–69 (2022).

244. Axe, E. L. *et al.* Autophagosome formation from membrane compartments enriched in phosphatidylinositol 3-phosphate and dynamically connected to the endoplasmic reticulum. *J. Cell Biol.* **182**, 685–701 (2008).

245. Valverde, D. P. *et al.* ATG2 transports lipids to promote

autophagosome biogenesis. *J. Cell Biol.* **218**, 1787–1798 (2019).

246. Nakatogawa, H., Ichimura, Y. & Ohsumi, Y. Atg8, a ubiquitin-like protein required for autophagosome formation, mediates membrane tethering and hemifusion. *Cell* **130**, 165–178 (2007).

247. Maruyama, T. *et al.* Membrane perturbation by lipidated Atg8 underlies autophagosome biogenesis. *Nat. Struct. Mol. Biol. 2021 287* **28**, 583–593 (2021).

248. Knorr, R. L. *et al.* Membrane Morphology Is Actively Transformed by Covalent Binding of the Protein Atg8 to PE-Lipids. *PLoS One* **9**, e115357 (2014).

249. Mi, N. *et al.* CapZ regulates autophagosomal membrane shaping by promoting actin assembly inside the isolation membrane. *Nat. Cell Biol. 2015 179* **17**, 1112–1123 (2015).

250. Zhou, F. *et al.* Rab5-dependent autophagosome closure by ESCRT. *J. Cell Biol.* **218**, 1908–1927 (2019).

251. Wu, Y. *et al.* PI3P phosphatase activity is required for autophagosome maturation and autolysosome formation. *EMBO Rep.* **15**, 973–981 (2014).

252. Tooze, J. *et al.* In exocrine pancreas, the basolateral

endocytic pathway converges with the autophagic pathway immediately after the early endosome. *J. Cell Biol.* **111**, 329–345 (1990).

253. Liou, W., Geuze, H. J., Geelen, M. J. H. & Slot, J. W. The autophagic and endocytic pathways converge at the nascent autophagic vacuoles. *J. Cell Biol.* **136**, 61–70 (1997).

254. Razi, M., Chan, E. Y. W. & Tooze, S. A. Early endosomes and endosomal coatomer are required for autophagy. *J. Cell Biol.* **185**, 305–321 (2009).

255. Jahreiss, L., Menzies, F. M. & Rubinsztein, D. C. The itinerary of autophagosomes: from peripheral formation to kiss-and-run fusion with lysosomes. *Traffic* **9**, 574–587 (2008).

256. Zhao, Y. G. & Zhang, H. Autophagosome maturation: An epic journey from the ER to lysosomes. *J. Cell Biol.* **218**, 757–770 (2019).

257. Ghislat, G. & Lawrence, T. Autophagy in dendritic cells. *Cell. Mol. Immunol.* **15**, 944–952 (2018).

258. Schmid, D., Pypaert, M. & Münz, C. Antigen-Loading Compartments for Major Histocompatibility Complex Class II Molecules Continuously Receive Input from

Autophagosomes. *Immunity* **26**, 79–92 (2007).

259. Mintern, J. D. *et al.* Differential use of autophagy by primary dendritic cells specialized in cross-presentation. *Autophagy* **11**, 906–917 (2015).

260. Romao, S. *et al.* Autophagy proteins stabilize pathogen-containing phagosomes for prolonged MHC II antigen processing. *J. Cell Biol.* **203**, 757–66 (2013).

261. Ligeon, L.-A., Romao, S. & Münz, C. Analysis of LC3-Associated Phagocytosis and Antigen Presentation. in 145–168 (Humana Press, New York, NY, 2017). doi:10.1007/978-1-4939-6581-6_10

262. Martinez, J. *et al.* Microtubule-associated protein 1 light chain 3 alpha (LC3)-associated phagocytosis is required for the efficient clearance of dead cells. *Proc. Natl. Acad. Sci. U. S. A.* **108**, 17396–401 (2011).

263. Sorice, M. *et al.* Autophagy generates citrullinated peptides in human synoviocytes: a possible trigger for anti-citrullinated peptide antibodies. *Rheumatology* **55**, 1374–1385 (2016).

264. Sugawara, E. *et al.* Autophagy promotes citrullination of VIM (vimentin) and its interaction with major histocompatibility complex class II in synovial fibroblasts.

Autophagy **16**, 946–955 (2020).

265. Sharifi, M. N., Mowers, E. E., Drake, L. E. & Macleod, K. F. Measuring Autophagy in Stressed Cells. *Methods Mol. Biol.* **1292**, 129 (2015).

266. Ge, L., Melville, D., Zhang, M. & Schekman, R. The ER–Golgi intermediate compartment is a key membrane source for the LC3 lipidation step of autophagosome biogenesis. *Elife* **2**, 1–23 (2013).

267. Brentville, V. A. *et al.* T cell repertoire to citrullinated self-peptides in healthy humans is not confined to the HLA-DR SE alleles; Targeting of citrullinated self-peptides presented by HLA-DP4 for tumour therapy. *Oncoimmunology* **8**, (2019).

268. Bicker, K. L., Subramanian, V., Chumanevich, A. A., Hofseth, L. J. & Thompson, P. R. Seeing Citrulline: Development of a phenylglyoxal-based probe to visualize protein citrullination. *J. Am. Chem. Soc.* **134**, 17015 (2012).

269. Neve, R. M. *et al.* A collection of breast cancer cell lines for the study of functionally distinct cancer subtypes. *Cancer Cell* **10**, 515–527 (2006).

270. Domcke, S., Sinha, R., Levine, D. A., Sander, C. &

Schultz, N. Evaluating cell lines as tumour models by comparison of genomic profiles. *Nat. Commun.* **4**, (2013).

271. Li, H. *et al.* Genomic analysis of head and neck squamous cell carcinoma cell lines and human tumors: a rational approach to preclinical model selection. *Mol. Cancer Res.* **12**, 571–582 (2014).

272. Mouradov, D. *et al.* Colorectal cancer cell lines are representative models of the main molecular subtypes of primary cancer. *Cancer Res.* **74**, 3238–3247 (2014).

273. Barretina, J. *et al.* The Cancer Cell Line Encyclopedia enables predictive modeling of anticancer drug sensitivity. *Nature* **483**, 603 (2012).

274. Garnett, M. J. *et al.* Systematic identification of genomic markers of drug sensitivity in cancer cells. *Nature* **483**, 570–575 (2012).

275. White, E., Karp, C., Strohecker, A. M., Guo, Y. & Mathew, R. Role of autophagy in suppression of inflammation and cancer. *Curr. Opin. Cell Biol.* **22**, 212 (2010).

276. Mathew, R. *et al.* Autophagy Suppresses Tumorigenesis Through Elimination of p62. *Cell* **137**, 1062 (2009).

277. Takamura, A. *et al.* Autophagy-deficient mice develop

multiple liver tumors. *Genes Dev.* **25**, 795 (2011).

278. Ding, Z. Bin *et al.* Association of autophagy defect with a malignant phenotype and poor prognosis of hepatocellular carcinoma. *Cancer Res.* **68**, 9167–9175 (2008).

279. Liang, X. H. *et al.* Induction of autophagy and inhibition of tumorigenesis by beclin 1. *Nature* **402**, 672–676 (1999).

280. Barnard, R. A. *et al.* Autophagy inhibition delays early but not late-stage metastatic disease. *J. Pharmacol. Exp. Ther.* **358**, 282–293 (2016).

281. Fung, C., Lock, R., Gao, S., Salas, E. & Debnath, J. Induction of Autophagy during Extracellular Matrix Detachment Promotes Cell Survival. *Mol. Biol. Cell* **19**, 797 (2008).

282. Lum, J. J. *et al.* Growth factor regulation of autophagy and cell survival in the absence of apoptosis. *Cell* **120**, 237–248 (2005).

283. Degenhardt, K. *et al.* Autophagy promotes tumor cell survival and restricts necrosis, inflammation, and tumorigenesis. *Cancer Cell* **10**, 51 (2006).

284. Guo, J. Y., Xia, B. & White, E. Autophagy-Mediated

Tumor Promotion. *Cell* **155**, 1216 (2013).

285. Mancias, J. D. & Kimmelman, A. C. Targeting Autophagy Addiction in Cancer. *Oncotarget* **2**, 1302 (2011).

286. Ahn, C. H. *et al.* Expression of beclin-1, an autophagy-related protein, in gastric and colorectal cancers. *APMIS* **115**, 1344–1349 (2007).

287. O'Donnell, J. S., Massi, D., Teng, M. W. L. & Mandala, M. PI3K-AKT-mTOR inhibition in cancer immunotherapy, redux. *Semin. Cancer Biol.* **48**, 91–103 (2018).

288. Vézina, C. & Kudelski, A. RAPAMYCIN (AY-22, 989), A NEW ANTIFUNGAL ANTIBIOTIC I. TAXONOMY OF THE PRODUCING STREPTOMYCETE AND ISOLATION OF THE ACTIVE PRINCIPLE. *J. Antibiot. (Tokyo).* **28**, 721–726 (1975).

289. Brown, E. J. *et al.* A mammalian protein targeted by G1-arresting rapamycin–receptor complex. *Nat. 1994 3696483* **369**, 756–758 (1994).

290. Dos, D. S. *et al.* Rictor, a Novel Binding Partner of mTOR, Defines a Rapamycin-Insensitive and Raptor-Independent Pathway that Regulates the Cytoskeleton. *Curr. Biol.* **14**, 1296–1302 (2004).

291. Peterson, T. R. *et al.* DEPTOR is an mTOR inhibitor

frequently overexpressed in multiple myeloma cells and required for their survival. *Cell* **137**, 873–886 (2009).

292. Kim, D. H. *et al.* GbetaL, a positive regulator of the rapamycin-sensitive pathway required for the nutrient-sensitive interaction between raptor and mTOR. *Mol. Cell* **11**, 895–904 (2003).

293. Kaizuka, T. *et al.* Tti1 and Tel2 are critical factors in mammalian target of rapamycin complex assembly. *J. Biol. Chem.* **285**, 20109–20116 (2010).

294. Hara, K. *et al.* Raptor, a binding partner of target of rapamycin (TOR), mediates TOR action. *Cell* **110**, 177–189 (2002).

295. Waldner, M., Fantus, D., Solari, M. & Thomson, A. W. New perspectives on mTOR inhibitors (rapamycin, rapalogs and TORKinibs) in transplantation. *Br. J. Clin. Pharmacol.* **82**, 1158 (2016).

296. Pearce, L. R. *et al.* Identification of Protor as a novel Rictor-binding component of mTOR complex-2. *Biochem. J.* **405**, 513–522 (2007).

297. Jacinto, E. *et al.* SIN1/MIP1 maintains rictor-mTOR complex integrity and regulates Akt phosphorylation and substrate specificity. *Cell* **127**, 125–137 (2006).

298. Li, J., Kim, S. G. & Blenis, J. Rapamycin: one drug, many effects. *Cell Metab.* **19**, 373 (2014).

299. Sarbassov, D. D. *et al.* Prolonged Rapamycin Treatment Inhibits mTORC2 Assembly and Akt/PKB. *Mol. Cell* **22**, 159–168 (2006).

300. Banaszynski, L. A., Liu, C. W. & Wandless, T. J. Characterization of the FKBP-rapamycin-FRB ternary complex. *J. Am. Chem. Soc.* **127**, 4715–4721 (2005).

301. Ganley, I. G. *et al.* ULK1·ATG13·FIP200 Complex Mediates mTOR Signaling and Is Essential for Autophagy. *J. Biol. Chem.* **284**, 12297 (2009).

302. Jung, C. H. *et al.* ULK-Atg13-FIP200 Complexes Mediate mTOR Signaling to the Autophagy Machinery. *Mol. Biol. Cell* **20**, 1992 (2009).

303. Sarbassov, D. D. *et al.* Prolonged Rapamycin Treatment Inhibits mTORC2 Assembly and Akt/PKB. *Mol. Cell* **22**, 159–168

304. Jhanwar-Uniyal, M. *et al.* Diverse signaling mechanisms of mTOR complexes: mTORC1 and mTORC2 in forming a formidable relationship. *Adv. Biol. Regul.* **72**, 51–62 (2019).

305. Pou, S. *et al.* Sontochin as a Guide to the Development

of Drugs against Chloroquine-Resistant Malaria. *Antimicrob. Agents Chemother.* **56**, 3475 (2012).

306. Andersag, H., Breitner, S. & Jung, H. Quinoline compound and process of. (1941).

307. Coatney, G. R. PITFALLS IN A DISCOVERY: THE CHRONICLE OF CHLOROQUINE*.

308. Trout, J. J., Stauber, W. T. & Schottelius, B. A. Increased autophagy in chloroquine-treated tonic and phasic muscles: An alternative view. *Tissue Cell* **13**, 393–401 (1981).

309. Mauthe, M. *et al.* Chloroquine inhibits autophagic flux by decreasing autophagosome-lysosome fusion. *Autophagy* **14**, 1435 (2018).

310. Jacquin, E. *et al.* Pharmacological modulators of autophagy activate a parallel noncanonical pathway driving unconventional LC3 lipidation. *Autophagy* **13**, 854 (2017).

311. Kawasaki, T. & Kawai, T. Toll-like receptor signaling pathways. *Front. Immunol.* **5**, 1–8 (2014).

312. Lu, N. *et al.* Two PI 3-Kinases and One PI 3-Phosphatase Together Establish the Cyclic Waves of Phagosomal PtdIns(3)P Critical for the Degradation of Apoptotic Cells.

PLOS Biol. **10**, e1001245 (2012).

313. Vlahos, C. J., Matter, W. F., Hui, K. Y. & Brown, R. F. A specific inhibitor of phosphatidylinositol 3-kinase, 2-(4-morpholinyl)- 8-phenyl-4H-1-benzopyran-4-one (LY294002). *J. Biol. Chem.* **269**, 5241–5248 (1994).

314. Blommaart, E. F. C., Krause, U., Schellens, J. P. M., Vreeling-Sindelárová, H. & Meijer, A. J. The Phosphatidylinositol 3-Kinase Inhibitors Wortmannin and LY294002 Inhibit Autophagy in Isolated Rat Hepatocytes. *Eur. J. Biochem.* **243**, 240–246 (1997).

315. Petiot, A., Ogier-Denis, E., Blommaart, E. F. C., Meijer, A. J. & Codogno, P. Distinct Classes of Phosphatidylinositol 3′-Kinases Are Involved in Signaling Pathways That Control Macroautophagy in HT-29 Cells. *J. Biol. Chem.* **275**, 992–998 (2000).

316. Dou, Z. *et al.* Class IA PI3-kinase p110β subunit promotes autophagy through Rab5 small GTPase in response to growth factor limitation. *Mol. Cell* **50**, 29 (2013).

317. Jewell, J. L. & Guan, K. L. Nutrient Signaling to mTOR and Cell Growth. *Trends Biochem. Sci.* **38**, 233 (2013).

318. Zhou, J. *et al.* Activation of lysosomal function in the

course of autophagy via mTORC1 suppression and autophagosome-lysosome fusion. *Cell Res. 2013 234* **23**, 508–523 (2013).

319. Liang, C. *et al.* Beclin1-binding UVRAG targets the class C Vps complex to coordinate autophagosome maturation and endocytic trafficking. *Nat. Cell Biol. 2008 107* **10**, 776–787 (2008).

320. Peplowska, K., Markgraf, D. F., Ostrowicz, C. W., Bange, G. & Ungermann, C. The CORVET Tethering Complex Interacts with the Yeast Rab5 Homolog Vps21 and Is Involved in Endo-Lysosomal Biogenesis. *Dev. Cell* **12**, 739–750 (2007).

321. Sato, T. K., Rehling, P., Peterson, M. R. & Emr, S. D. Class C Vps Protein Complex Regulates Vacuolar SNARE Pairing and Is Required for Vesicle Docking/Fusion. *Mol. Cell* **6**, 661–671 (2000).

322. Jiang, P. *et al.* The HOPS complex mediates autophagosome-lysosome fusion through interaction with syntaxin 17. *Mol. Biol. Cell* **25**, 1327–1337 (2014).

323. Takáts, S. *et al.* Interaction of the HOPS complex with Syntaxin 17 mediates autophagosome clearance in Drosophila. *Mol. Biol. Cell* **25**, 1338–1354 (2014).

324. Schmid, D., Pypaert, M. & Münz, C. Antigen-Loading Compartments for Major Histocompatibility Complex Class II Molecules Continuously Receive Input from Autophagosomes. *Immunity* **26**, 79–92 (2007).

325. Pan, C., Kumar, C., Bohl, S., Klingmueller, U. & Mann, M. Comparative Proteomic Phenotyping of Cell Lines and Primary Cells to Assess Preservation of Cell Type-specific Functions* □ S. (2009). doi:10.1074/mcp.M800258-MCP200

326. Basu, A. Regulation of Autophagy by Protein Kinase C-ε in Breast Cancer Cells. *Int. J. Mol. Sci. 2020, Vol. 21, Page 4247* **21**, 4247 (2020).

327. Guan, F. *et al.* Curcumin Suppresses Proliferation and Migration of MDA-MB-231 Breast Cancer Cells through Autophagy-Dependent Akt Degradation. *PLoS One* **11**, e0146553 (2016).

328. Ambjørn, M. *et al.* IFNB1/interferon-β-induced autophagy in MCF-7 breast cancer cells counteracts its proapoptotic function. *https://doi.org/10.4161/auto.22831* **9**, 287–302 (2012).

329. Sivaprasad, U. & Basu, A. Inhibition of ERK attenuates autophagy and potentiates tumour necrosis factor-α-induced cell death in MCF-7 cells. *J. Cell. Mol. Med.* **12**,

1265–1271 (2008).

330. Chen, Y., Liersch, R. & Detmar, M. The miR-290-295 cluster suppresses autophagic cell death of melanoma cells. *Sci. Reports 2012 21* **2**, 1–10 (2012).

331. Park, H. J. *et al.* Melasolv induces melanosome autophagy to inhibit pigmentation in B16F1 cells. *PLoS One* **15**, e0239019 (2020).

332. Elgendy, M., Sheridan, C., Brumatti, G. & Martin, S. J. Oncogenic Ras-induced expression of Noxa and Beclin-1 promotes autophagic cell death and limits clonogenic survival. *Mol. Cell* **42**, 23–35 (2011).

333. Melnikova, V. O., Bolshakov, S. V., Walker, C. & Ananthaswamy, H. N. Genomic alterations in spontaneous and carcinogen-induced murine melanoma cell lines. *Oncogene* **23**, 2347–2356 (2004).

334. Foster, D. A. Phosphatidic acid signaling to mTOR: Signals for the survival of human cancer cells. *Biochim. Biophys. Acta - Mol. Cell Biol. Lipids* **1791**, 949–955 (2009).

335. Chen, Y., Zheng, Y. & Foster, D. A. Phospholipase D confers rapamycin resistance in human breast cancer cells. *Oncogene* **22**, 3937–3942 (2003).

336. Fingar, D. C. & Blenis, J. Target of rapamycin (TOR): an integrator of nutrient and growth factor signals and coordinator of cell growth and cell cycle progression. *Oncogene* **23**, 3151–3171 (2004).

337. Vaghela, P. T cell recognition of stress-induced post-translational modifications. (2022).

338. Pavel, M. *et al.* Contact inhibition controls cell survival and proliferation via YAP/TAZ-autophagy axis. *Nat. Commun. 2018 91* **9**, 1–18 (2018).

339. Zhang, W. Optimal timing of autophagy occurrence induced by earle's balanced salts solution in DLD-1,HCT-116,A2780,CHO,Hep G2 and SMMC7721 cancer cell lines. (2016).

340. Sahani, M. H., Itakura, E. & Mizushima, N. Expression of the autophagy substrate SQSTM1/p62 is restored during prolonged starvation depending on transcriptional upregulation and autophagy-derived amino acids. *Autophagy* **10**, 431–441 (2014).

341. Eloranta, K. *et al.* Chloroquine Triggers Cell Death and Inhibits PARPs in Cell Models of Aggressive Hepatoblastoma. *Front. Oncol.* **10**, 1138 (2020).

342. Eskelinen, E. L. *et al.* Inhibition of autophagy in mitotic

animal cells. *Traffic* **3**, 878–893 (2002).

343. Baba, M., Ohsumi, Y. & Osumi, M. Anaysis of the Membrane Structures Involved in Autophagy in Yeast by Freeze-Replica Method. *Cell Struct. Funct.* **20**, 465–471 (1995).

344. Eskelinen, E.-L. To be or not to be? Examples of incorrect identification of autophagic compartments in conventional transmission electron microscopy of mammalian cells. *Autophagy* **4**, 257–260 (2008).

345. Young, A. R. J. *et al.* Starvation and ULK1-dependent cycling of mammalian Atg9 between the TGN and endosomes. *J. Cell Sci.* **119**, 3888–3900 (2006).

346. Mizushima, N. *et al.* Mouse Apg16L, a novel WD-repeat protein, targets to the autophagic isolation membrane with the Apg12-Apg5 conjugate. *J. Cell Sci.* **116**, 1679–1688 (2003).

347. Itakura, E., Kishi, C., Inoue, K. & Mizushima, N. Beclin 1 forms two distinct phosphatidylinositol 3-kinase complexes with mammalian Atg14 and UVRAG. *Mol. Biol. Cell* **19**, 5360–5372 (2008).

348. Matsunaga, K. *et al.* Two Beclin 1-binding proteins, Atg14L and Rubicon, reciprocally regulate autophagy at

different stages. *Nat. Cell Biol.* **11**, 385–396 (2009).

349. Sun, Q. *et al.* Identification of Barkor as a mammalian autophagy-specific factor for Beclin 1 and class III phosphatidylinositol 3-kinase. *Proc. Natl. Acad. Sci. U. S. A.* **105**, 19211–19216 (2008).

350. Axe, E. L. *et al.* Autophagosome formation from membrane compartments enriched in phosphatidylinositol 3-phosphate and dynamically connected to the endoplasmic reticulum. *J. Cell Biol.* **182**, 685–701 (2008).

351. Ravikumar, B., Moreau, K., Jahreiss, L., Puri, C. & Rubinsztein, D. C. Plasma membrane contributes to the formation of pre-autophagosomal structures. *Nat. Cell Biol.* **12**, 747–757 (2010).

352. Fan, W., Nassiri, A. & Zhong, Q. Autophagosome targeting and membrane curvature sensing by Barkor/Atg14(L). *Proc. Natl. Acad. Sci. U. S. A.* **108**, 7769–7774 (2011).

353. Tian, W. *et al.* An antibody for analysis of autophagy induction. *Nat. Methods* **17**, 232–239 (2020).

354. Takáts, S. *et al.* Autophagosomal Syntaxin17-dependent lysosomal degradation maintains neuronal function in

Drosophila. *J. Cell Biol.* **201**, 531–539 (2013).

355. Kumar, S. *et al.* Phosphorylation of Syntaxin 17 by TBK1 Controls Autophagy Initiation. *Dev. Cell* **49**, 130-144.e6 (2019).

356. Proikas-Cezanne, T., Ruckerbauer, S., Stierhof, Y. D., Berg, C. & Nordheim, A. Human WIPI-1 puncta-formation: a novel assay to assess mammalian autophagy. *FEBS Lett.* **581**, 3396–3404 (2007).

357. Polson, H. E. J. *et al.* Mammalian Atg18 (WIPI2) localizes to omegasome-anchored phagophores and positively regulates LC3 lipidation. *Autophagy* **6**, 506–522 (2010).

358. Scacioc, A. *et al.* Structure based biophysical characterization of the PROPPIN Atg18 shows Atg18 oligomerization upon membrane binding. *Sci. Rep.* **7**, (2017).

359. Sanjuan, M. A. *et al.* Toll-like receptor signalling in macrophages links the autophagy pathway to phagocytosis. *Nature* **450**, 1253–1257 (2007).

360. Kimura, T. *et al.* Cellular and molecular mechanism for secretory autophagy. *http://dx.doi.org/10.1080/15548627.2017.1307486* **13**, 1084–1085 (2017).

361. Johansen, T. & Lamark, T. Selective Autophagy: ATG8 Family Proteins, LIR Motifs and Cargo Receptors. *J. Mol. Biol.* **432**, 80–103 (2020).

362. Li, W. *et al.* Selective autophagy of intracellular organelles: recent research advances. *Theranostics* **11**, 222 (2021).

363. Lamark, T. & Johansen, T. Aggrephagy: Selective disposal of protein aggregates by macroautophagy. *Int. J. Cell Biol.* (2012). doi:10.1155/2012/736905

364. Singh, R. *et al.* Autophagy regulates lipid metabolism. *Nature* **458**, 1131–1135 (2009).

365. Mancias, J. D., Wang, X., Gygi, S. P., Harper, J. W. & Kimmelman, A. C. Quantitative proteomics identifies NCOA4 as the cargo receptor mediating ferritinophagy. *Nat. 2014 5097498* **509**, 105–109 (2014).

366. Jiang, S. *et al.* Starch binding domain-containing protein 1/genethonin 1 is a novel participant in glycogen metabolism. *J. Biol. Chem.* **285**, 34960–34971 (2010).

367. Liou, W., Geuze, H. J., Geelen, M. J. H. & Slot, J. W. The Autophagic and Endocytic Pathways Converge at the Nascent Autophagic Vacuoles. *J. Cell Biol.* **136**, 61 (1997).

368. Gordon, P. B. & Seglen, P. O. Prelysosomal convergence of autophagic and endocytic pathways. *Biochem. Biophys. Res. Commun.* **151**, 40–47 (1988).

369. Eskelinen, E. L. Maturation of autophagic vacuoles in Mammalian cells. *Autophagy* **1**, 1–10 (2005).

370. Berg, T. O., Fengsrud, M., Strømhaug, P. E., Berg, T. & Seglen, P. O. Isolation and Characterization of Rat Liver Amphisomes: EVIDENCE FOR FUSION OF AUTOPHAGOSOMES WITH BOTH EARLY AND LATE ENDOSOMES. *J. Biol. Chem.* **273**, 21883–21892 (1998).

371. Strømhaug, P. E., Berg, T. O., Fengsrud, M. & Seglen, P. O. Purification and characterization of autophagosomes from rat hepatocytes. *Biochem. J.* **335 (Pt 2**, 217–224 (1998).

372. Mizushima, N., Ohsumi, Y. & Yoshimori, T. Autophagosome Formation in Mammalian Cells. *CELL Struct. Funct.* **27**, 421–429 (2002).

373. Jin, M. & Klionsky, D. J. Regulation of autophagy: Modulation of the size and number of autophagosomes. *FEBS Lett.* **588**, 2457 (2014).

374. Hailey, D. W. *et al.* Mitochondria Supply Membranes for Autophagosome Biogenesis during Starvation. *Cell* **141**,

656–667 (2010).

375. Axe, E. L. *et al.* Autophagosome formation from membrane compartments enriched in phosphatidylinositol 3-phosphate and dynamically connected to the endoplasmic reticulum. *J. Cell Biol.* **182**, 685–701 (2008).

376. Andrejeva, G. *et al.* De novo phosphatidylcholine synthesis is required for autophagosome membrane formation and maintenance during autophagy. *Autophagy* **16**, 1044–1060 (2020).

377. Axe, E. L. *et al.* Autophagosome formation from membrane compartments enriched in phosphatidylinositol 3-phosphate and dynamically connected to the endoplasmic reticulum. *J. Cell Biol.* **182**, 685–701 (2008).

378. Yen, W. L. *et al.* The conserved oligomeric Golgi complex is involved in double-membrane vesicle formation during autophagy. *J. Cell Biol.* **188**, 101–114 (2010).

379. Punnonen, E. L., Pihakaski, K., Mattila, K., Lounatmaa, K. & Hirsimäki, P. Intramembrane particles and filipin labelling on the membranes of autophagic vacuoles and lysosomes in mouse liver. *Cell Tissue Res. 1989 2582* **258**, 269–276 (1989).

380. Ni, M., Zhou, H., Wey, S., Baumeister, P. & Lee, A. S. Regulation of PERK Signaling and Leukemic Cell Survival by a Novel Cytosolic Isoform of the UPR Regulator GRP78/BiP. *PLoS One* **4**, e6868 (2009).

381. Eid, N., Ito, Y., Maemura, K. & Otsuki, Y. Elevated autophagic sequestration of mitochondria and lipid droplets in steatotic hepatocytes of chronic ethanol-treated rats: An immunohistochemical and electron microscopic study. *J. Mol. Histol.* **44**, 311–326 (2013).

382. Gao, W. *et al.* Biochemical isolation and characterization of the tubulovesicular LC3-positive autophagosomal compartment. *J. Biol. Chem.* **285**, 1371–83 (2010).

383. Eskelinen, E.-L. Fine Structure of the Autophagosome. *Methods Mol. Biol.* **445**, 11–28 (2008).

384. Ireland, J. M. & Unanue, E. R. Processing of proteins in autophagy vesicles of antigen-presenting cells generates citrullinated peptides recognized by the immune system. *Autophagy* **8**, 429–430 (2012).

385. Rosenbaum, P. *et al.* Vaccine Inoculation Route Modulates Early Immunity and Consequently Antigen-Specific Immune Response. *Front. Immunol.* **12**, 1362 (2021).

386. Paul, D. *et al.* Phagocytosis Dynamics Depends on Target Shape. *Biophys. J.* **105**, 1143 (2013).

387. Dieu, M. C. *et al.* Selective Recruitment of Immature and Mature Dendritic Cells by Distinct Chemokines Expressed in Different Anatomic Sites. *J. Exp. Med.* **188**, 373–386 (1998).

388. Blood, D. J.- & 1997, undefined. Dendritic cells: unique leukocyte populations which control the primary immune response. *cir.nii.ac.jp*

389. Caux, C. *et al.* B70/B7-2 is identical to CD86 and is the major functional ligand for CD28 expressed on human dendritic cells. *J. Exp. Med.* **180**, 1841–1847 (1994).

390. Nijman, H. W. *et al.* Antigen capture and major histocompatibility class II compartments of freshly isolated and cultured human blood dendritic cells. *J. Exp. Med.* **182**, 163–174 (1995).

391. Castellino, F., Zhong, G., Immunology, R. G.-H. & 1997, U. Antigen presentation by MHC class II molecules: invariant chain function, protein trafficking, and the molecular basis of diverse determinant capture. *Elsevier* (1997).

392. Binnewies, M. *et al.* Unleashing Type-2 Dendritic Cells to

Drive Protective Antitumor CD4+ T Cell Immunity. *Cell* **177**, 556-571.e16 (2019).

393. Labeur, M. S. *et al.* Generation of Tumor Immunity by Bone Marrow-Derived Dendritic Cells Correlates with Dendritic Cell Maturation Stage. *J. Immunol.* **162**, 168–175 (1999).

394. Inaba, K. *et al.* Generation of large numbers of dendritic cells from mouse bone marrow cultures supplemented with granulocyte/macrophage colony-stimulating factor. *rupress.org*

395. Twitty, C. G., Jensen, S. M., Hu, H.-M. & Fox, B. A. Tumor-Derived Autophagosome Vaccine: Induction of Cross-Protective Immune Responses against Short-lived Proteins through a p62-Dependent Mechanism. *Clin. Cancer Res.* **17**, 6467–6481 (2011).

396. Johnstone, R. M., Adam, M., Hammond, J. R., Orr, L. & Turbide, C. Vesicle formation during reticulocyte maturation. Association of plasma membrane activities with released vesicles (exosomes). *J. Biol. Chem.* **262**, 9412–9420 (1987).

397. Altieri, S. L., Khan, A. N. H. & Tomasi, T. B. Exosomes from plasmacytoma cells as a tumor vaccine. *J. Immunother.* **27**, 282–288 (2004).

398. Bu, N., Li, Q. L., Feng, Q. & Sun, B. Z. Immune protection effect of exosomes against attack of L1210 tumor cells. *Leuk. Lymphoma* **47**, 913–918 (2006).

399. Wolfers, J. *et al.* Tumor-derived exosomes are a source of shared tumor rejection antigens for CTL cross-priming. *Nat. Med.* **7**, 297–303 (2001).

400. Altieri, S. L., Nazmul, A., Khan, H. & Tomasi, T. B. Exosomes from Plasmacytoma Cells as a Tumor Vaccine. *J. Immunol.* (2004).

401. Yao, Y. *et al.* Dendritic cells pulsed with leukemia cell-derived exosomes more efficiently induce antileukemic immunities. *PLoS One* **9**, (2014).

402. Zitvogel, L. *et al.* Eradication of established murine tumors using a novel cell-free vaccine: dendritic cell-derived exosomes. *Nat. Med.* **4**, 594–600 (1998).

403. Théry, C. *et al.* Molecular Characterization of Dendritic Cell-Derived Exosomes: Selective Accumulation of the Heat Shock Protein Hsc73. *J. Cell Biol.* **147**, 599 (1999).

404. Szczepanski, M. J., Szajnik, M., Welsh, A., Whiteside, T. L. & Boyiadzis, M. Blast-derived microvesicles in sera from patients with acute myeloid leukemia suppress natural killer cell function via membrane-associated

transforming growth factor-β1. *Haematologica* **96**, 1302 (2011).

405. Iero, M. *et al.* Tumour-released exosomes and their implications in cancer immunity. *Cell Death Differ.* **15**, 80–88 (2008).

406. Xiang, X. *et al.* Induction of myeloid-derived suppressor cells by tumor exosomes. *Int. J. Cancer* **124**, 2621 (2009).

407. Clayton, A. & Tabi, Z. Exosomes and the MICA-NKG2D system in cancer. *Blood Cells. Mol. Dis.* **34**, 206–213 (2005).

408. Hellwinkel, J. E. *et al.* Glioma-derived extracellular vesicles selectively suppress immune responses. *Neuro. Oncol.* **18**, 497 (2016).

409. Abusamra, A. J. *et al.* Tumor exosomes expressing Fas ligand mediate CD8+ T-cell apoptosis. *Blood Cells. Mol. Dis.* **35**, 169–173 (2005).

410. Clayton, A., Al-Taei, S., Webber, J., Mason, M. D. & Tabi, Z. Cancer exosomes express CD39 and CD73, which suppress T cells through adenosine production. *J. Immunol.* **187**, 676–683 (2011).

411. Sorice, M. *et al.* Autophagy generates citrullinated

peptides in human synoviocytes: a possible trigger for anti-citrullinated peptide antibodies. *Rheumatology* **55**, 1374–1385 (2016).

412. Helft, J. *et al.* GM-CSF Mouse Bone Marrow Cultures Comprise a Heterogeneous Population of CD11c+MHCII+ Macrophages and Dendritic Cells. *Immunity* **42**, 1197–1211 (2015).

413. Wang, J. C. E. *et al.* An 11-color Flow Cytometric Assay for Identifying, Phenotyping, and Assessing Endocytic Ability of Peripheral Blood Dendritic Cell Subsets in A Single Platform. *J. Immunol. Methods* **341**, 106 (2009).

414. Wen, H., Hao, J. & Li, S. K. Characterization of Human Sclera Barrier Properties for Transscleral Delivery of Bevacizumab and Ranibizumab. *J. Pharm. Sci.* **102**, 892 (2013).

415. Shibutani, S. T. & Yoshimori, T. A current perspective of autophagosome biogenesis. *Cell Res.* **24**, 58 (2014).

416. Pustylnikov, S., Sagar, D., Jain, P. & Khan, Z. K. Targeting the C-type Lectins-Mediated Host-Pathogen Interactions with Dextran. *J. Pharm. Pharm. Sci.* **17**, 371 (2014).

417. Uribe-Querol, E. & Rosales, C. Phagocytosis: Our Current

Understanding of a Universal Biological Process. *Front. Immunol.* **11**, 1066 (2020).

418. Dickson, R. B., Willingham, M. C. & Pastan, I. H. Receptor-mediated endocytosis of alpha 2-macroglobulin: inhibition by ionophores and stimulation by Na+ and HCO3(-). *Ann. N. Y. Acad. Sci.* **401**, 38–49 (1982).

419. Platt, C. D. *et al.* Mature dendritic cells use endocytic receptors to capture and present antigens. *Proc. Natl. Acad. Sci. U. S. A.* **107**, 4287–4292 (2010).

420. McAleer, J. P. & Vella, A. T. Understanding how lipopolysaccharide impacts CD4 T cell immunity. *Crit. Rev. Immunol.* **28**, 281 (2008).

421. Tough, D. F., Sun, S. & Sprent, J. T Cell Stimulation In Vivo by Lipopolysaccharide (LPS). *J. Exp. Med.* **185**, 2089–2094 (1997).

422. Madura Larsen, J. *et al.* BCG stimulated dendritic cells induce an interleukin-10 producing T-cell population with no T helper 1 or T helper 2 bias in vitro. *Immunology* **121**, 276 (2007).

423. Kamath, A. T., Sheasby, C. E. & Tough, D. F. Dendritic Cells and NK Cells Stimulate Bystander T Cell Activation

in Response to TLR Agonists through Secretion of IFN-αβ and IFN-γ. *J. Immunol.* **174**, 767–776 (2005).

424. Blander, J. M. & Medzhitov, R. Regulation of phagosome maturation by signals from toll-like receptors. *Science* **304**, 1014–1018 (2004).

425. Magarian Blander, J. & Medzhitov, R. Toll-dependent selection of microbial antigens for presentation by dendritic cells. *Nat. 2006 4407085* **440**, 808–812 (2006).

426. Rodig, S. J. *et al.* MHC proteins confer differential sensitivity to CTLA-4 and PD-1 blockade in untreated metastatic melanoma. *Sci. Transl. Med.* **10**, (2018).

427. Roemer, M. G. M. *et al.* Major Histocompatibility Complex Class II and Programmed Death Ligand 1 Expression Predict Outcome After Programmed Death 1 Blockade in Classic Hodgkin Lymphoma. *J. Clin. Oncol.* **36**, 942–950 (2018).

428. Mortara, L. *et al.* CIITA-induced MHC class II expression in mammary adenocarcinoma leads to a Th1 polarization of the tumor microenvironment, tumor rejection, and specific antitumor memory. *Clin. Cancer Res.* **12**, 3435–3443 (2006).

429. Park, I. A. *et al.* Expression of the MHC class II in triple-negative breast cancer is associated with tumor-infiltrating lymphocytes and interferon signaling. *PLoS One* **12**, (2017).

430. Andres, F. *et al.* Expression of the MHC Class II Pathway in Triple-Negative Breast Cancer Tumor Cells Is Associated with a Good Prognosis and Infiltrating Lymphocytes. *Cancer Immunol. Res.* **4**, 390–399 (2016).

431. Johnson, D. B. *et al.* Melanoma-specific MHC-II expression represents a tumour-autonomous phenotype and predicts response to anti-PD-1/PD-L1 therapy. *Nat. Commun.* **7**, (2016).

432. Ahn, C. H. *et al.* Expression of beclin-1, an autophagy-related protein, in gastric and colorectal cancers. *APMIS* **115**, 1344–1349 (2007).

433. Delaney, J. R. *et al.* Haploinsufficiency networks identify targetable patterns of allelic deficiency in low mutation ovarian cancer. *Nat. Commun.* **8**, (2017).

434. Richardson, P. J. & Luzio, J. P. Immunoaffinity purification of membrane fractions from mammalian cells. *Subcell. Biochem.* **12**, 221–241 (1988).

435. Brooks, A. R. *et al.* Transcriptional silencing is associated

with extensive methylation of the CMV promoter following adenoviral gene delivery to muscle. *J. Gene Med.* **6**, 395–404 (2004).

436. Bozzacco, L. & Yu, H. Identification and quantitation of MHC class II-bound peptides from mouse spleen dendritic cells by immunoprecipitation and mass spectrometry analysis. *Methods Mol. Biol.* **1061**, 231 (2013).

437. Steimle, V., Siegrist, C. A., Mottet, A., Lisowska-Grospierre, B. & Mach, B. Regulation of MHC class II expression by interferon-gamma mediated by the transactivator gene CIITA. *Science* **265**, 106–109 (1994).

438. Castelli, F. A. *et al.* HLA-DP4, the Most Frequent HLA II Molecule, Defines a New Supertype of Peptide-Binding Specificity. *J. Immunol.* **169**, 6928–6934 (2002).

439. Robinson, J., Mistry, K., Mcwilliam, H., Lopez, R. & Marsh, S. G. E. IPD—the Immuno Polymorphism Database. *Nucleic Acids Res.* **38**, D863 (2010).

440. Robinson, J. *et al.* IPD-IMGT/HLA Database. *Nucleic Acids Res.* **48**, D948 (2020).